MASTER THESIS

Purification and characterization of ice nuclei from birch pollen

carried out at the

Institute for Materials Chemistry
TU Wien

under the supervision of

Univ.Prof. Dipl.-Chem. Dr. rer.nat Hinrich Grothe

by

Florian Reyzek, B.Sc.

Vienna, 22.03.2023

DIPLOMARBEIT

Aufreinigung und Charakterisierung von Eiskeimen aus Birkenpollen

durchgeführt am
Institute for Materials Chemistry
TU Wien

unter der Anleitung von
Univ.Prof. Dipl.-Chem. Dr. rer.nat Hinrich Grothe

durch
Florian Reyzek, B.Sc.

Wien, 22.03.2023

Eidesstattlich Erklärung

Ich, Florian Reyzek, erkläre hiermit an Eides statt, dass ich die vorliegende Arbeit selbstständig verfasst, andere als die angegebenen Quellen und Hilfsmittel nicht benutzt, und die den benutzten Quellen wörtlich und inhaltlich entnommenen Stellen als solche kenntlich gemacht habe.

Affidavit

I, Florian Reyzek, hereby declare that I have authored this thesis independently, that I have not used other than the declared sources and resources, and that I have explicitly marked all material which has been quoted either literally or by content from the sources.

_____   _____
Ort, Datum   Florian Reyzek

*"Develop success from failures. Discouragement and failure are
two of the surest stepping stones to success."*

Dale Carnegie
$(1888 - 1955)$

Abstract

Progressing climate change demands understanding of Earth's climate and its influencing factors. One of the most challenging tasks is currently the influence of aerosol particles on the climate which is still quite uncertain. Numerous aerosols, such as dust, soot, and biological particles, can act as heterogeneous ice nuclei (IN) and trigger the freezing of supercooled liquid cloud droplets. Without the presence of IN, cloud droplets can be supercooled down to $-38\,°C$, thus ice clouds would only occur at rather high altitudes. The phase state of the droplets has a major impact on cloud properties, such as the albedo, precipitation, and cloud lifetime.

IN of biological origin, such as bacteria, fungi, or pollen, can have remarkably high onset freezing temperatures. Interestingly, for tree pollen solubilized macromolecules are responsible for the ice nucleation activity and not the pollen grains themselves. In addition, these ice-nucleating macromolecules (INMs) were found on other tree tissues. In general, nano-sized INMs exceed micrometer-sized pollen grains in number by several orders of magnitude, and thus the emission of INMs from the biosphere might play a more important role than previously thought.

Still, the chemical composition and structure of INMs remain largely unknown. In this work, we extracted INMs from birch pollen with water to shine a light on. In order to purify and concentrate the extracted INMs, we used ice affinity purification, which enabled us to perform further characterization experiments with INM at varying concentrations.

The birch pollen INMs show onset temperatures of up to $-6\,°C$, much higher than the $-15\,°C$ previously reported by many studies. Interestingly, the $10\,kDa$ filtrate of the INM sample still showed ice nucleation activity. Thus, the INMs can be much smaller than the previously reported $100\,kDa$. Fluorescence-, infrared-, and circular dichroism spectroscopy were used to understand the chemical composition of the INMs. The spectra showed polysaccharide and protein signals. Also, the INMs were found to be heat sensitive as the ice nucleation activity decreased with increased temperature and duration of heat treatments. In sum, this led us to hypothesize that the INMs are agglomerates, made up of small subunits which can also act as IN. The agglomerates might be proteinaceous, polysaccharides, or even a combination of both.

Kurzfassung

In Zeiten des Klimawandels wird es immer wichtiger, dass wir das Klima unserer Erde besser verstehen. Das Klima ist ein komplexes System bestehend aus vielen Variablen, welche natürlich und durch den Menschen beeinflusst werden. Obwohl wir einige dieser Variablen bereits sehr gut verstehen, so haben wir doch noch einiges zu erforschen. Das wahrscheinlich wichtigste Beispiel ist der Einfluss von Aerosolen. Diverse Aerosole, wie Staub, Ruß und biologische Partikel, können als Eiskeim in Wolken wirken. Diese inititiieren das Gefrieren von unterkühlten Wassertropfen in Wolken. Wolkentropfen können bis zu $-38\,°C$ unterkühlt werden, daher würde es ohne Eiskeime nur in großer Höhe Eis in Wolken geben. Der Eisanteil hat jedoch großen Einfluss auf die Eigenschaften der Wolke, unter anderem das Albedo und die Bildung von Niederschlag.

Vor allem biologische Eiskeime zeichnen sich durch eine hohe Gefrier-Effizienz aus. Unter anderem Bakterien, Pilze bzw. deren Sporen und Pollen sind biologische Eiskeime. Bei den meisten biologischen Eiskeimen wurde festgestellt, dass wasserlösliche Makromoleküle für die Eisnukleationsaktivität verantwortlich sind. Die Eiskeime von Birkenpollen wurden darüber hinaus auch auf den Blättern und dem Holz der Birken gefunden. Ganz generell gibt es wesentlich mehr Eiskeime als Pollen und daher ist es umso wichtiger die Eiskeime und deren Emission in die Atmosphäre besser zu verstehen, um deren potenzielle atmosphärische Relevanz evaluieren zu können. Trotzdem ist die Zusammensetzung der Birken Eiskeime noch kaum bekannt. Aus diesem Grund, liegt der Fokus dieser Arbeit auf der Analyse von Birken Eiskeimen.

Die Eiskeime wurden mit Reinstwasser von Birkenpollen extrahiert. Das Extrakt wurde mittels Eisaffinität aufgereinigt und dabei um einen Faktor 10 aufkonzentriert. Die aufgereinigte Probe wurde im Anschluss mit diversen Methoden analysiert. Dabei haben wir herausgefunden, dass der Eiskeim das Gefrieren der unterkühlten Tropfen schon bei $-6\,°C$ ermöglicht, viel höher als die $-15\,°C$, welche zuvor berichtet wurden. Weiters haben wir mittels Filtration herausgefunden, dass der Eiskeim eine Größe von unter $10\,kDa$ aufweist, viel kleiner als die zuvor berichteten $100\,kDa$. Mittels Fluoreszenz-, Infrarot- und Zirkulardichroismus Spektroskopie haben wir die chemische Zusammensetzung untersucht, dabei haben wir sowohl Protein als auch Polysaccharid Signale gemessen. Darüber hinaus haben wir beobachtet, dass die Eiskeime teilweise hitzelabil sind, da ihre Eiskeim-Aktivität mit erhöhter Temperatur und Dauer immer weiter gesunken ist. Mit der Summe der Ergebnisse stellen wir die Hypothese auf, dass die Eiskeime vermutlich große Agglomerate aus kleinen Untereinheiten sind, welche ebenso als Eiskeim wirken können. Wahrscheinlich sind die Agglomerate eine Kombination aus Proteinen und Polysacchariden.

Preface

This Master thesis was supervised by Univ. Prof. Dr. Hinrich Grothe. In addition, Dr. Janine Fröhlich and Ass.Prof. Dr. Konrad Meister provided guidance and expertise over the course of the project.

The experiments were mainly carried out at the Max Planck Institute for Chemistry in Mainz (Germany) in the period from October 2021 to March 2022, in the group of Dr. Janine Fröhlich.

Additional experimental work was carried out at the Max Planck Institute for Polymer Research in Mainz (Germany), in the group of Ass.Prof. Dr. Konrad Meister and at the Vienna Universtiy of Technology (TU Wien) in the group of Univ. Prof. Dr. Hinrich Grothe.

Acknowledgments

First, I want to express my gratitude to **Prof. Hinrich Grothe** for the opportunity to participate in his research group and supervise this work.

I would like to thank **Janine Fröhlich** for giving me the opportunity to work under her guidance at the Max Planck Institute for Chemistry in Mainz and for making me feel welcome even before my first arrival.

Further, I want to thank **Konrad Meister** for the opportunity to work in his lab at the Max Planck Institute for Polymer research and for valuable input, discussions, and guidance all throughout this work.

A special thanks to **Teresa Seifried**, who first brought me to the topic of ice nucleation. Although we were far apart at most times during this work, I could always turn to her for any advice.

Another special thanks to **Nadine Bothen**. She helped tremendously with the experimental work and troubleshooting when something went wrong. Also, our discussions were always fruitful, and above all, she became a good friend and helped me gain a foothold in Mainz.

I am grateful to **Luisa Scolari**, **Jürgen Gratzl**, **Stefan Werkovits**, **Paul Bieber** and **Ayse Koyun** and all other colleagues at TU Wien for motivating and supporting me, especially during the writing process.

Thanks to all my colleagues in Mainz, I truly felt welcome from the first day on. A special thanks to **Ralph Schwidetzky** for guidance and productive discussion. Also, thanks to **Nina Kropf** for helping me whenever I needed supplies and troubleshooting in the lab. I also want to thank **Jean Pierre** for being a great colleague and friend.

I would like to express my deepest gratitude to my family, my parents, **Renate** and **Michael**, and my brother **Daniel**. They always supported me and provided security and space to follow my interests.

*I dedicate this work to my love **Victoria**. Thank you for always being there and supporting me in anything I do.*

Contents

Contents

Chapter 1

Introduction and theoretical background

The *Anthropocene* is the latest proposed geological epoch. A time named after the human influence on the global climate and thereby many ecological and geological systems [1]. A surge in human-caused greenhouse gas emissions is the main cause of the immense impact. The Earth's climate is a complex and rigid system sensitive to interferences. The intergovernmental panel on climate change (IPCC) has recently reported that human-induced warming reached approximately $1\,°C$ above pre-industrial levels in 2017 [2]. With an increase of $0.2\,°C$ per decade, it is obvious that the goal of the Paris climate agreement of $1.5\,°C$ is in close proximity. Nonetheless, the effects of climate change are already significant, with an increasing amount and more intense extreme weather events, like droughts or floods. An extremely worrying example where global warming is directly visible is the steady decline of glaciers especially in the alpine region. Moreover, many species are reaching their limits in their ability to adapt to the apparent changes already. This results in the loss of biodiversity which can lead to reducing the ability of nature to provide the essential services humans depend on, such as food supply [3].

Atmospheric research is the basis for understanding and predicting future climate changes needed to understand and assess the risks involved. Moreover, it is necessary for planning and execution of the necessary measures to limit impacts and preserve biodiversity and a habitable climate. The following paragraphs aim to give a basic understanding of the Earth's climate and its influencing factors.

1.1 The Earth's climate - a complex system

1.1.1 Weather vs. climate

The word "climate" is derived from the Greek word κλίμα (klima), referring to a slope linked to temperature gradients from the Equator to Pole [5]. In its modern meaning, the climate is the long-term composite of the weather conditions at a certain place or region. It encompasses means, variabilities, and extremes of a number of meteorological variables, these include temperature, pressure, humidity, wind velocity, precipitation, cloud coverage, and many others. On a short scale, where these variables affect the daily life of humans and all other life on Earth, is called weather. The main difference
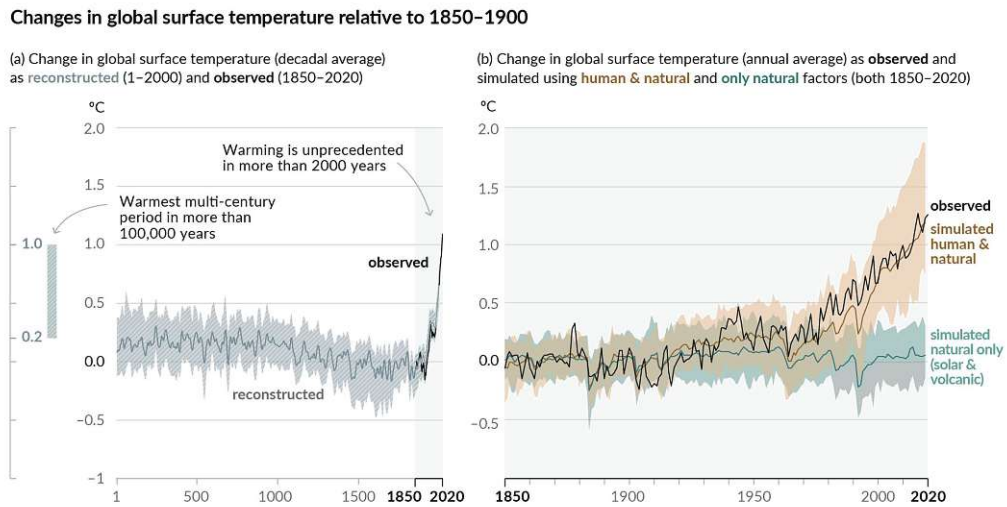
Changes in global surface temperature relative to 1850–1900

(a) Change in global surface temperature (decadal average)
as reconstructed (1–2000) and observed (1850–2020)

(b) Change in global surface temperature (annual average) as **observed** and
simulated using **human & natural** and **only natural** factors (both 1850–2020)

Figure 1.1: History of global temperature change and causes of recent warming: (a) Changes in global surface temperature reconstructed from paleoclimate archives (solid grey line, years 1–2000) and from direct observations (solid black line, 1850–2020). (b) Changes in global surface temperature over the past 170 years (black line). Figure SPM.1 from IPCC [4].

is the time scale: Weather is usually defined by a time scale of a few days. Climate, on the other hand, has a normal time scale of 30 consecutive years, defined by the World Meteorological Organization (WMO), in which the data are averaged. [5]

A broader definition nowadays would furthermore include a set of hydrospheric, cryospheric, and biospheric variables, in addition to the atmospheric variables. Parameters of the hydrological cycle make the set of hydrospheric variables, while parameters of snow and ice form the cryospheric variables. At the same time, biospheric variables contain information on interactions between the land and ocean surface with the atmosphere. Figure 1.2 tries to grasp the complexity of these interconnected parameters in a schematic illustration.

Apart from all the complexity and changes in climate, there is at least one constant. Weather and therefore climate all take place in a thin gas layer surrounding planet Earth, called the atmosphere.

1.1.2   The Earth's atmosphere

Earth's atmosphere is essential for terrestrial life, although it makes up only about 1 % of the Earth's radius. Through different mechanisms, the atmosphere protects life by absorbing harmful radiation, regulating temperature, and creating the pressure needed for liquid water to exist. [7]

While the pressure of the atmosphere decreases exponentially with increasing altitude, the temperature has a varying gradient. The temperature determines the division of the atmosphere into four layers. Each subsequent layer has an opposite gradient. Starting from the Earth's surface the troposphere stretches up to about 12 km to the tropopause. The height varies, while it is smaller at the poles it is larger at the equator. Temperature and moisture generally decrease with altitude in the
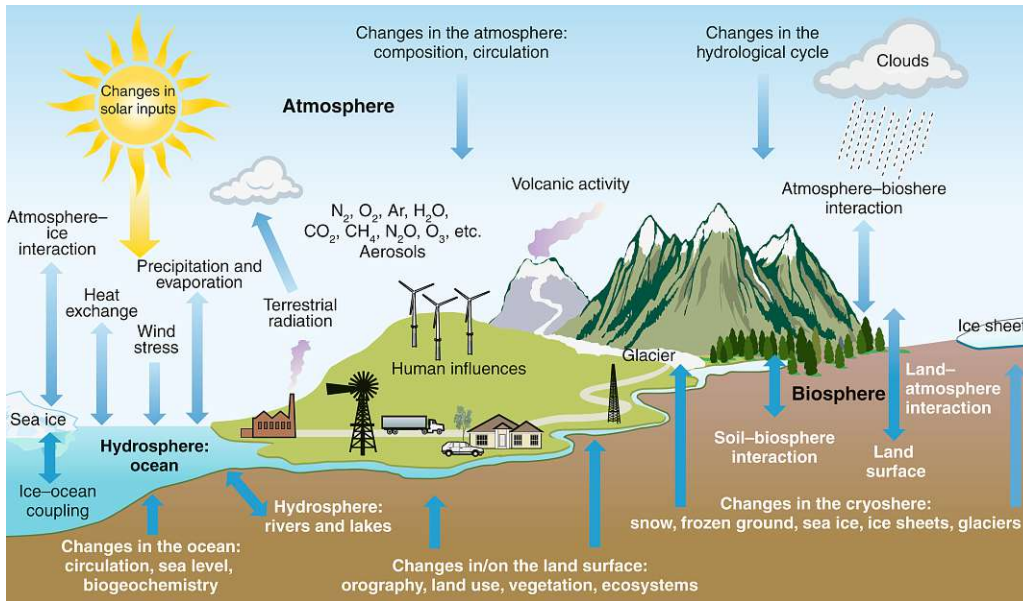
Figure 1.2: The complex climate system. Figure 1.1 from Barry & Hall-McKim [6].

troposphere. The second layer is the Stratosphere, where the temperature begins to increase with altitude. This is due to the UV absorption by ozone at around 20 km to 40 km. After the stratopause, the mesosphere with a decreasing temperature stretches from about 50 km to 80 km. After reaching the coldest temperatures in mesopause the thermosphere begins. Here temperature increases again due to short wavelength UV absorption of molecular and atomic oxygen. The outermost layer is called the exosphere, usually, it is not considered part of the atmosphere due to its very low density. [5, 7]
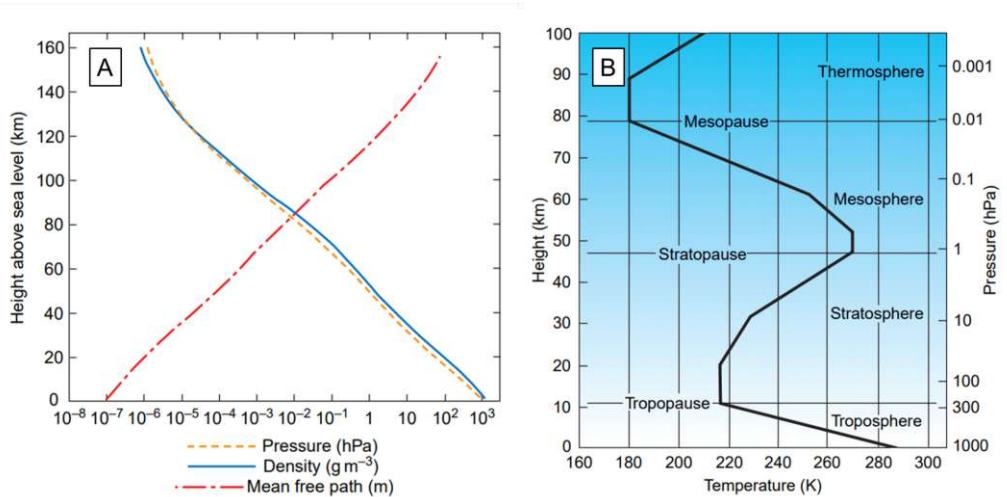
Figure 1.3: Pressure (A) and temperature (B) gradient of the Earth's atmosphere. Adapted from Wallace & Hobbs [8].

The troposphere from the greek word τρόπος, is the most turbulent layer with the highest amount of water vapor. The bottom of the troposphere is highly influenced

by the Earth's surface, through the transfer of heat and momentum. This layer is called the planet boundary layer and is varying in height depending on location, a good average is about 1 km. Everything above is considered the free troposphere. The heat transfer leads to a process called convection, caused by warm air close to the Earth's surface rising and adiabatic cooling and decreasing infrared (IR) radiation with increasing altitude. Convection is the main drive for vertical mixing in the troposphere. Thereby, water vapor is transported from the surface up throughout the troposphere. Decreasing temperature and pressure, as well as the presence of aerosol particles, lead to the condensation of vapor and the formation of clouds.

1.1.3 Clouds

A cloud is defined as an ensemble of hydrometeors suspended in the air. Clouds come in many different appearances. They can be classified into four types: low-level clouds (*stratus*, *stratocumulus*), mid-level clouds (*altocumulus*, *altostratus*), high-level clouds (*cirrus*, *cirrocumulus*, *cirrostratus*), and clouds with vertical development (*cumulunimbus*) [7, 9].

Moreover, clouds can be classified by their phase state. Warm clouds consist purely of liquid water droplets. They are usually low-level clouds and close to the surface. Their temperature can be above or below 0 °C. These clouds can be supercooled down to −38 °C, before the droplets will freeze homogeneously. Most high-level clouds like *cirrus* consist purely of ice crystal, thus they are called ice- or cold clouds. In between are mixed-phase clouds consist of ice crystals as well as liquid droplets. [7, 9]

Cloud formation is a complex process depending on many variables, such as temperature, saturation, and the presence of aerosol particles. Some aerosol particles are cloud-condensation nuclei (CCN) and act like a seed for a cloud droplet to grow. Without a CCN a droplet can only start forming at quite low temperatures and very high supersaturation, since the condensation process of pure water is kinetically hindered. Likewise, the freezing process of a pure water droplet is also hindered which explains why cloud droplets can be supercooled down to −38 °C before pure water droplets will freeze. Similar to CCN certain aerosol particles called ice nuclei (IN) can allow the droplets to freeze at higher temperatures. Section 1.2 will focus on the theory behind these processes.

1.2 Classical nucleation theory

1.2.1 Homogeneous nucleation

In thermodynamics, a phase transition is a physical transition between two states of a medium, e.g state of matter (see figure 1.4). Some phase transitions require a nucleation process. Nucleation describes a phase transition where a cluster of a thermodynamic stable or metastable phase forms and grows within the surrounding metastable parent phase. These transitions include for example formation of ice from liquid water (ice nucleation) or the formation of aerosol particles (gas to particle conversion). Classical nucleation theory (CNT) describes nucleation as a stochastic process driven by thermodynamic and kinetic parameters. [9–13]

While ice melts at the melting point of water (0 °C at atmospheric pressure) liquid water can remain in a supercooled state prior freezing. Hereby, the Gibbs free energy
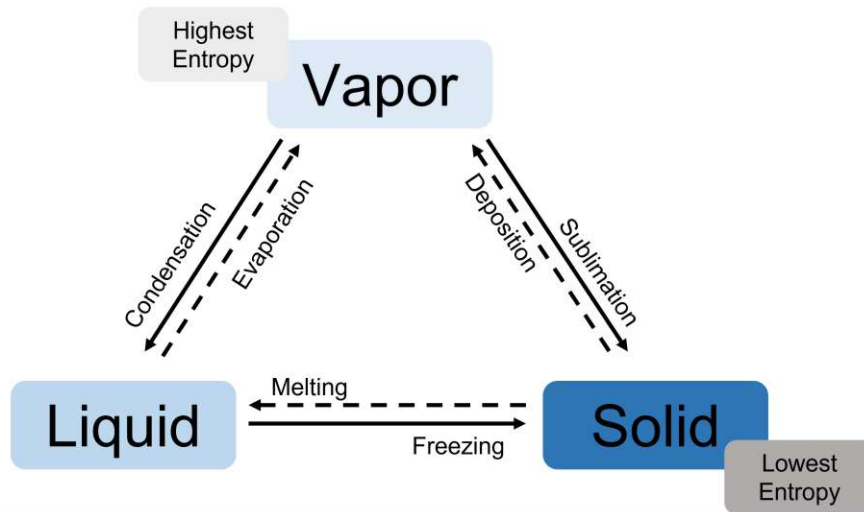
Figure 1.4: Phases and transitions between them. Solid arrows indicate changes leading to decreased entropy.

G of ice is lower than that of water but an energy barrier hinders the transition. The metastable liquid phase lies within an energy valley and an energy barrier needs to be overcome for the phase transition to occur. Due to the minimum principle of G thermodynamically, the system has no reason to increase its energy to overcome this barrier. Nevertheless, statistical fluctuations of intermolecular bonds by thermal energy lead to cluster formation of the new phase, resulting in a much lower energy barrier. These clusters form and dissipate by random chance. This is where CNT bridges the thermodynamic and atomistic view of a system. The stable thermodynamic macrostate is a temporal and spatial average of infinite microstates. The atomistic view however allows for microscale fluctuations on a short time scale. In this sense, the cluster needs to reach a sufficient size to overcome the energy barrier. [10]

Following is a derivation for the energy barrier impeding the formation of a cluster within a parent phase for the liquid to the solid transition of water adapted from Lohmann *et al.* [10] and Murray *et al.* [14].

Figure 1.5 illustrates two states. State 1 is the parent phase containing N water molecules and has the Gibbs free energy G_1. The Gibbs free energy per mole, of the parent phase, is the chemical potential μ_{old}.

$$G_1 = N\mu_{old} \tag{1.1}$$

State 2, after the homogeneous formation of a cluster containing n molecules with G_n and the remaining parent phase with $N - n$ water molecules and a Gibbs free energy for the whole system of G_2. Where μ_{new} is the chemical potential of the newly formed cluster and $G_{ex}(n)$ is the excess Gibbs energy needed for the formation of a new interface between the two phases.

$$G_2 = (N - n)\,\mu_{old} + G(n) \tag{1.2}$$

$$G(n) = n\mu_{new} + G_{ex}(n) \tag{1.3}$$
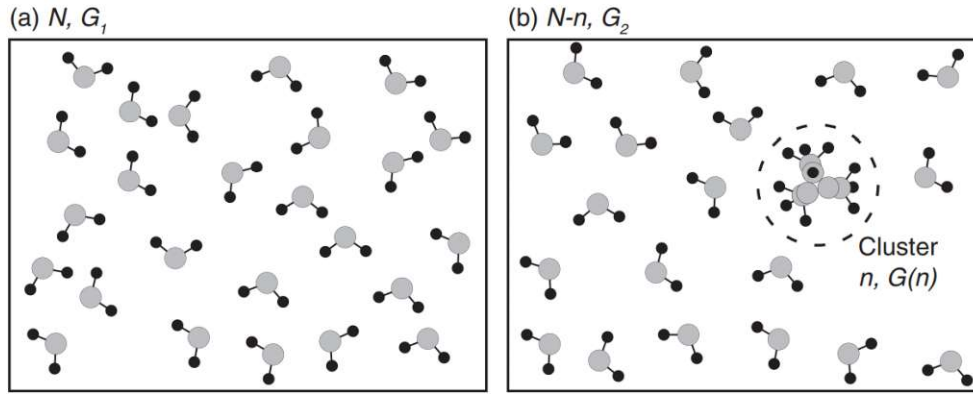
Figure 1.5: Scematic before and after homogeneous cluster formation. (a) State 1: parent phase with N molecules and G_1. (b) State 2: parent phase with N-n molecules and G_2, and cluster with n molecules and G_g. Adapted from Lohmann *et al.* [10]

The difference between G_2 and G_1 describes the work $W(n)$ needed for cluster formation.

$$W(n) = \Delta G_{cl} = G_2 - G_1 = n\Delta\mu + G_{ex}(n) \qquad (1.4)$$

$\Delta\mu$ denotes the difference $\Delta\mu = \mu_{new} - \mu_{old}$ and can be approximated as follows:

$$\Delta\mu(p, T) = -k_B T \ln(S) \qquad (1.5)$$

Where k_B is the Boltzmann constant, T is the temperature, p is the pressure and S is the saturation, which is defined as the fraction of the vapor pressure of the phases.

$$S = \frac{p_{parent}}{p_{cluster}} \qquad (1.6)$$

Assuming as a spherical cluster of a radius r, G_{ex} can be expressed as:

$$G_{ex} = 4\pi r^2 \sigma \qquad (1.7)$$

Where σ is the energy of the interface between the new and parent phases, also referred to as surface tension. The assumption of a spherical cluster further allows the expression to calculate the number n of molecules in a cluster:

$$n = \frac{4\pi r^3}{3\nu} \qquad (1.8)$$

Where ν is the molecular volume of the condensed phase. Inserting equations 1.5, 1.7, and 1.8 into equation 1.4 leaves the Gibbs free energy associated with homogeneous nucleation, or the formation of a cluster.

$$\Delta G_{cl} = -\frac{4\pi r^3}{3\nu} k_B T \ln(S) + 4\pi\sigma r^2 \qquad (1.9)$$

$$\Delta G_v = -\frac{4\pi r^3}{3\nu} k_B T \ln(S) \qquad (1.10)$$

$$\Delta G_s = 4\pi\sigma r^2 \tag{1.11}$$

The resulting equation cannot just be used to describe the freezing process of water but is a general term that can be applied to processes like the condensation from gas to aerosol particles. The second term is a surface-driven term ΔG_s and contributes positively to ΔG_{cl}, hindering the process from happening spontaneously. The first term is a volume-driven term ΔG_v. It is positive for $S > 1$, not allowing nucleation. However, the term is negative at supersaturation $S < 1$, such as supersaturated vapor or supercooled water. Generally, the volume term ΔG_v dominates for large radii r.
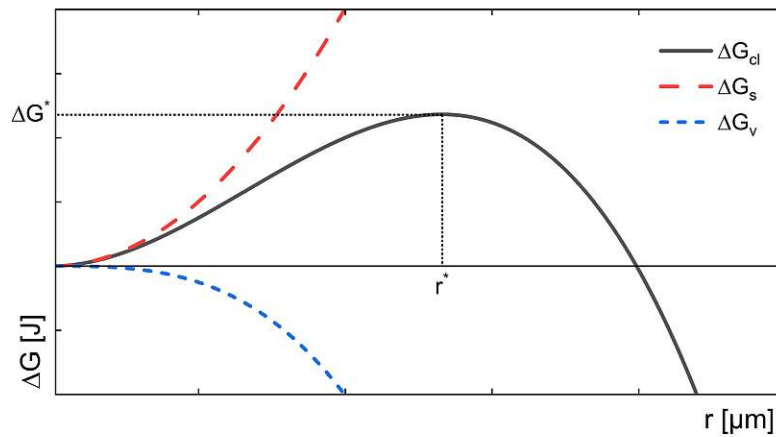
Figure 1.6: Schematic of the Gibbs free energy as a function of the cluster radius for homogeneous nucleation. The dotted lines mark the maximum of ΔG_{cl} corresponds to the critical cluster size r^*.

Figure 1.6 shows the dependence of the surface ΔG_s and the volume driven term ΔG_v of the Gibbs free energy of the cluster formation ΔG_{cl} on the cluster radius r. The resulting curve ΔG_{cl} increases at low radii due to surface-driven term, after a maximum ΔG^* the curve decreases and becomes negative, resulting in spontaneous cluster growth. The corresponding radius r^* is called the critical radius. Cluster below that size will dissipate again, but clusters reaching and overcoming this size are called embryo and will continue growing into an ice crystal. The critical radius can be derived from equation 1.9 as:

$$r^* = \frac{2\sigma\nu}{k_B T \ln(S)} \tag{1.12}$$

By inserting equation 1.12 into 1.9 the Gibbs free energy of the critical radius can be given as:

$$\Delta G^* = \frac{16\pi\sigma^3\nu^2}{3\left(k_B T \ln(S)\right)^2} \tag{1.13}$$

Both equations 1.13 and 1.12 emphasize the dependency of the critical radius size on the temperature T, the saturation S, and the surface tension σ. For example, the lower the temperature the smaller the critical cluster radius. At this point, it should

be noted that CNT has its weaknesses. It assumes the parameters such as density, saturation, and surface tension (interfacial energy) are the same for a macroscopic crystal and a nanoscopic cluster. However, for example, the interfacial energy is thought to be size-dependent [14].

For an investigation of the nucleation rate, we can start with thermodynamics by using a Boltzmann distribution to express the number of ice clusters N_{cl} per unit volume using ΔG^*. Where N_l expresses the number volume-based density of molecules in the liquid parent phase.

$$N_{cl} = N_l \exp\left(-\frac{\Delta G}{k_B T}\right) \tag{1.14}$$

From a kinetic perspective, the nucleation rate gives the number of water molecules, which can potentially be incorporated into the cluster. The following approach is a shortened version adapted from Ickes *et al.* [11] In order to estimate a nucleation rate the flux of available water molecules has to be accounted for. This flux can be expressed as a Boltzmann distribution since it can be understood as a diffusive flux Φ.

$$\Phi = \frac{k_B T}{h} \exp\left(-\frac{\Delta g^{\#}}{k_B T}\right) \tag{1.15}$$

Where h denotes Planck's constant and $\Delta g^{\#}$ the activation energy for the transfer of a water molecule across the water–ice boundary. Φ can be interpreted as a rate of collisions, a probability of bond breaking and molecular reorganization [15], or the frequency at which molecules overcome the activation energy barrier [16]. Using a second kinetic prefactor, the Zeldovich factor Z, the nucleation rate K at which water molecules are transferred into a cluster can be predicted by the following equation. Where n_S is the number of molecules in the jumping distance around the cluster surface and $4\pi r_{cl}^2$ is the cluster surface.

$$K = n_s 4\pi r_{cl}^2 Z \Phi \tag{1.16}$$

Combining the thermodynamic (equation 1.14) and kinetic (equation 1.16) approach a steady-state nucleation rate can be expressed

$$J_{hom} = K N_l \exp\left(-\frac{\Delta G}{k_B T}\right) \tag{1.17}$$

which can be summarized to

$$J_{hom} = C \exp\left(-\frac{\Delta g^{\#}}{k_B T}\right) \exp\left(-\frac{\Delta G}{k_B T}\right) \tag{1.18}$$

where the prefactors are combined to a single factor C and leaving two exponents, for the kinetic and thermodynamic approaches respectively.

To summarize, CNT describes homogeneous nucleation as a stochastic process where the probability of a cluster reaching and overcoming the critical size depends on the temperature, time, and volume of the parent phase. The lower the temperature, the smaller the critical size. Moreover, the probability of observing critical cluster formation, e.g. ice formation, increases the longer the observation time, hence more

collisions of molecules, and similar the larger the volume, hence more molecules colliding.

In order to connect the theory with experimental data we can consider a freezing experiments, where the freezing temperature of an ensamble of N_{total} droplets is observed. The number of frozen droplets at a certain temperature $n_{frozen}(T)$ can be observed, and a fraction of frozen droplets f_{ice} can be derived. According to CNT f_{ice} is dependent on the temperature T, the droplet volume V and the homogeneous freezing rate J_{hom} and can be written as:

$$f_{ice} = \frac{n_{frozen}}{N_{total}} = 1 - \exp\left(-J_{hom}Vt\right) \tag{1.19}$$

1.2.2 Heterogeneous nucleation

Until now the parent phase was pure and no other surface was introduced. The process where a foreign surface lowers the energy barrier ΔG^* is called heterogeneous nucleation. There are several different adaptions trying to describe heterogeneous nucleation. One of these approaches it the contact angle theory, which is a theory that can be used to describe heterogeneous nucleation. Therefore, a simplified Arrhenius approach of homogeneous nucleation $J_{hom,A}$ can be adapted using a correction factor $\varphi < 1$.

$$J_{hom,A} = A\exp\left(-\frac{\Delta G^*}{k_B T}\right) \tag{1.20}$$

$$J_{het,A} = A\exp\left(-\frac{\Delta G^*\varphi}{k_B T}\right) \tag{1.21}$$

with

$$\varphi = \frac{(2+m)(1-m)^2}{4} \tag{1.22}$$

m is the cosine of the contact angle given by the Young equation,

$$m = \cos\theta = \frac{\sigma_{SV} - \sigma_{SL}}{\sigma_{LV}} \tag{1.23}$$

The contact angle θ is defined with the surface tension between sloid-vapor σ_{SV}, solid-liquid σ_{SL}, and liquid-vapor σ_{LV}.

Nowadays most heterogeneous nucleation theories developed are more accurate but also more complex. Still, the basic idea of the contact angle theory, reducing the energy barrier is used in many theories. Moreover, Murray *et al.* [14] proposed the θ value as semi-empirical measure of how efficient an IN is, meaning the contact angle in these cases should not be thought of as actual angle but rather an easily comparable value.

1.3 Ice nucleation in an atmospheric context

1.3.1 Homogeneous ice nucleation

In the previous section, CNT was applied to the freezing process and gives a detailed description of why this happens. This section aims to connect the theory of CNT with environmental and experimental observations.

The phase diagram of water (see figure 1.4 A) shows the thermodynamic favored state of water at a certain temperature and pressure. For example the red dot at $1\,\mathrm{atm}$ and $0\,^\circ\mathrm{C}$ ($273.15\,\mathrm{K}$) shows an equilibrium between the ice and liquid water. Following the dotted line toward lower temperatures, ice is the favored state. The transition from liquid water to solid ice is called freezing. This phase transition, as mentioned in the previous paragraphs, requires nucleation in order to take place, as the transition is kinetically hindered. This energetic barrier allows the water to supercool, hence, remain in a liquid state although ice would be favored by thermodynamics. On the other hand, the opposing process, melting (solid to liquid), does not require nucleation and happens spontaneously. This results in a freeze-thaw hysteresis as indicated in figure 1.7 B.
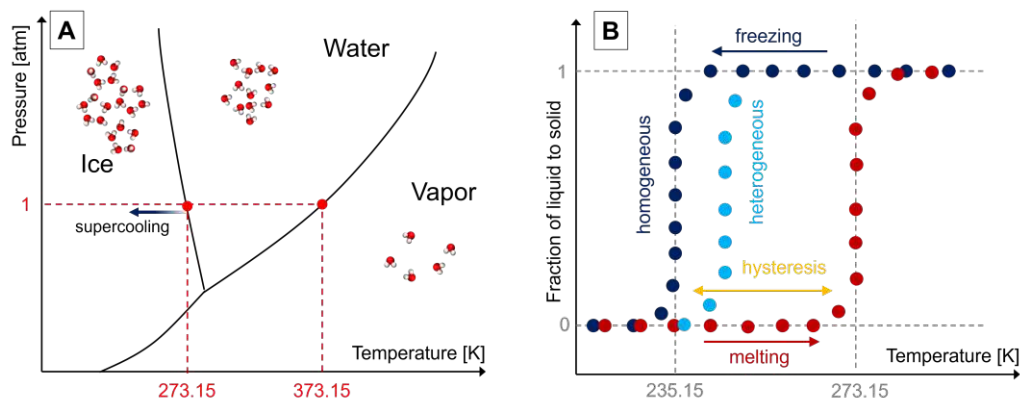
Figure 1.7: Schematic illustration of the phase diagram of water and the freeze-thaw-hysteresis of water droplets. Inspired by Bieber *et al.* [17].

The freeze-thaw hysteresis can be experimentally observed. When pure water droplets are cooled below their freezing point they will remain liquid. For example pure water droplets with a diameter of $10\,\mu\mathrm{m}$, a typical cloud sized droplet, can be supercooled to about $-38\,^\circ\mathrm{C}$ (ca. $235\,\mathrm{K}$) before freezing. However, melting is observed at the melting point. Observing multiple droplets allows to calculate a fraction of frozen droplets f_{ice} (or fraction of liquid droplets $f_{lq} = f_{ice}^{-1}$). Which can be used to determine the homogeneous nucleation rate as mentioned in equation 1.19.

In an atmospheric context, cloud droplets can reach temperatures below $-38\,^\circ\mathrm{C}$ and freeze. However, IN are often present inducing heterogeneous freezing at higher temperatures, as indicated in figure 1.7 B.

1.3.2 Heterogeneous ice nucleation

If a foreign substance is involved in nucleation, and therefore freezing process, it is referred to as heterogeneous ice nucleation. The ice nucleating particles (INPs) or ice

nucleating macromolecules (INMs) help by reducing the energy barrier a cluster needs to overcome for spontaneous and continuous crystal growth to occur. Although clouds could reach temperatures that allow homogeneous ice nucleation, many droplets freeze at higher temperatures. Hence, heterogeneous ice nucleation is an important process for cloud glaciation. Generally, ice formation in the atmosphere can occur via four different pathways [10, 15, 18]:

- **Immersion freezing:** Hereby the freezing is initiated from within a droplet. Hence, the IN is already immersed in the droplet. Upon cooling, freezing is initiated. This mode is independent of saturation. However, cloud immersion freezing requires the prior existence of cloud droplets and thus relative humidity near water saturation or highly effective CCN.

- **Condensation freezing:** Requires an IN is present in subsaturated air. When saturation approaches condensation on the IN surface takes place, before freezing. Interestingly, at water saturation, the critical radius for ice nucleation in liquid water is smaller than that for droplet nucleation. Hence, it is possible, that a stable ice germ forms within a water embryo. Hereby, the freezing stabilizes the water embryo. Since most IN can act as CCN at low supersaturation, this pathway can only occur in a narrow range of saturation values, before the IN acts as CCN prior to immersion freezing.

- **Contact freezing:** When a supercooled cloud droplet collides with an IN and freezing occurs it is referred to as contact freezing. This pathway requires a droplet and therefore takes place at saturation. A special pathway called "contact nucleation inside out" can take place below saturation [19]. Furthermore, if the colliding particle is another ice crystal it is called secondary ice formation.

- **Deposition freezing:** In this mode water vapor directly deposits as ice on the surface of the IN. The ambient air needs to be supersaturated concerning ice. Deposition nucleation takes place in cirrus clouds when vapor deposits onto IN like mineral dust. It is not yet clear if deposition nucleation truly exists. It may only appear like it, while in reality, a liquid phase forms in the pores of the IN before nucleation, like condensation freezing. However, deposition freezing does not seem to be important for the formation of mixed-phase clouds.

Figure 1.8 illustrates the different pathways for heterogeneous ice nucleation. Depending on altitude, and thereby temperature and saturation, different freezing modes may occur. For mixed-phase clouds, which often do not reach temperatures allowing homogeneous freezing, immersion freezing is the most dominant mode. Also, LIDAR observations showed that liquid droplets are required before ice crystals form in mixed-phase clouds [10].

Regardless of the mode of ice nucleation, two contradicting theories have been developed. Either heterogeneous ice nucleation is viewed as a deterministic or a stochastic process, the latter being derived from CNT. The latter model assumes a time-dependent process. Although the energy barrier is lowered by the IN the freezing process remains stochastic. Accordingly, multiple droplets with identical IN will always have the same probability of a cluster reaching the critical size per unit time by random fluctuations. Therefore, the sequence in which the droplets freeze is
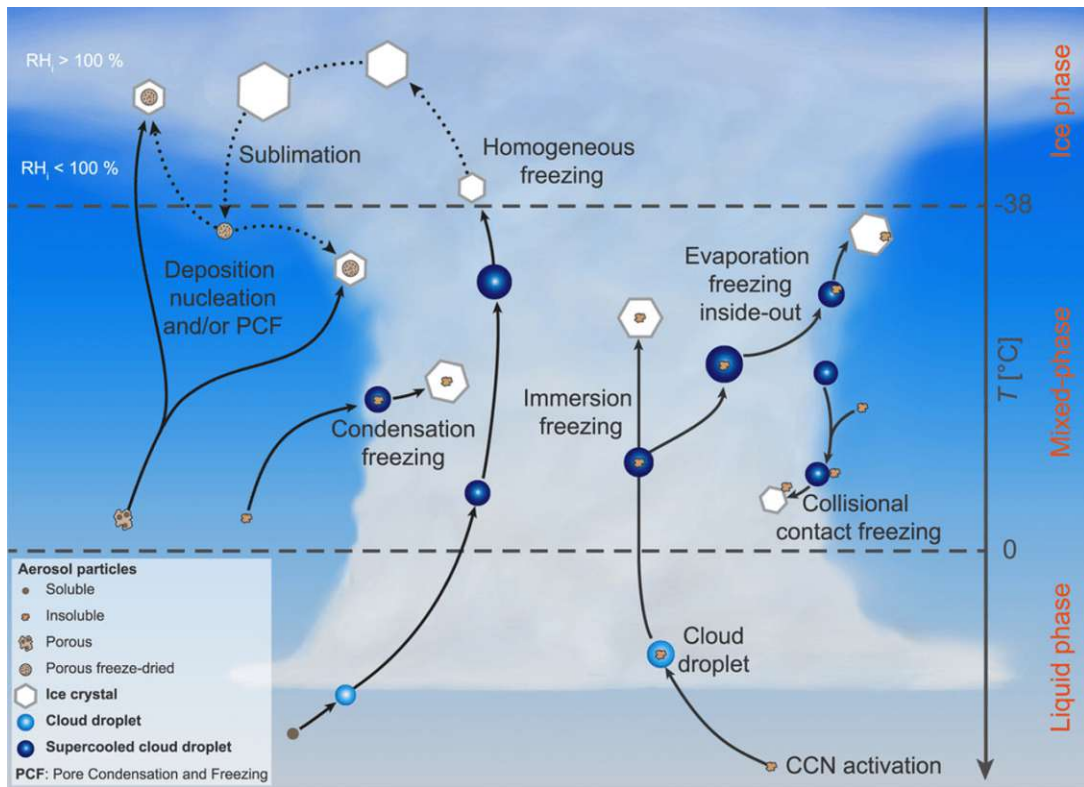
Figure 1.8: Different modes of heterogeneous ice nucleation. From Kanji *et al.* [20] ©American Meteorological Society. Used with permission.

random, at constant temperature and supersaturation. In addition, the fraction of frozen droplets f_{ice} will increase over time, if held at constant ambient conditions. [10]

On the other hand, the deterministic, singular, hypothesis assumes each IN has a certain temperature or supersaturation at which it will trigger the nucleation event. Hence, f_{ice} will not change with increasing time at constant ambient conditions. Additionally, in a repeated freezing experiment the sequence in which freezing is triggered will always be the same. [10]

Still, no clear evidence for either hypothesis has been reported. While some experimental studies, focusing on the time dependence, supported the stochastic model it has to be noted, that the immersion freezing experiments are much more sensitive to temperature, IN size, or contact angle compared to time. The process might very well have both a stochastic and a deterministic component, some studies attempt to introduce a hybrid model, e.g. Niedermeier *et al.* [21]. However, many experimental studies focusing on different IN, rather than the underlying process, use the cumulative nucleus concentration N_m for evaluation of their experiments, as is done in this work. N_m is calculated using a formula introduced by Vali [22], see equation 4.2 in section 4.3.1. It is based on f_{ice} and assumes the time component to be much less important, hence negligible.

1.3.3 Requirements for ice nuclei

Overall, the number of IN in the atmosphere concerning total particle concentration is rather low, as only one in about one million particles acts as IN [23, 24]. Although this number can vary depending on location. While the past chapters discussed theories of heterogeneous ice nucleation, the question of what makes a good IN remains.

Historically, Pruppacher & Klett [23] proposed several characteristic properties for effective IN based on the past empirical data: (i) water insolubility (ii) chemical bond similarity (e.g. hydroxyl groups), (iii) Crystallographic similarity to ice, and (iv) active sites (e.g. lattice mismatches, cracks, etc.).

Most of these criteria were fitted to the back then well-studied inorganic IN such as mineral dust or soot. It is thought that active sites can be responsible for the ice nucleating activity (INA), e.g. a hydrophilic site, lattice mismatch, or cracks. Since the number of these sites increases with surface area, larger IN are thought to be more efficient. [25]. However, there is some studies, suggesting, smaller particles are making up the majority of atmospheric IN [20, 26]. Chemical bond similarity, such as hydroxyl groups, have a high affinity to water and are therefore thought to be important features of IN. Which was shown by Kanji *et al.* [27], as the functionalization of these groups led to a reduction in INA. Furthermore, AgI and soot are known IN, their activity is mainly attributed to the similarities in the crystallographic structure to ice [28, 29].

However, there are numerous examples not fulfilling these criteria. For example, ammonium sulfate particles, among other water-soluble salts, act as efficient IN [30]. Furthermore, many biological IN do not fulfill the criteria. Examples are the cell membrane-bound protein *inaZ*, responsible for the INA of *P. syringae* [31]. In addition, the activity of many biological IN are correlated to various soluble macromolecules [32, 33]. More about these macromolecules will be discussed in section 1.5.

1.4 Ice nuclei in the Earth's atmosphere

1.4.1 Atmospheric aerosol particles

Aerosols, in an atmospheric context, describes dispersed particles in the gas phase. Aerosol particles can range from a few nanometers to several micrometers. They are classified into primary aerosol particles - directly emitted into the atmosphere - and secondary aerosol particles - formed in the atmosphere through physical and chemical processes. Primary aerosol particles are of natural (e.g. sea spray, mineral dust, spores, etc.) or anthropogenic origin (e.g. combustion, agriculture, etc.). Often they are also classified by their chemistry into inorganic (e.g. sea salt, soot, sulfate, etc.), organic (e.g. secondary organic aerosols (SOA), brown carbon from biomass burning) and biological aerosol particles, also bioaerosol particles (e.g. pollen, bacteria, spores, etc.).

aerosol particles have a huge impact on human life. They influence air quality and hence public health. At the same time, they also interfere with Earth's radiation budget and the formation and properties of clouds, two big factors in the Earth's climate. A direct effect is the influence on the radiation budget. aerosol particles can reflect incoming radiation and absorb outgoing radiation. Arguably more important is their impact on clouds. Some aerosol particles act as CCN or IN, and thus are important for cloud formation, phase state, and precipitation. Clouds also interfere with the radiation budget. Generally, they have a higher albedo than land or ocean, thus reflecting more incoming radiation and hence a cooling effect. A warming effect can be observed when longwave radiation is absorbed. These two effects are opposite and can compensate for each other. Moreover, high altitude ice clouds (*cirrus*) and low altitude clouds have a net warming effect. However, the overall net effect remains uncertain, since the balance is highly influenced by the ratio of liquid droplets to solid ice crystals [34, 35], the lower the ice content, the more radiation is reflected.

In addition, aerosol particles influence the formation of precipitation. More than half of precipitation initiates via the ice phase of mixed-phase clouds [36]. Both effects show the high impact IN concentrations can have on weather and the climate. Hence it is essential to understand the distribution of IN in the atmosphere.

1.4.2 Pollen and their ice nucleating abilities

Various aerosol particles can act as IN. Examples of important IN are mineral dust, soot, volcanic ash, sea salt, and biological IN. Mineral dust, emitted from deserts and arid regions, is often considered the most important IN in the atmosphere due to the relatively high abundance [14, 37]. At the same time biological IN, e.g. pollen, spores, and bacteria nucleate freezing at higher temperatures than most inorganic substances. Especially when it comes to atmospherically relevant IN, almost exclusively biological IN are active above $-15\,°C$, in the immersion freezing mode [33, 37, 38]. A prominent example of highly active biological IN is *P. syringae*, this bacteria has a freezing onset temperature of only $-2\,°C$ in the immersion freezing mode [39]. The fungi *Mortirella alpina* and *Fusarium avenaceum* show onset temperatures up to $-6\,°C$ and $-2\,°C$, respectively [33, 40]. Pollen is, compared to bacteria or fungi, active at lower temperatures at about $-15\,°C$ and lower [41]. Birch pollen showed the highest freezing onset temperatures among pollen, a simple reason why many studies have focused on them, especially the species *Betula pendula* [42–46].

Pollen is present in quite high numbers, especially during their respective blooming season. Still, their influence on atmospheric ice nucleation is highly debated. Pollen have sizes from 10 μm to 100 μm, making them rather large particles, thus it is assumed that they are not transported to high enough altitudes where they could initiate freezing in mixed-phase clouds. However, pollen can release sub pollen particles (SPPs) with size ranging from 0.25 μm to 4.5 μm [47–50]. These smaller particles can be transported further and higher than the larger pollen grains. In fact, SPPs were found to be active as CCN [51–53]. SPPs are emitted under relatively high humidity or in contact to rain through a process called pollen rupture. This is also correlated to the phenomenon of thunderstorm asthma, where increased numbers of asthma attacks are reported after thunderstorms, which is linked to pollen rupture and the thereby released allergens [54, 55].

A a study by Pummer *et al.* [32] reported that the INA of pollen is actually caused by macromolecules found in and on pollen, rather than the actual grain. Hence, they suggest the name ice nucleating macromolecule (INM). Furthermore, Burkart *et al.* [47] suggests that SPPs could act as potential carriers for the INMs since they found the SPPs of silver birch (*Betula pendula*) not to be ice nucleation active. INMs were actually found all over the surface of *Betula pendula* trees [56, 57]. This suggests the number of INMs potentially emitted from a single birch tree to be much higher and the emission to be at least partly independent from the pollination season. Recently we also reported, that not only the surface of birch but also of pine trees (*P. sylvestris*) can act as source for INMs [58]. Since birch and pine trees are widely found all over Eurasia, this poses them as massive reservoirs of INMs. While the INA of pollen and the respective INMs have been the subject of several lab studies [32, 46, 56, 57, 59–61], the actual emission of the INMs remains unknown.

Generally, the emission flux of primary biological aerosol particles (PBAP) and specifically pollen is quite challenging. Global PBAP emissions are estimated to be around 78 Tg/yr [62], where pollen make up to 44 Tg/yr [62]. Another estimate for pollen emission is about 84.5 Tg/yr, showing just how uncertain these estimates are. For comparison, global mineral dust emissions are about 5000 Tg/yr, which explains why biological IN and pollen (INMs) are often neglected in climate models. On the other hand, we can use this argument for the need for better measurement techniques for PBAP, pollen, and biological IN. Pollen monitoring, for example, is still mostly done offline using Hirst traps, with a time resolution of days. More recently online pollen monitoring is tested with various fluorescence-based techniques [63–65]. Another promising method is to use drones to measure the emission fluxes of biological IN [17].

The motivation of this work is a different approach, if we understand the chemistry of biological IN, we can specifically monitor related trace substances and measure them. Therefore, the first step is to characterize pollen INMs.

1.5 Macromolecules responsible for biological ice nucleation activity

Plants growing in cold environments developed various mechanisms to survive freezing temperatures, usually lethal to a single cell. Various biological molecules, e.g. protein, glycoproteins, and polysaccharides can interact with ice formation. On the one hand ice nucleation active substances, induce freezing usually outside the cell. On the other

hand anti-freeze substances (such as anti-freeze proteins (AFPs)) inhibit ice growth. Both with involved in important processes to prevent frost damage [46]. Hence, it is not surprising that the suspendable macromolecules responsible for the ice nucleation ability of birch pollen were also found all over the trees tissue [56, 57]. Much smaller organisms, such as bacteria or fungi, have developed similar strategies. In contrast to complex organisms (e.g. plants), cell membrane-bound proteins were identified to be responsible for the INA of various bacteria [66].

The ice nucleating ability of *P. syringae*, nucleating at $-2\,°C$ [39], was traced to the gene *inaZ* decoding for a cell membrane-bound protein [31]. Since then various other genes were found (*inaA*, *inaE*, *inaQ*, etc.) [67–69]. Pandey *et al.* [70] suggested an alternating hydrophilic and hydrophobic pattern allows water ordering, thus promoting ice nucleation. However, Lukas *et al.* [71] showed, the simple water ordering is insufficient to explain the INA. The INA of fungi is suggested to be also caused by proteins [33, 72], however, there is no clear evidence yet. Similarly, pollen INMs have not yet been clearly classified. Fungi and pollen are much more complex organisms than bacteria, thus making it harder to pinpoint the INMs.

Figure 1.9 (c) illustrates the main components of a birch pollen grain. The grain is protected by a robust and chemically inert sporopollenin layer, the exine. Underneath is the intine, a cellulose-pectin layer. The inside is filled with cytoplasmic material, including polysaccharides (e.g. starch) proteins, and lipids. In all images of figure 1.9 the pores are visible, which is where the pollen rupture, as described in section 1.4.2.
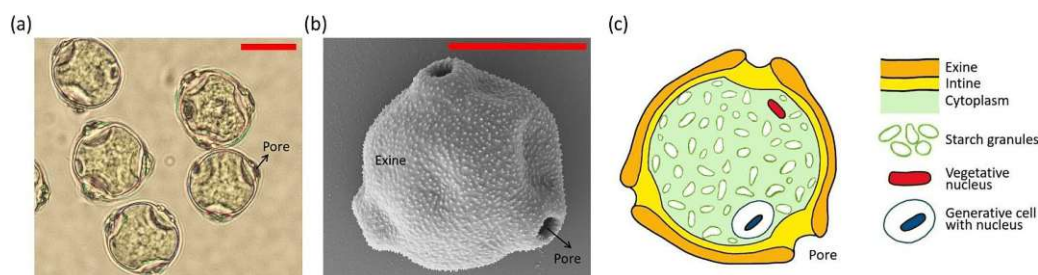

Figure 1.9: Different views of *Betula pendula* grains. (a) Light microscope image (scale bar $10\,μm$). (b) Electron microscope image (scale bar $10\,μm$). (c) Schematic illustration of the main components of a birch pollen grain. Adapted from Burkart *et al.* [47].

INMs from birch pollen are usually studied using birch pollen washing water (BPWW). These simple aqueous extracts can be tested for INA and chemically analyzed. The INMs were able to nucleate freezing at an onset temperature of around $-18\,°C$. Some studies suggest the birch INMs to consist of polysaccharides [32, 46, 59]. The main arguments for polysaccharides are high temperature stability, of up to $187\,°C$, and various chemical (e.g. guanidinium chloride for denaturation) and enzymatic experiments (e.g. papain for digestion of proteins), aimed to destroy or digest proteins and lipids, which only showed minor influence on the INA [32, 46, 59]. Further supported by IR and Raman spectra showing high quantities of hydroxyl groups, associated with the sugar monomers. In contrast, other studies suggest proteins to be at least involved [47, 73, 74], sometimes contradicting arguments for polysaccharide. For example, Tong *et al.* [73] observed a diminished INA after proteinaceous components were extracted from the birch pollen extract. Also, Burkart *et al.* [47] argue for proteinaceous involvement, supported by fluorescence measurements and a decrease in

16

INA after treatment with subtilisin A and urea. Where urea interferes with protein folding and subtilisin A is used for the digestion of proteins. Burkart *et al.* [47] suggest, that glycoproteins could be the answer, which explains polysaccharide and proteinaceous signals.

While the chemistry of the INMs is highly debated, the size of >100 kDa was reported consistently [32, 46, 47], similar to bacterial IN sizes which range from 120 kDa to 180 kDa [75, 76].

Interestingly, Dreischmeier *et al.* [46] additionally reported, that birch pollen show antifreeze activity in addition to the INA. They suggest hydroxyl groups could be responsible for both activities, in accordance with Davies [77]. This is supported by experiments using borate, which forms esters and effectively shields the hydroxyl groups. Finally, they suggest the major difference between the substances seems to be the size, where the antifreeze ability was only visible at sizes well below 100 kDa. Size seems to be quite important for pollen INMs and their properties. The INMs with sizes >100 kDa are big, this could be achieved by aggregation or agglomeration of various subunits, possibly proteinaceous and polysaccharides. While aggregates are rather smaller clusters of molecules held together by chemical bonds, agglomerates are comparatively loosely connected subunits, which can be dissembled rather easily.

Chapter 2

Research objective and motivation

Advances in atmospheric research lead to a better understanding of Earth's climate and its influencing factors. Weather forecasts and climate models steadily increase in their accuracy. However, while increasing computing power and advances in mathematics can help models, they will only be as good as the data they are based on. According to the IPCC, the physical understanding of aerosol-cloud interactions is rather limited. One important category of aerosol particles are IN. Although they occur in comparatively low numbers, their influence on the climate by altering cloud properties, such as albedo or lifetime, is substantial. Several aerosol particles act as IN, the most efficient IN are of biological origin. An incomplete understanding of these biogenic aerosol particles, as well as their emission and transport, pose a big gap. As weather extremes and climate change approach relentlessly this gap is in urgent need to be closed.

This work focuses on birch pollen and biogenic aerosol particles, which have been identified as efficient IN about five decades ago [78]. Only recently macromolecules were identified as IN rather than the pollen themselves [32]. These were not only found on pollen but all over the tree's tissues [56], thus they are present in extraordinary amounts. Meanwhile, lots of other biological material has been found as efficient IN such as bacteria, fungi, algae, or lichen [33, 40, 79]. Besides these important discoveries, the exact working mechanism of biogenic IN has not yet been found. Moreover, accurate measurements of emission fluxes and advances in the understanding of the atmospheric impact of these IN depend on the elucidation of the chemical composition and structure of these IN.

Climate change is one of the major problems of the generation Z and is the root for the motivation of this work. **This thesis aims to combine several advanced analytical methods with novel purification methods to take a step towards the chemical understanding of INMs from birch pollen.** The findings can further help the complete chemical and structural elucidation. Which will in turn be a major step towards understanding the nucleation mechanism of birch pollen INMs. This mechanism might very well be similar to those of many other biogenic IN and further increase our understanding of the impact on clouds and the climate.

Chapter 3

Methods

This chapter aims to provide the essential theoretical background to understand the most important aspects of this thesis. Not-well-established methods like the measurement of ice nucleation will be described in detail. More established methods will be described briefly focusing on the underlying principles.

3.1 Freezing assays

Freezing assays are used to study the influence of potential ice nuclei (IN) on the freezing temperature of water. The term freezing assay is a collective term for a wide variety of measurement setups. This chapter aims to give the background to understand what freezing assays are. Moreover, examples of setups will be given and in addition advantages and disadvantages of different setups will be discussed.

The general idea of a freezing assay is to cool an aqueous sample until freezing. Samples containing potential IN are prepared and their freezing behavior is observed. If the sample contains IN heterogeneous freezing occurs otherwise homogeneous freezing will take place. The metric used to distinguish between these processes is the freezing temperature. The freezing point of pure water marks the threshold for homogeneous freezing. Higher freezing temperatures are caused by an IN and are therefore heterogeneous freezing. Naturally, in a sample containing multiple IN, only the INA at the highest temperature can be seen in one measurement, due to the sample being frozen. Therefore no additional freezing can be triggered.

Numerous freezing assays have been developed to study ice nucleation. Most freezing assays, especially for the study of atmospheric ice nucleation, are based on immersion freezing (see section 1.2.2) since it is the dominant heterogeneous freezing process in clouds. Immersion freezing assays have high variations in working principles. They include methods like a single-particle levitation method [80], a continuous-flow diffusion chambers [81], and droplet freezing assays (DFAs). This chapter will mainly focus on DFAs like the Twin-plate ice nucleation assay "TINA" [82] which was mainly used for this thesis. Miller *et al.* [83] gives a good overview of DFAs, containing a table listing most assays developed between 2000 and the date of publication. As the name suggests DFAs are methods based on sample droplets being cooled down until freezing. These assays consist of three main components: droplet generation, cooling mechanism, and detection.

Droplet generation implementations include emulsifying aqueous droplets in hydrophobic solvents, pipetting, piezo-driven droplet generation, microfluidics, and cavities on a chip. This is a crucial component since it determines the number and volume of droplets. Higher droplet numbers lead to higher certainties and higher sample throughput. The latter is also true for higher droplet volumes but comes at a price since homogeneous freezing is volume-dependent. Droplet volumes range from picoliter-sized droplets (e.g. emulsions and microfluidics) to microliter-sized droplets (pipetting). Droplet numbers vary from a few tens to over ten thousand. These droplets are then placed on plates coated with hydrophobic substances, in well-plates as used for polymerase chain reaction (PCR), and directly or indirectly (e.g. a glass slide) on the cooling surface later used for the experiment.

Over time, also various cooling mechanisms have been developed, ranging from cold stages - typically made of one or more Peltier elements - to cooling blocks and liquid cooling baths. The implementations set the ranges for working temperature and range of cooling rate. The slower the cooling the longer the measurement time but in general the more accurate the freezing point determination. Further, it can restrict detection types.

Lastly, the freezing can be detected manually by visual inspection, automated optically using software, pyroelectric, and by infrared thermal detection. The optical detection is possible due to the different optical densities of water and ice, which in most cases lets ice appear darker than liquid water. Further, it can be observed by a volume change and therefore a sudden change in appearance. On the other side, the latent heat which is freed during a freezing event is used for the pyroelectric and infrared detection methods. The latter can be implemented using an IR camera observing the droplets. They can also be directly placed on a pyroelectric detector which can then detect the heat flow.

All different implementations all have their advantages and disadvantages, which have to be weighed depending on the sample of interest. For example, micro-liter assays allow for a high sample throughput but show high homogeneous freezing temperatures, limiting the detection of IN with low freezing onset temperatures.

In the following paragraphs, the setups which were used for this thesis will be briefly explained.

Twin-plate ice nucleation assay - TINA

The Twin-plate ice nucleation assay TINA was developed by Dr. Anna T. Kunert in the group of Dr. J. Fröhlich (Max Planck Institute for Chemistry) and is published under Kunert *et al.* [82]. Small microliter-sized droplets are pipetted into two 384-well plates (as used for PCR). These plates are then placed on aluminum cooling blocks and cooled by a thermostat through a complex flow system allowing highly accurate cooling rates and temperatures. Two infrared cameras mounted above each 384-well plate detect the latent heat freed during droplet freezing. The evaluation is automated.

Vienna optical droplet crystallization analyzer - VODCA

This picoliter assay was developed by Dr. B. Pummer and P. Baloh in the group of Prof. H. Grothe (Technical University Vienna) and is published by Pummer *et al.* [32]. This assay uses sample droplets emulsified in paraffin oil on top of a glass slide.

The slide is placed on a Peltier element which is then used to cool down the droplets in a closed cell to avoid evaporation. The freezing of the droplets is recorded via a microscope camera. The recorded file is then used to manually detect the freezing events by observing a change in the optical density leading to a darker appearance of the droplet.
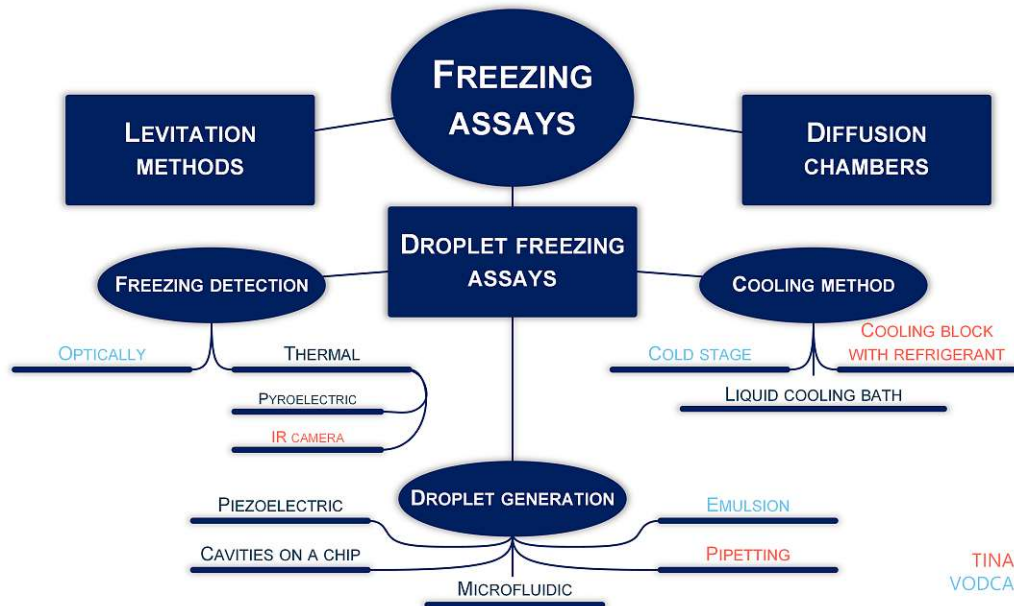

Figure 3.1: Overview of freezing assay setup possibilities with special focus on droplet freezing assays like the ones used for this thesis. Droplet freezing assays are made up of three major components: droplet generation, cooling method, and freezing detection. For each, a variety of actual realization possibilities are given under a categorical name. By color, the setups used in this thesis are marked - Twin-plate ice nucleation assay "TINA" and Vienna optical droplet crystallization analyzer "VODCA". This graph does not include all possible setup types due to the wide variety.

3.2   Ice affinity purification

Ice affinity purification (IAP) is a simple yet effective method used to purify ice-affine molecules, like ice-binding proteins (IBPs). Raymond & Fritsen [84] first used IAP to purify ice active substances from cyanobacteria, green algae, and moss crude extracts. Since then multiple reports of IAP have come up [85–89]. In most reports, IAP was used to purify antifreeze proteins (AFPs) until Lukas *et al.* [71] used IAP to purify ice nucleating proteins from a *P. syringae* sample.

All IAP methods work on the same basic principle and use the affinity of ice-binding molecules (IBMs) to ice. The idea is that if the ice grows slow enough, the engulfment of impurities is low due to the minimized supercooling [87]. Therefore, IAP setups take crude sample and cause slow ice growth by cooling the sample, and thereby IBMs tend to be embedded into the growing ice layer. Afterward, the IBM enriched ice layer is separated from the remaining liquid fraction and melted to gain a purified sample.

Multiple different IAP methods have been developed since Raymond & Fritsen [84], which can semi-purify samples containing ice-active substances by partly freezing an sample and centrifuging it, to partition ice and liquid fractions. Kuiper *et al.* [90] used a cold finger immersed in a crude protein extract. By constantly stirring the crude extract higher purification rates were achieved. Later, Marshall *et al.* [88] developed rotary ice-shell purification, where purification is achieved by growing an ice layer on the interior surface of a rotating round bottom flask. This method was then also used by Lukas *et al.* [71] to purify IN from *P. syringae.* Adar *et al.* [87] developed the falling water ice affinity purification (FWIP), where a commercially available ice machine is used to perform IAP. It allows IAP to be performed from half to hundreds of liters of IBM solution, posing a key advantage compared to other methods.

In this work, a setup developed by Dr. Ralph Schwidetzky (Max Planck Institute for Polymer Research), was used [91]. Similar to FWIP it allows an IAP on a large scale. At the heart of the setup is a cooled metal slide, where the crude sample slowly flows down into a sample reservoir, from there the sample is pumped to the top of the slide again. Figure 3.2 shows a schematic illustration of the setup.
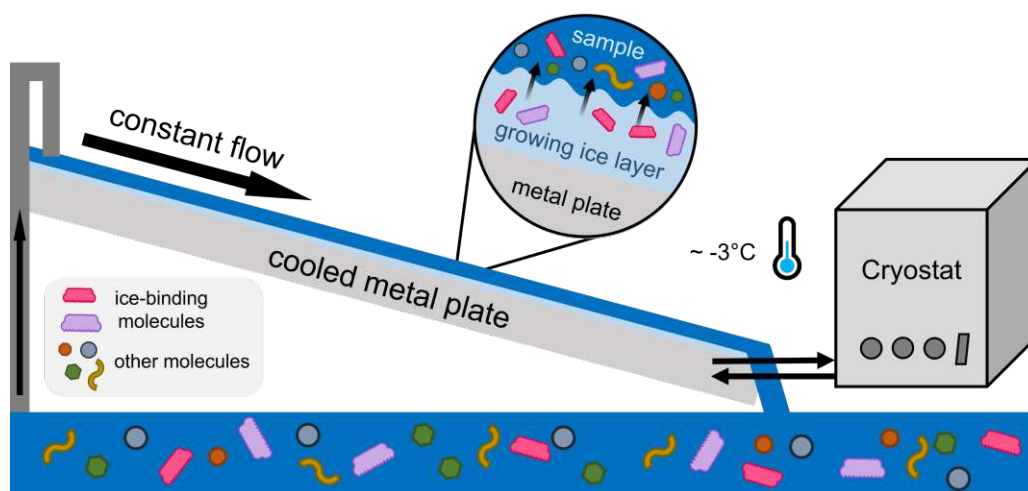

Figure 3.2: Schematic illustration of ice affinity purification. The sample is constantly pumped down a cooled metal plate, where an ice layer starts to form. Ice-binding molecules bind to ice, while other molecules are washed down by the constant flow. Figure adapted from Ralph Schwidetzky, Max Planck Institute for Polymer Research [91].

3.3 Optical spectroscopy

Spectroscopic methods are among the oldest analytical methods in chemistry. They are based on the interaction between electromagnetic radiation (EM), or photons, and matter. Energy is exchanged between matter and the EM field. When EM energy is absorbed by matter, atoms and molecules are brought into excited quantum states. This energy is absorbed in the form of atomic, molecular, or electronic motions. On the other hand, this energy can also be emitted by excited atoms or molecules relaxing them to a lower or the ground quantum state. Out of these simple interactions, numerous spectroscopic measurement techniques were developed. UV/VIS-, infrared (IR), and

circular dichroism(CD)-spectroscopy are all absorption based, while fluorescence-spectroscopy is an emission-based technique. [92–94]

The energy E_{sum} of a particle (e.g. atom or molecule) is the sum of several different contributions: rotational E_{rot}, vibrational E_{vib} and electronic E_{el} energy. According to quantum mechanics all energies are quantized, therefore the sum must also be quantized. [92–94]

$$E_{sum} = E_{el} + E_{vib} + E_{rot}$$
$$E_{el} >> E_{vib} >> E_{rot}$$

$$(3.1)$$

Atoms and molecules can absorb or emit EM radiation and transition between states. Since these states are quantized this leads to a finite number of transitions for an atom or molecule, which builds the basis for spectroscopy. The energy of the absorbed or emitted EM radiation has to be equal to the energy difference ΔE of the energy states of a certain transition, figure 3.3 shows schematically shows electronic, vibrational, and rotational transitions for a diatomic molecule. In spectroscopy this energy is mostly given as wavelength, frequency or wavenumber, which is connected as described in equation 3.2, where h is Planck's constant ($h =6.626 \times 10^{-34}\,\mathrm{J\,s^{-1}}$), ν is the frequency, c is the speed of light ($c =2.998 \times 10^{8}\,\mathrm{m\,s^{-1}}$), λ is the wavelength, and $\tilde{\nu}$ is the wavenumber. [92–94]

$$\Delta E = h\nu = h\frac{c}{\lambda} = hc\tilde{\nu}$$

$$(3.2)$$

Quantization limits the number of transitions in atoms and molecules, furthermore selection rules limit the number of allowed transitions, due to symmetry. Selection rules can be mathematically derived. The limited number of transitions allows the link between certain transitions to chemical properties such as elemental or molecular information. [92–94]

3.3.1 Infrared spectroscopy

IR describes EM radiation with wavelengths spanning from about $780\,\mathrm{nm}$ to $1\,\mathrm{mm}$ (equal to $12\,800\,\mathrm{cm^{-1}}$ to $10\,\mathrm{cm^{-1}}$). The energy of IR radiation is in the range of vibrational transitions in molecules and intermolecular vibrations. This is used for IR spectroscopy, hereby absorption of IR radiation is measured and linked to molecular information, bond strength, and bond length. IR spectroscopy is a versatile method that can be used for numerous purposes, e.g. catalytic activity, structure elucidation of organic molecules, and much more. In this work, it was used to understand the chemical composition of a complex biological sample.

IR spectroscopy can be used to identify carbohydrates and even quantify them in aqueous solutions like fruit juices. The identification of a certain carbohydrate or sugar becomes increasingly complicated the bigger the molecule. The method can also be used to analyze proteins and peptides, also commonly found in biological samples. To some extent, it can be used to determine enzymatic activities or the secondary structure of proteins. In general, proteins show quite distinctive signals, the amide bands (I, II, III) which are used to find and differentiate proteins in samples. [95]
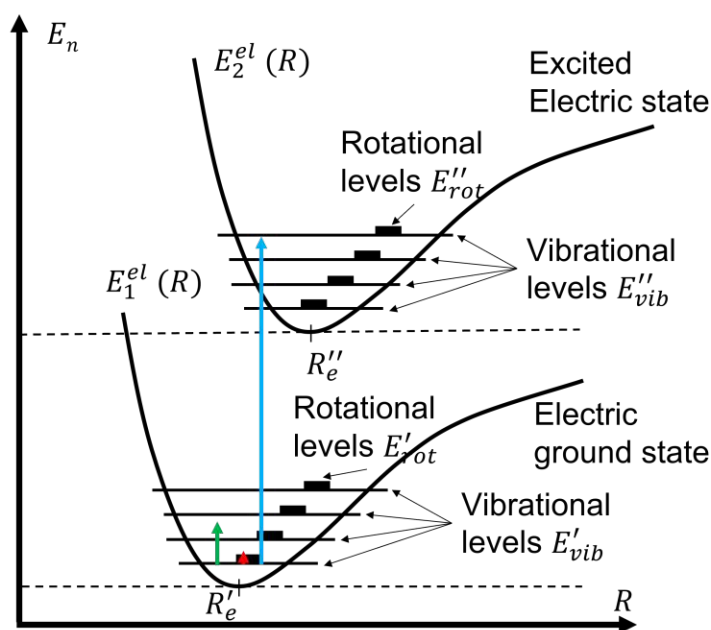
Figure 3.3: Schematic illustration of the energy levels of a diatomic molecule consisting of rotational, vibrational, and electronic states. Arrows mark electronic (blue), vibrational (green) and rotational (red) excitations. Adapted from Demtröder [92].

3.3.2 Protein quantification using spectroscopic methods

Absorption spectroscopy in the UV/VIS range (UV 100 nm to 380 nm and VIS 380 nm to 780 nm) is also a versatile and well-established method with numerous applications. In this work absorption spectroscopy was used for protein quantification. Various staining techniques such as the Biuret, Lowry, BCA, or Bradford assay were developed. All of these are assays stain proteins using different chemical reactions or by binding to side chains of proteins. The specific absorption of the reagent at a certain wavelength is then used to quantify the amount of protein in the sample. Not all methods require reagents, by simply measuring the absorption of a purified protein sample at 280 nm, the protein content can be estimated, due to the absorption from aromatic amino acids. [96]

All these methods have their strengths and weaknesses due to inferences. In general, the purer a sample the easier and more robust the result.

Bradford assay The Bradford assay is one of the most used protein assay since it is quite robust. The assay uses Coomassie brilliant blue G-250 dye (see figure 3.4) which exists in three different forms: anionic, neutral, and cationic, which are all absorbing at different wavelength ranges. Under acidic conditions and the presence of proteins, the dye unspecifically binds to cationic and hydrophobic side chains of proteins. This leads to the shift of the maximum absorption of the dye to about 595 nm, which can then be used to quantify protein concentrations with the help of protein standards of defined concentrations. [96, 97]
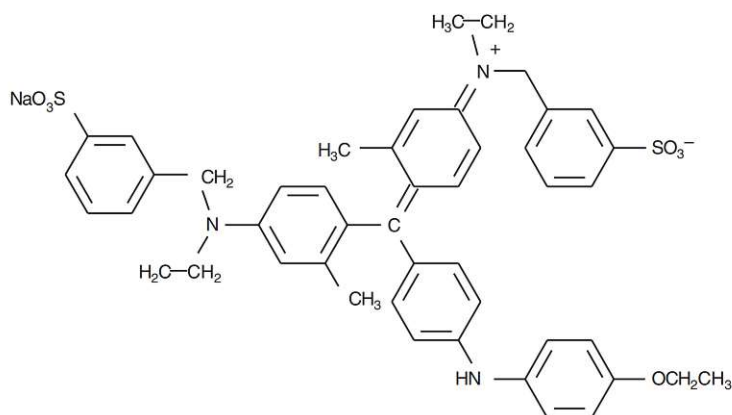
Figure 3.4: Bradford assay reagent: Coomassie brilliant blue G-250 as sulfonate. Adapted from Kurreck *et al.* [96].

3.3.3 Circular dichroism spectroscopy

Circular dichroism (CD) can also be used for absorption spectroscopy. EM radiation can be polarized, this refers to the direction of the electric field vector in respect to the direction of propagation. For example, if radiation is linear polarized the direction of the electric field vector remains the same. Moreover, radiation can be right or left circularly polarized, figure 3.5. Interestingly, linear polarization is actually a result of a constant ratio of right and left circularly polarized radiation over time. [96, 98]

Optically active molecules, e.g. chiral molecules, can interact with polarized EM radiation and can influence the polarization plane. This is famously used for polarimetry, a simple method to determine sugar concentrations. Thereby the polarization plane is changed, due to the different speeds of the left and right circularly polarized light. This difference leads to a phase shift to each other and appears as a shift of the polarization plane. [96, 98]

CD spectroscopy on the other hand takes advantage of the different absorption of left and right circularly polarized light. This method is widely used to determine the secondary structures of proteins because this method is particularly sensitive to changes in secondary structures of proteins. [96, 98]

3.3.4 Fluorescence spectroscopy

Fluorescence describes a phenomenon, where EM radiation is absorbed by matter and re-emitted with a longer wavelength, hence lower energy, which is known as the Stokes shift. Figure 3.6 demonstrates this principle in a so-called Jablonski diagram. An electron transitions to a higher electronic state (from S_0 to S_1 or S_2) by absorbing a photon $h\nu_A$. Thereafter energy conversions can take place, e.g. thermal or vibrational. When the electron relaxes to the ground state a photon can be emitted $h\nu_F$, which is observed as fluorescence. A similar phenomenon is phosphorescence, where the electron in the excited state undergoes intersystem crossing into a triplet T_1 state. The relaxation from a triplet to a singlet state is not allowed, due to symmetry selection
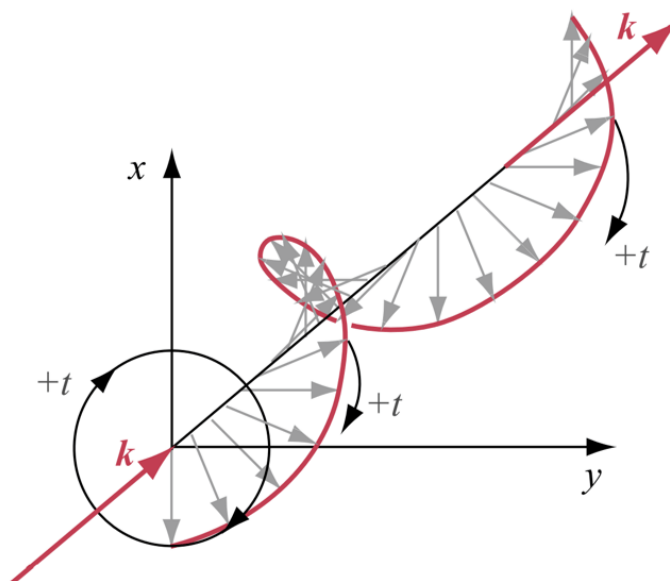
Figure 3.5: Schematic illustration of left-hand circularly polarized electromagnetic radiation. The grey arrows indicate the direction of the electric field vector, perpendicular to k. Adapted from Hertel & Schulz [93].

rules, but can still happen. The lifetime of this state is much longer resulting in a much longer duration where emission takes place, typical for phosphorescence. [99]

Photoluminescence spectroscopy is a mainly based on fluorescence. Thereby excitation wavelength can be varied as well as the observed emission wavelength. Typically one is fixed and the other is scanned through a certain range. When varying both emission and excitation wavelength an excitation-emission map is measured. The technique can be used for the analysis of biological samples, due to the intrinsic fluorescence property of most biological molecules. [99]
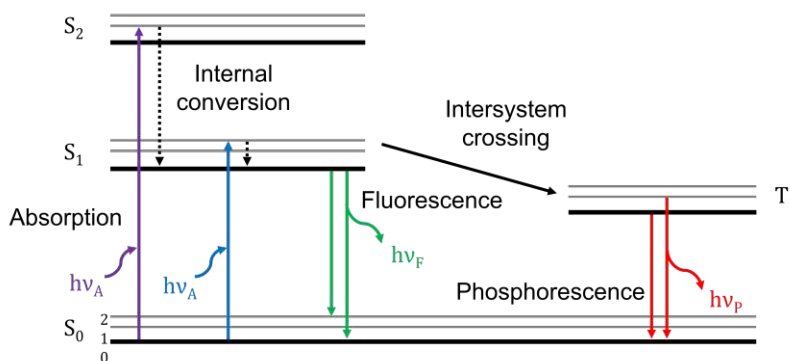

Figure 3.6: Schematic illustration the principle of fluorescence. A Jablonski diagram of electrons excited by absorbing photons and emitting photons while relaxation.

3.4   Liquid chromatography

Liquid chromatography is an analytical technique used to separate, characterize and purify various compounds from a mixture. The separation is based on the interaction of an analyte within a mobile phase (e.g. a solvent) and a stationary phase. The interactions can be based on e.g. polarity, size, and charge. Liquid chromatography is mostly used as high-performance liquid chromatography (HPLC). Thereby high pressures are applied increasing time and separation efficiency.
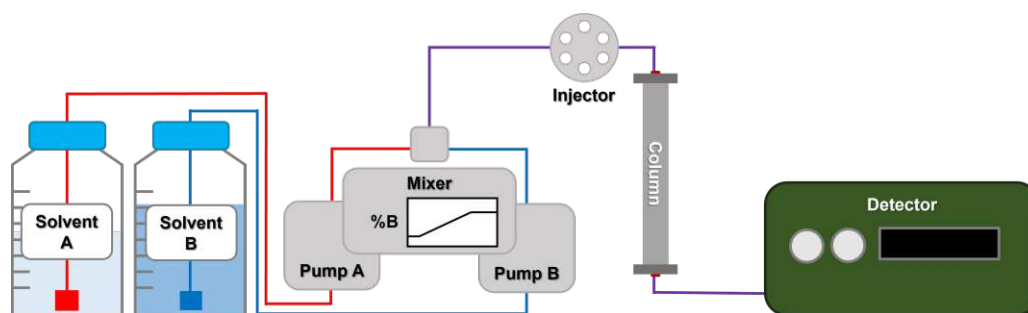

Figure 3.7: Schematic illustration of an HPLC setup.

The separation of the sample compounds starts with the injection into the HPLC system. The sample is brought into the mobile phase which is pumped through a column containing the stationary phase. The mobile phase can be alternated during separation to achieve better separation or decrease measurement times. After separation, the compounds can be detected in various ways depending on the sample. The simplest detection methods are based on absorption at a specific wavelength or conductivity. Furthermore, HPLC can be coupled with mass spectrometry (HPLC-MS) or inductively-coupled plasma (ICP) methods. This makes HPLC a versatile method for various applications. Figure 3.7 shows a schematic illustration of a HPLC setup.

Size exclusion chromatography   Size exclusion chromatography (SEC) is a special form of chromatography where analytes are separated by particle size. The stationary phase usually is a highly porous silica-based material. Smaller analytes can enter the pores and therefore have a longer retention time in the column. For biological samples, SEC can be used for desalting, as the ions are much smaller than the biological molecules. Moreover, from SEC a distribution of molecular weights can be estimated since the size correlates with the mass. [96]

3.5   Gel electrophoresis

Similar to chromatography electrophoresis is a separation technique. In contrast to chromatography, gel electrophoresis separates analytes by their mobility in an electric field. Electric mobility depends on the charge, size, and numerous other factors. For bioanalytics, the most commonly used methods are capillary electrophoresis and SDS Page. [96, 97]

SDS-Page   SDS-Page is a qualitative method used to separate proteins by size. The name is a composition of the two main characteristics of the method. Sodium dodecyl

sulfate (SDS) is an anionic detergent. It covers the intrinsic charges of proteins resulting in micelles with constant charge per mass ratios. In addition, the samples are heat denatured at 95 °C and can be treated with thiol reagents, breaking apart disulfide bonds. This treatment leads to stretched amino acid chains with a constant mass to size ratio. Thus, proteins are ideally exclusively separated by size. The second part of the name Page refers to the matrix where the separation takes place, a polyacrylamide gel. These gels are widely used due to their mechanical stability and colorless appearance. Polyacrylamide gels are relatively simple to prepare and the porosity can easily be adjusted in the preparation process, according to the sample needs. [96, 97]

SDS-Page is a simple and handy method. However, the method is limited when it comes to glycoproteins. As they tend to bind far fewer SDS, migration is extremely slow and separation is limited. Although, sample preparation with Tris-borate-EDTA buffer charges the sugar moieties, accelerating the migration velocity. [97]

3.6 Dynamic light scattering

Dynamic light scattering (DLS), also known as photon correlation spectroscopy, is a method used among others to determine the size of particles in suspension. When a suspension of particles in Brownian motion is excited by a monochromatic laser beam (usually in the VIS range, e.g. 650 nm), the incoming light shifts to a smaller wavelength after scattering, also known as a Doppler shift. DLS takes advantage of this shift, as it provides information about the size, distribution, shape, and structure of the particles. Generally, light scattered by large particles propagates slowly with a comparatively larger Doppler shift, while scattered by small particles it fluctuates quickly with a smaller Doppler shift. However, the Doppler shifts are quite small posing a challenge for instrumentation. [100, 101]

In DLS the hydrodynamic diameter D_H of a particle is measured. Therefore the velocity of the particle under Brownian motion is observed which is defined by its translational diffusion coefficient D_t. For spherical particles the hydrodynamic diameter D_H can be derived from the diffusion coefficient Using the Stokes-Einstein equation 3.3, where k_B is the Boltzmann constant ($k_B = 1.380 \times 10^{-23}$ J K^{-1}), T is the temperature, and η is the solvent viscosity. [100, 101]

$$D_H = \frac{k_B T}{3 \pi \eta D} \tag{3.3}$$

The measured D_H represents the diameter of a hypothetical hard sphere having the same diffusion coefficient as the examined particle. This poses a strong limitation of the method if the structural information of the particle measured is unknown. Using different equations for D_t, e.g. for rod-like particles, this problem can be minimized. Still, D_H is not solely affected by the shape, but also by surface texture and structure. Furthermore, the surface charge can influence D_H in presence of electrolytes forming a layer around the particle, increasing its size [100, 101]. Uncertainties in these measurements for standardized samples lie in the range of 2 %, however, for more complex samples such as biological molecules uncertainties may quite well be in the range of 10 % if not higher.

Chapter 4

Experimental part

4.1 Sample preparation

4.1.1 *Betula pendula* pollen

The birch pollen investigated were of the species *Betula pendula* (silver birch) (Pharmallerga CZ, Czech Republic). They were harvested from two different growing regions, the Czech Republic (A) and Slovakia (B), figure 4.1 shows the approximate locations of the trees.

According to the distributor, the pollen were harvested by hand in march 2020 (pollen A) and march 2019 (pollen B). Each batch contained pollen from five different trees growing at varying growing sites (forest, park, roadside). After collection the pollen were dried at a temperature $\leq 26\,^{\circ}\text{C}$ for 7 days. The pollen were air and shake sifted in multiple steps to remove foreign material. They were dried again to a moisture content of $5.3\,\%$.
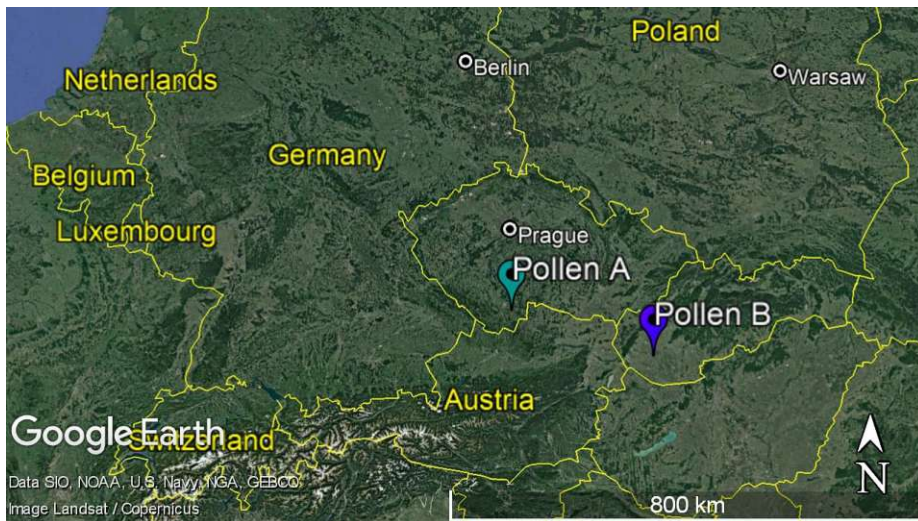

Figure 4.1: Map of approximate birch tree locations of which the pollen were collected. Image adapted from Google Earth©, https://earth.google.com/, last access: 05th July 2022.

4.1.2 Birch pollen washing water

Prior to the analysis of the INMs from birch pollen, they were extracted with water to prepare birch pollen washing water (BPWW). This was the base sample for all experiments. The procedure to prepare BPWW is the following:

1. 50 mg birch pollen per mL BPWW were weighed.

2. The according amount of ultra-high quality (UHQ) water was added cautiously to prevent dust formation.

3. While occasionally shaken the pollen were extracted for 6 h.

4. Subsequently the suspension was centrifuged for 5 min at romm temperature (RT) with 3500 rpm.

5. Thereafter the supernatant was filtered through a 0.2 µm syringe filter.

The prepared BPWW was then stored at $-20\,^{\circ}\mathrm{C}$ if not immediately used. BPWW was prepared in batches, the batches were numbered successively.
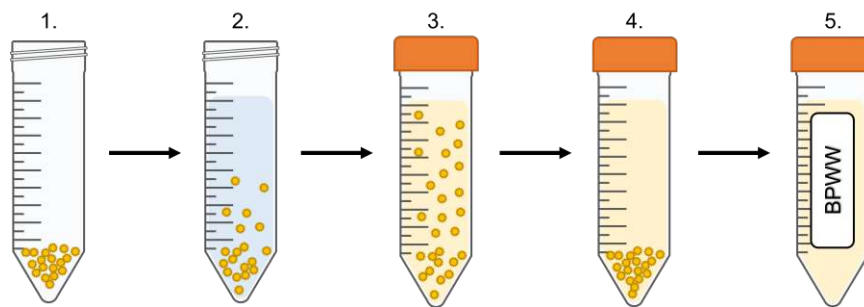

Figure 4.2: Schematic illustration of the preparation of birch pollen washing water (BPWW).

4.1.3 Freeze drying of samples

In order to allow a direct comparison of INM concentration before and after IAP, some samples were freeze dried. The remaining dry powder was then re-suspended in a defined amount of water in order to get a standardized concentration of freeze-dry-residue. Therefore, the liquid sample was frozen at $-80\,^{\circ}\mathrm{C}$ for at least 15 min in a tube or plastic box prior to freeze drying (Alpha 2-4 LDplus, Christ, Germany). Freeze drying duration varied between a few hours and days depending on the amount of sample. The dry residue was then weighed and suspended in a defined amount of UHQ water. If not otherwise noted, the standard "after freeze drying"-concentration was $7.2\,\mathrm{mg\,mL^{-1}}$.

4.1.4 UHQ water

UHQ water was used for the preparation of BPWW and for the ice nucleation background measurements. The procedure for preparation is as follows:

1. Pure water was obtained from a MilliQ water purification system.

2. The water was autoclaved for 20 min at 120 °C.

3. After cooling it was filtered three times through a 0.1 μm sterile PES (polyethersulfone) vacuum filter.

4. The obtained UHQ water was stored at RT until used.

4.2 Experiments

To characterize the birch INMs, various treatments were performed with the pollen and BPWW before the ice nucleation measurements. Moreover, sample aliquots were analyzed with further methods described below.

4.2.1 Pollen milling

An aliquot of pollen was milled using a swing mill (MM400, RETSCH, Germany). Two aliquots were milled dry and one wet.

Dry-milling procedure The pollen were transferred to a steel container. Prior to each milling step, the container was cooled with liquid nitrogen (at −196 °C) for approximately 2 min, to increase the porosity of the pollen and prevent frictional heat from altering the sample. The pollen were milled three times for 60 s at a swing rate of 25 Hz. The milled pollen were transferred out of the container and BPWW was prepared.

Wet-milling procedure The pollen and about 5 mL UHQ were added to the steel container. The sample was milled three times for 3 min at 25 Hz. The sample was not cooled at any time. Afterwards the wet mixture was quantitatively transferred to a falcon and the steel container was washed three times. From the mixture, BPWW was prepared.

Figure 4.3: (a) Swing mill (MM400, RETSCH) with a steel container, containing pollen, left and a counter weight right. (b) Pollen after milling in the steel container.

4.2.2 Filtrations

BPWW was filtered to gain information about the size and to purify the INMs. Therefore, centrifugal molecular weight cut-off (MWCO) filters of 10, 30, 50, 100 and

300 kDa (Vivaspin©15R/20, Sartorius) were used. The filter material is polyethersulfone (PES) or Hydrosat©(HS) in the case of the 10 kDa filter, which is a twin PES membrane.

Procedure

1. About 10 mL samples were pipetted to the filter.

2. The filter was centrifuged at 3000 xg (*times gravitational force*), relative centrifugal force) for 30 min at 4 °C.

3. The filtrate was transferred to a falcon.

4. 10 mL water was step-wise added to the supernatant, to wash it off the membrane. It was then transferred to another falcon.

Before sample filtration, the filter was washed five times with UHQ water. Therefore, 10 mL water was pipetted to the filter and it was centrifuged (Megafuge 40R, Thermo Scientific, Germany) at 3000 xg at 4 °C for 5 min.The filters were immediately used or stored at 4 °C, with UHQ water to keep the membrane wet.

4.2.3 Ice affinity purification

Ice affinity purification (IAP) was used to purify and concentrate INMs from BPWW. As the name suggests this method uses the high affinity of ice-binding molecules (IBMs) to ice surfaces to separate them from other molecules. Thereby IBMs are incorporated in a slowly forming ice layer. For background information see section 3.2.

Setup   Figure 3.2, shows a schematic illustration of the used setup, built by Ralph Schwidetzky (Max Planck Institute for Polymer Research) [91]. Sample (BPWW) is constantly pumped over a metal plate cooled by a cryostat to a high subzero temperature. As the sample slowly flows down an ice layer forms, where IBMs tend to stick and other molecules are washed down by the constant flow.

Procedure   About 800 mL BPWW were prepared and diluted with about 2075 mL UHQ water to reach a sufficient volume for IAP. The sample was transferred to the collecting container and the pump started to pump the sample to the top of the plate. The cryostat was started and the temperature was set to −3.5 °C to cool the plate. The plate was not pre-cooled to avoid immediate freezing of the first droplets. After 1 h, the pump was stopped. The resulting ice layer was then freeze-dried (see section 4.1.3).

4.2.4 Heat treatment

BPWW was heat treated, to test the heat stability of the INMs. Therefore an aliquot of BPWW (between 750 µL to 1500 µL) was pipetted to a microtube, which was sealed with parafilm. BPWW aliquots were incubated at 40 °C, 78 °C and 98 °C for 1 h, and one at 98 °C for 24 h and 100 rpm on a Thermomixer (Accublock™Mini, Labnet International Inc. USA). After the specified duration, the samples were cooled to RT and analyzed the same day.

4.3   Measurements

4.3.1   Ice nucleation measurements

For this thesis, two different droplet-freezing assays were used. First, the twin-plate ice nucleation assay (TINA) and second the Vienna optical droplet crystallization analyzer (VODCA). While VODCA uses picoliter droplets allowing the measurement of cloud-sized droplets, TINA uses microliter-sized droplets allowing a higher sample throughput, the difference in analyzed volume therefore is about six orders of magnitude. Compared to the background given in section 3.1 this section will focus on the setups used and give detailed measurement procedures.

Twin-plate ice nucleation assay - TINA

Setup   The idea of the twin-plate ice nucleation assay (TINA) is simple, two 384-well plates (as used for PCR) each containing sample droplets are gradually cooled down until the droplets freeze [82]. A schematic illustration of TINA is shown in figure 4.4. The core of TINA are two aluminum cooling blocks shaped to hold the 384-well plates. The plates can be loaded with sample droplets between $1\,\mu L$ to $20\,\mu L$. The loaded well plates are put onto the cooling blocks and cooled down using a silicon-based coolant tempered by an external refrigeration bath circulator (CC-508 with Pilot ONE, Peter Huber Kältemaschinenbau AG, Germany) and various temperature sensors allowing precise temperature control. The cooling rate is adjustable and temperature ranges from $-1\,°C$ to $-55\,°C$. For freezing detection, an IR camera (Seek Thermal Compact XR, Seek Thermal Inc., USA) is mounted above each plate recording the cooling process.
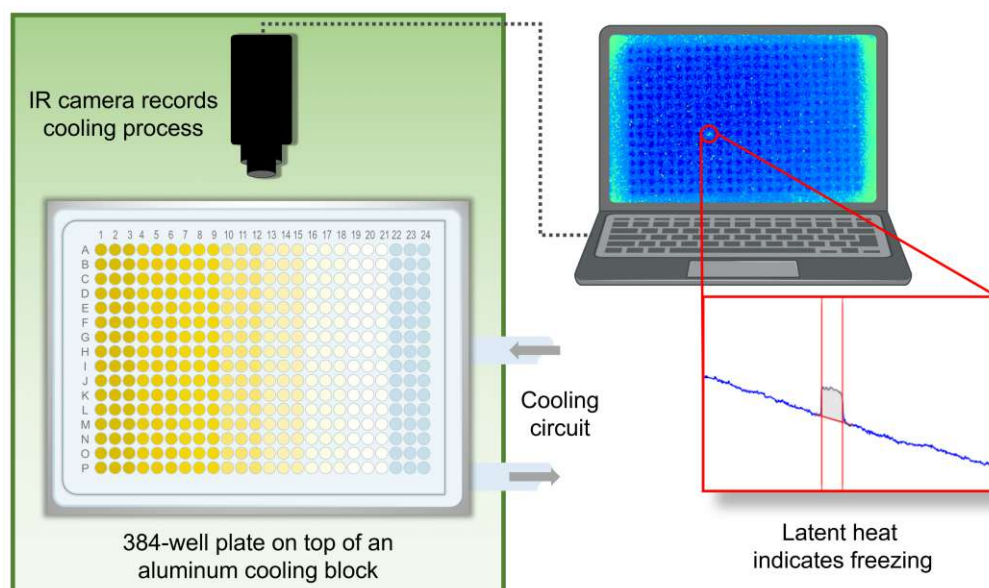

Figure 4.4: Schematic illustration of the twin-plate ice nucleation assay (TINA), shown with only one 384-well plate. Each well contains a sample droplet. The plates sit on top of a cooling block. An infrared (IR) camera above records the cooling process. A spike in the signal, caused by the latent heat freed during freezing, marks the freezing of a droplet.

Procedure Typically in a single run, eight different samples or dilutions of a sample are measured with 96 droplets each.

- In each well of the two 384-well plates a droplet is pipetted by a pipetting robot. The default droplet volume is $3\,\mu$L.

- The plates are placed onto the aluminum cooling blocks and the camera position is adjusted.

- Afterwards, the cooling and the recordings are started. The standard procedure is a cooling rate of $1\,\mathrm{K\,min^{-1}}$ starting at $0\,^\circ$C and ending at $-35\,^\circ$C.

Freezing detection The recordings are analyzed using a self-developed software from the MPIC. Therefore specific pixel regions are binned to build the signal for each well. The IR signal steadily decreases due to the decreasing temperature. The freezing of a droplet can be detected by observing a spike in the signal due to the freed latent heat (see figure 4.4. Thereby a table is created listing the number of freezing events per $0.1\,^\circ$C bin.

Vienna optical droplet crystallization analyzer - VODCA

Setup The basic principle of VODCA is cooling picoliter-sized sample droplets stabilized in an oil emulsion which is cooled down until the droplets freeze [32]. VODCA is made up of two main parts: a cryo-cell used to cool the emulsion and a microscope-mounted camera (MDC320 microQ L3CMOS, Hengtech, Germany) to observe it. A schematic illustration can be seen in Figure 4.5.

The heart of the cryo-cell is a cold stage consisting of a Peltier element (High Tech Peltier-element, Quick-cool QC-31-1.4-3.7M, Qick-OHM Küpper and Co, Germany) and a cooling circuit. Due to the Peltier effect, the Peltier element heats up on one side and cools down on the other when an electric current is applied. By adjusting the current the cooling rate can be adjusted between $0.1\,\mathrm{K/min}$ to $10\,\mathrm{K/min}$, this is done by a programmable power supply (DP831 A LXI, Rigol, USA) using the software LabView©. The sample-oil-emulsion is placed on a glass slide on top of the Peltier element. A thermo-couple (PCE-T312 typ K, PCE, Germany) also mounted to the top of the element using thermo-glue (Wärmeleitkleber, WLK DK10, Fischer Elektronik, Germany) is used to measure the temperature. The excess heat on the warm side is removed from the system by a cooling circuit made up of a copper block flushed with iced water. The cryo-cell itself is a closed cell that can be flushed with nitrogen prior to measurement to ensure an inert environment. A window in the cell lid allows the observation of the sample, to avoid condensation a steady air stream is applied above it.

The cryo-cell is mounted on a microscope (Olympus BX, Japan). Through an objective, a camera records the sample during measurement.

Procedure

- A sample-oil-emulsion is prepared by pipetting $2\,\mu$L of the sample and $4\,\mu$L oil mixture (90 wt% paraffin and 10 wt%) to a glass slide. It is then mixed using a pipette tip until it appears cloudy.
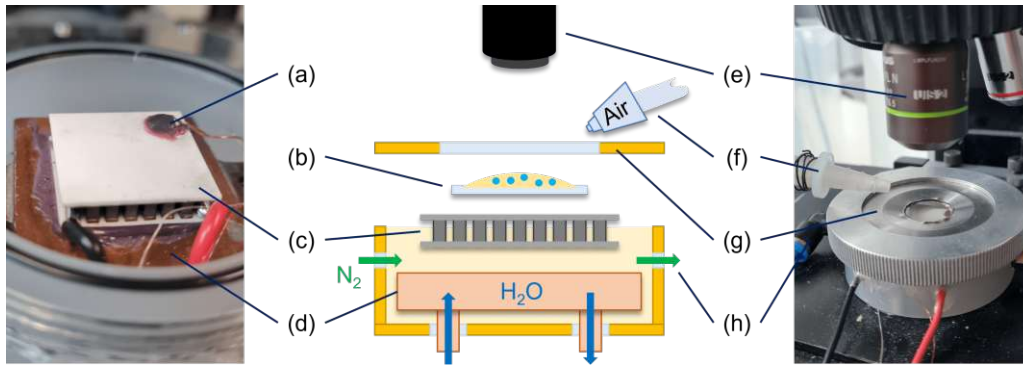
Figure 4.5: The Vienna Optical Droplet Crystallization Analyzer (VODCA). In the middle is a schematic illustration of the cryo-cell made up of (a) a thermo-couple, (b) a glass slide with the oil-sample emulsion, (c) a Peltier element, (d) a copper block flushed with iced water, (e) a camera connected to a microscope, (f) an air nozzle to avoid condensation on the lid (g), (h) a nitrogen line to flush the cell. On the right is a picture of the cryo-cell, and on the left from the cold stage within.

- The glass slide is placed in the cryo-cell onto the Peltier element. The cryo-cell is closed and flushed with dry nitrogen for about 5 min. Meanwhile, the camera focus is set to a region of interest and the steady air stream is turned on.

- The cooling rate is set to $10\,\mathrm{K\,min^{-1}}$ and the starting temperature is set to $0\,°\mathrm{C}$ and the end temperature to $-40\,°\mathrm{C}$. The recording and cooling are started using Labview©. Additionally, photos can be taken as well.

- After the first measurement the sample can be moved to a different region of interest by moving the microscope stage and cooled down again to increase the number of droplets measured. Usually, a single sample is measured four times.

Freezing detection Labview© is used to record the samples, it automatically overlays the current temperature in the video by using the data from the thermo-couple. The videos or photos are afterwards observed and freezing events are manually counted, they can be detected since frozen droplets appear darker due to the increased optical density (see figure 4.6). Only droplets with diameters between $15\,\mathrm{\mu m}$ to $40\,\mathrm{\mu m}$ are counted. Thereby a table is created with the number of freezing events per temperature which is then further evaluated as explained in Section 4.3.1.

Data evaluation

After a measurement run with TINA or VODCA we get information about the freezing of each sample droplet. This data is converted to a list with number of freezing events per $0.1\,°\mathrm{C}$ bin. From this, we can then calculate the fraction of frozen droplets $f_{ice}(T)$, as shown in equation 4.1, where s is the number of freezing events within a temperature bin and a is the total number of evaluated droplets.

$$f_{ice}(T) = \frac{\sum_{i=0}^{j} s}{a} \qquad 0 \leq j \leq a \tag{4.1}$$
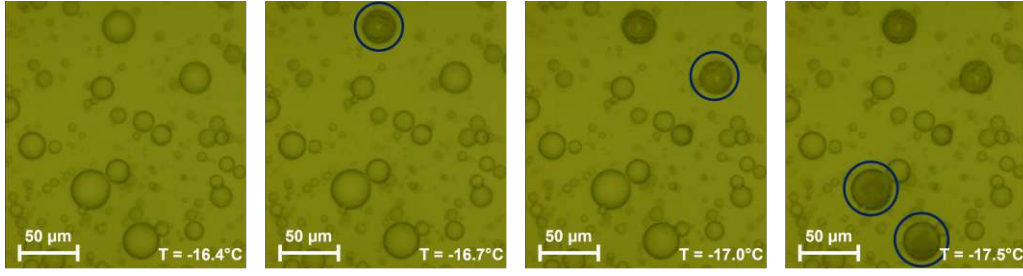
Figure 4.6: Evaluation of measurement data from VODCA. Frozen droplets appear darker than liquid droplets. Photos or a video of a measurement are evaluated manually and freezing events are detected.

A freezing curve is the plot of $f_{ice}(T)$ against T, an example is given in 4.7. It contains qualitative information, for example, the freezing onset temperature T_{on} - the temperature at which the first droplet froze.

To get quantitative information the cumulative ice nucleation number concentration $N_m(T)$ can be calculated using equation 4.2, adopted from [82]. It is based on an equation from Vali [22] which assumes ice nucleation as a time-independent process (see section 1.3.2). Thereby V_{wash} is the volume of the initial suspension, V_{drop} is the average droplet volume (TINA: 3 µL, VODCA: 8.2 pL), d is the dilution factor, and m is the mass of the particles in the initial suspension (e.g. birch pollen).

$$N_m(T) = -\ln\left(1 - \frac{\sum_{i=0}^{j} s}{a}\right) \cdot \frac{V_{wash}}{V_{drop}} \cdot \frac{d}{m} \tag{4.2}$$

In figure 4.7 the $f_{ice}(T)$ and the N_m plots are given for a BPWW dilution series measured with TINA. We can see three different freezing onset temperatures at about $-6\,°C$, $-15\,°C$ and $-18\,°C$ marked by a knee in the N_m plot highlighted by the colored regions. Another important aspect to note is f_{ice} curves show purely qualitative information and dilutions are necessary to extract quantitative information from INA measurements. This is because a sample that freezes purely heterogeneously, e.g. dilution 10^{-6} in the f_{ice} graph of figure 4.7 which freezes between $-16\,°C$ to $-18\,°C$, can be seen as a signal overflow similar to as is it occurs for example at optical emission spectroscopy. The dilutions allow the extraction of quantitative information because, samples are diluted until no INA is visible anymore, from the dilution factors quantitative information is gained.

Error analysis The Gaussian error propagation is used to calculate the uncertainty for each measurement. The error for $N_m(T)$ is calculated as seen in equation 4.3 and are illustrated by error bars in the N_m plots. Data points with uncertainties higher than $100\,\%$ are excluded.

$$\delta N_m(T) = \sqrt{\left(\frac{\frac{V_{wash}}{V_{drop}} \cdot \frac{d}{m}}{1 - \frac{\sum_{i=0}^{j} s}{a}} \cdot \frac{\sqrt{\sum_{i=0}^{j} s}}{a}\right)^2} \tag{4.3}$$
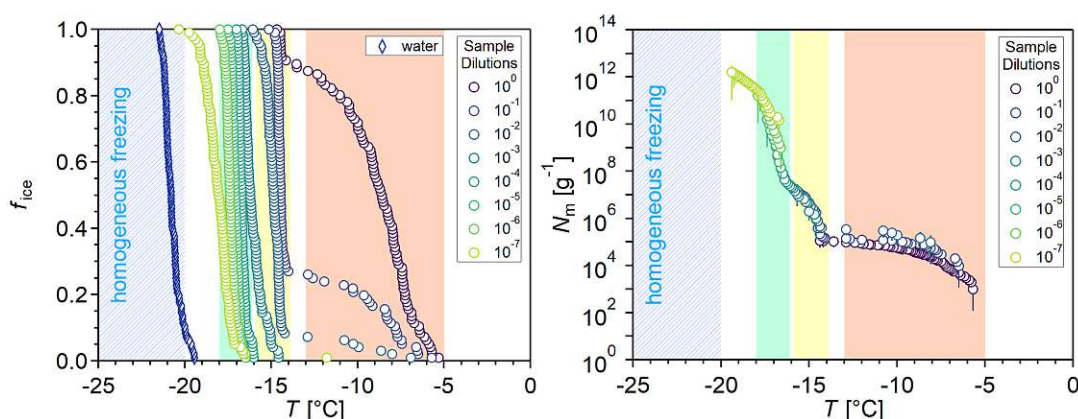
Figure 4.7: Example of an $f_{ice}(T)$ and an $N_m(T)$ plot of BPWW measured using TINA. Three different freezing onset temperatures can be recognized by a knee in the N_m plot at about $-6\,°C$, $-15\,°C$ and $-18\,°C$ - also marked by the colored regions. While both plots show qualitative information, the N_m plot additionally contains quantitative information.

4.3.2   Size exclusion chromatography

For size exclusion chromatography (SEC) a HPLC 1260 Infinity II system (Agilent Technologies) with a PSS Proteema Micro column (250 x 4.6 mm i.g., 3 μm, volume 4.15 mL; Agilent Technologies) was used. The HPLC system consisted of a binary pump, an autosampler with a thermostat, a column thermostat, and a photodiode array detector. As mobile phase a 150 mM NaH_2PO_4, adjusted to ph 7 with 10 M $NaOH_{(aq)}$ was used. The system was operated with a constant flow rate of 0.3 mL/min. Absorbance at 220, 280, 357 and 425 nm was measured. For optimal signal and column loading, each sample was injected multiple times with varying injection volumes, starting with the lowest volume. Before the first measurement, the system flushed with pure mobile phase for at least 30 min. Between different samples a blank run was carried out. The procedure was adapted from Liu *et al.* [102].

4.3.3   Gelelectrophoresis

Sodium dodecyl sulfate polyacrylamide gel electrophoresis (SDS-Page) was performed to analyze BPWW. Three different gels were used: 4–20 % Mini-Protean©TGX, Stain-free™gel, 10 % Mini-Protean©TGX™gel, and a self casted 15 % gel. The first gel type did not need dying, while Coomassie blue dying was used for the latter two gel types. The gels were run using a PowerPac™Basic (Bio-Rad Laboratories, USA) and analyzed with an imaging system (Western Workflow, Bio-Rad Laboratories, USA). The procedure was adapted from Ziegler *et al.* [103].

Procedure

1. The gel was mounted inside a gel chamber, that was filled with Tris/Glycine/SDS-buffer.

   (a) The buffer was prepared by diluting 1 part 10x Tris/Glycine/SDS-buffer (Bio-Rad Laboratories, USA) with 9 parts water.

2. The samples were prepared and loaded onto the gel.

   (a) One part sample was mixed with one part 2x Laemmli sample buffer - containing 65.8 mM Tris-HCl (pH 6.8, Carl Roth), 26.3 % glycerol (v/v, Carl Roth), 2.1 % SDS (Carl Roth), 0.02 % bromophenol blue (Sigma Aldrich) - and about 0.2 vol% β-mercaptoethanol.

   (b) The mixture was incubated for 5 min at 98 °C (or at RT for the heat-treated samples).

   (c) After incubation the samples were immediately loaded onto the gel.

3. The gel was usually run at a constant voltage of 150 V.

4. Afterwards the gels were dyed (if necessary) and imaged.

4.3.4 Bradford assay

For protein quantification, a Quick Start Bradford Protein Assay (Bio-Rad Laboratories, USA) was performed according to the manufacturer's standard test tube protocol. A series of seven high-purity BSA standards over 25–1500 µg mL^{-1} was prepared for calibration (see table 4.1). UHQ water was used as blank. The samples needed no preparation. 5 µL of standards, blank, and samples were pipetted into separate wells of a 96-well plate, before 250 µL QuickStart Bradford Dye 1x (Bio-Rad Laboratories, USA) were added. After 5 min of incubation, the absorbance at 595 nm was measured using a photometer (Multiskan GO, Thermo Scientific, Germany). The procedure was adapted from Reinmuth-Selzle *et al.* [104].

Vial	V(H$_2$O) µL	V(BSA Standard) µL	c(BSA) µg mL^{-1}
A (stock)	0	300 (stock)	2000
B	125	375 (stock)	1500
C	325	325 (stock)	1000
D	175	175 (B)	750
E	325	325 (C)	500
F	325	325 (E)	250
G	325	325 (F)	125
H	400	100 (G)	25
I	400	0	0 (blank)

Table 4.1: Dilution scheme of the standard preparation (B-H) for the Bradford assay.

4.3.5 Circular dichroism spectroscopy

Circular dichroism (CD) spectra were recorded on a J-1500 CD-Spectrometer (Jasco, USA). Samples were measured in a 350 µL quartz cuvette (Hellma Analytics, Germany), with a path length of 1 mm. At RT samples spectra from 190 nm to 250 nm with a scan rate of 5 nm min^{-1} were recorded with a data pitch of 0.2 nm and data integration time of 2 s. Samples were diluted about 1:5 (1 part sample to 5 parts overall) with

water. Water was measured as background. Spectra were background subtracted and processed using the Spectra Manager Analysis program from JASCO. The procedure was adapted from Schwidetzky *et al.* [105].

4.3.6 Infrared spectroscopy

Fourier-transform-infrared (FTIR) spectroscopic measurements were conducted with a Vertex 80v (Bruker, Germany) containing a liquid nitrogen-cooled MCT (mercury cadmium telluride) detector. The spectrometer operates at a pressure of 2 mbar. The internal reflection element (IRE) in the attenuated total reflection (ATR) cell (GladiATR™, Pike Technologies, USA) was a diamond crystal. OPUS 6.5 software (Bruker, Germany) was used for evaluation and instrument control. The crystal surface was flushed with dry nitrogen. For each measurement, 128 scans were accumulated at a resolution of $0.5 \, cm^{-1}$. For measurement, the IRE was coated with a thin layer of soluble sample components. Therefore, about 30 µL samples were pipetted onto the IRE and dried using a steady stream of dry nitrogen. Post-processing of the spectra included normalization and removal of the IRE signal between $1900 \, cm^{-1}$ to $2350 \, cm^{-1}$. The procedure was adapted from Felgitsch *et al.* [56].

4.3.7 Fluorescence spectroscopy

Fluorescence excitation-emission maps (FEEM) were recorded using an FSP920 spectrometer (Edinburgh Instruments, UK) with a Xe900 xenon arc lamp (450 W) and an S900 single photon photomultiplier. Samples were measured in a quartz glass cuvette (500 µL, Hellma Quartz (Suprasil©, Germany). The measurement parameters include: dwell time of 0.25 s, monochromator step widths of 5 nm (excitation and emission), first and second order excitation was prevented using an offset of 10 nm and a 295 nm low-pass filter. Water was measured as blank and before the measurements, a background correction scan was performed. The procedure was adapted from Burkart *et al.* [47].

4.3.8 Dynamic light scattering

Dynamic light scattering (DLS) was measured using a Submicron Particle Sizer Nicomp 380 (Entegris, USA) with a fixed scattering angle of 90° and a laser wavelength of $\lambda = 632.8 \, nm$. DLS measurements were performed on undiluted samples. The procedure was adapted from Schwidetzky *et al.* [106, 107].

Chapter 5

Results and discussion

5.1   Background measurements of INA setups

Before and during sample measurements background measurements were carried out. For this purpose UHQ water (for preparation details see section 4.1.4) was measured with TINA and VODCA.

Figure 5.1 shows background measurements with TINA and VODCA. The background measurements with TINA show freezing temperatures of $-20\,°\mathrm{C}$ with some single droplets starting to freeze as high as $-6\,°\mathrm{C}$. Except for sample 4 (light blue), no more than $4\,\%$ of droplets froze before $-20\,°\mathrm{C}$, for sample 4 it was $7.3\,\%$. Water 4 was not used for any sample. The VODCA background measurements show freezing temperatures of about $-32\,°\mathrm{C}$ with T_{on} at $-30\,°\mathrm{C}$.

From this data, homogeneous freezing is derived. For TINA INA below $-20\,°\mathrm{C}$ will be considered as homogeneous freezing and therefore background, for VODCA this value is set to $-32\,°\mathrm{C}$.
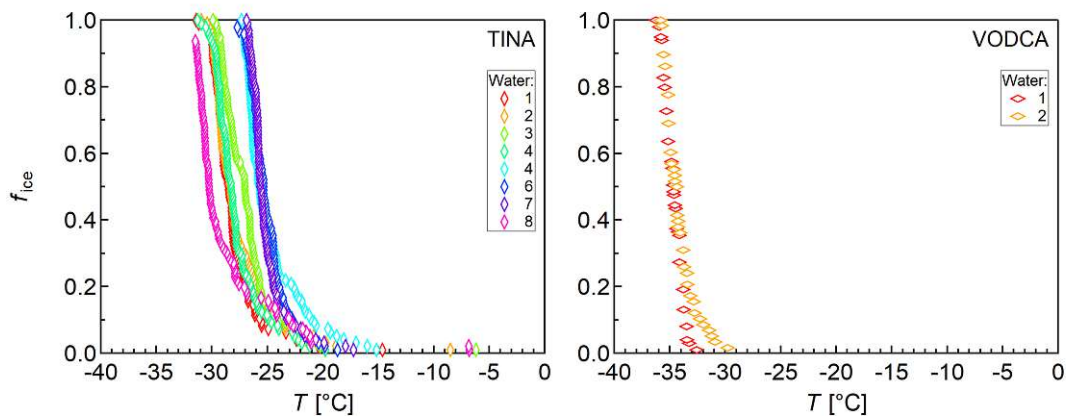

Figure 5.1: Fraction of frozen droplets f_{ice} of UHQ water. Left: TINA measurements of eight different UHQ water measurements. Right: VODCA measurements of two different UHQ water background measurements. The freezing temperature of UHQ water for TINA is around $-20\,°\mathrm{C}$, and for VODCA it is around $-32\,°\mathrm{C}$. The TINA and VODCA samples 1 and 2 are not the same.

5.2 Ice nucleation activity of birch pollen

To study the ice nucleation activity of INMs from *Betula pendula* pollen, they were extracted using water and measured with the freezing assay TINA. Pollen from the Czech Republic (A) and Slovakia (B) was analyzed.

The cumulative number of INMs ($N_m(T)$) per gram pollen has been calculated using equation 4.2. Figure 5.2 depicts two measurements of pollen A (top and middle, turquoise) and a single measurement of pollen B (bottom, purple). In general, INMs from both pollen show similar activity with three different T_{on} at about $-6\,°C$, $-15\,°C$ and $-18\,°C$, marked by a sharp incline of the curve at these temperatures. While pollen B show higher numbers of INMs at $-6\,°C$ temperatures, the INMs at $-15\,°C$ and $-18\,°C$ occur in similar concentrations. The figure also shows the variability of INM concentrations between the two measurements from pollen A, especially the number of INMs active above $-15\,°C$ varies between the two measurements. N_m values for the three temperatures are listed in table 5.1.

These measurements reveal a new onset temperature (T_{on}) at $-6\,°C$ of birch INMs, since previously only T_{on} at $-15\,°C$ and $-18\,°C$ were reported [32, 44–46, 108]. The following experiments, in section 5.2, were performed to find out the origin of this newly found activity.

Table 5.1: $N_m(T)$ values of BPWW per gram pollen from the measurements of pollen A and B.

Temperature	$N_m(T)$ of Pollen A		$N_m(T)$ of Pollen B
[°C]	#1 [g^{-1}]	#2 [g^{-1}]	[g^{-1}]
$-7\,°C$	-	1.40×10^2	2.31×10^3
$-15\,°C$	2.30×10^6	3.02×10^6	2.33×10^5
$-18\,°C$	1.22×10^{10}	1.08×10^{11}	1.45×10^{11}

5.2.1 Possible contamination of birch pollen

To verify the new finding of INA with T_{on} of $-6\,°C$ from birch pollen INMs, the possibility of microorganism contamination was tested for. Therefore, microorganisms found in the unfiltered BPWW were cultivated in three different culture media: potato dextrose agar (figure 5.3(c)), malt extract agar, and soy broth (figure 5.3(b)). Further soy broth was diluted - 1:1 (medium:water) - to simulate lower nutrient concentration.

Bacterial contamination was found on soy broth and potato dextrose agar. The cultivated bacteria were then tested for their ice nucleation activity. The bacteria in soy broth were measured directly, and pure soy broth was used as a blank measurement for reference. The bacteria from the agar plate were scraped down and transferred into UHQ water to produce an aqueous solution, this was repeated with a clean plate to create a blank sample.

The freezing curve of the cultivated contamination is depicted in figure 5.3 on the left. The bacteria shows activity at $-15\,°C$ in pure soy broth, at $-20\,°C$ in diluted soy broth, and after agar cultivation. Since both blank measurements froze at $-25\,°C$, it is concluded that the bacteria are ice nucleation active, even at two different temperatures
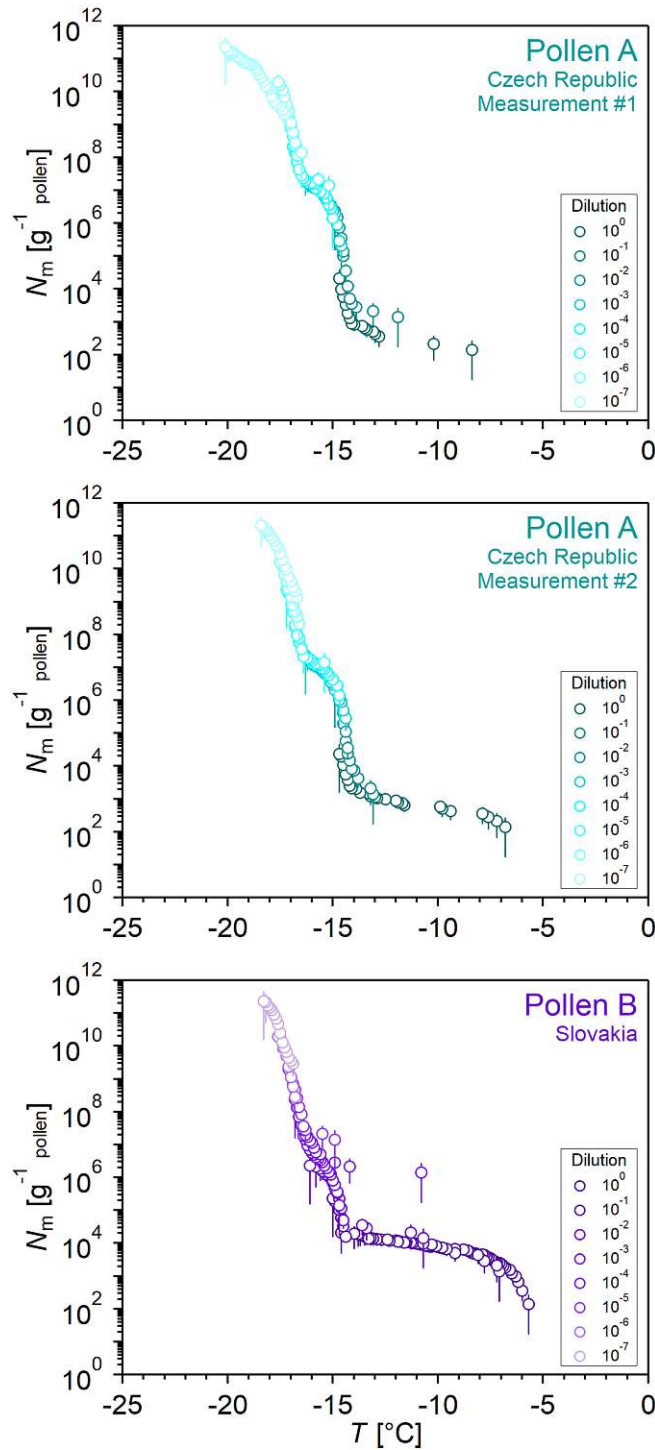
Figure 5.2: Cumulative number of INMs ($N_m(T)$) per gram pollen in BPWW from pollen of two different growing regions measured with TINA. The error was calculated using the Gaussian error propagation. Top & middle: Graphs of two different measurements of pollen A, a variability of concentrations of INMs active above $-15\,°C$ can be seen. Bottom: One measurement of pollen B, showing a much higher number of INMs active above $-15\,°C$.

$(-15\,°C$ and $-20\,°C)$. Still, the activity is well below $-6\,°C$. Figure 5.3 (d) shows microscopy pictures of the bacteria. The bacteria are in the size range of $2\,\mu m$ to $5\,\mu m$, and therefore can be removed with $0.2\,\mu m$ filters which are in the standard procedure for preparing BPWW (see section 4.1).
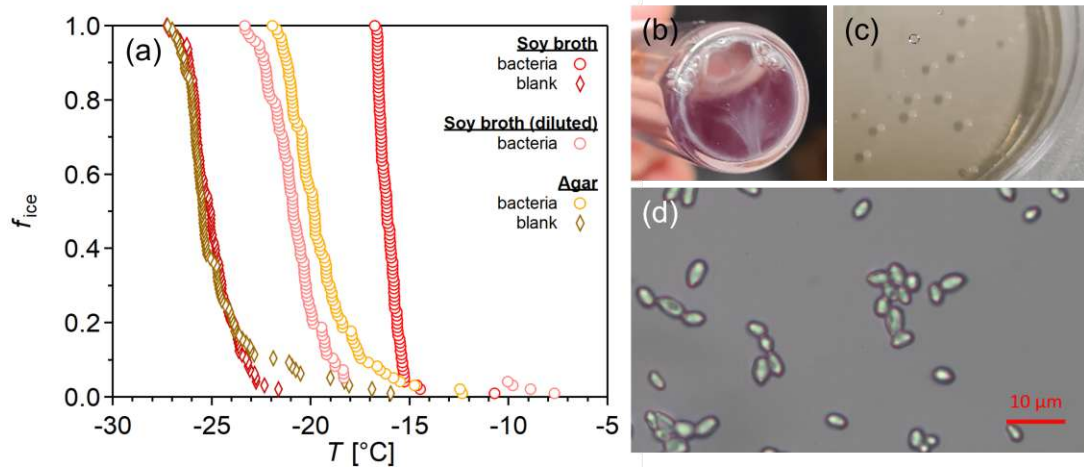

Figure 5.3: (a) Freezing curve of the bacterial BPWW contamination under three different growing conditions measured with TINA. The blank measurements serve as background. Bacterial contamination growing in soy broth (b) and on potato dextrose agar (c). (d) Microscopy pictures of the contamination (bright field, 100x objective with oil immersion).

5.2.2 Comparison of INA using different measurement setups

Another approach for the verification of the $-6\,°C$ activity was to compare the same samples measured with different ice nucleation assays. Therefore the BPWW was additionally measured using the VODCA setup.

Figure 5.4 depicts N_m per gram residue after freeze-drying of BPWW measured with TINA and VODCA - this calculation was necessary for the ice affinity measurements, more information is given in section 4.2.3 - and such is not comparable to figure 5.2. Figure 5.4, shows TINA measures a T_{on} of $-5.7\,°C$ and VODCA of $-15.6\,°C$. The N_m values start at $9.8 \times 10^2\,g^{-1}$ with TINA and at $2.2 \times 10^8\,g^{-1}$ with VODCA. Further, that the N_m curves overlap at N_m of $2.2 \times 10^8\,g^{-1}$ to $1.6 \times 10^{10}\,g^{-1}$ and temperatures of $-15.6\,°C$ to $-19.4\,°C$ (see table 5.2). Thus, the two measurements coincide. While the VODCA measurement is a good representation of the previously reported INA of birch pollen, it does not contradict the activity found with the TINA setup.

The N_m curve measured using VODCA reaches down to $-32\,°C$, this is possible due to the lower homogeneous freezing temperature of the setup (as described in section 5.1). On the other hand, the TINA setup shows higher sensitivity since the starting N_m value is about a factor 10^6 lower.

5.2.3 Influence of storage conditions on the freezing behaviour

In another experiment, the potential influence of storage conditions on the freezing behaviour was tested. Therefore an aliquot of dry pollen was stored at $-20\,°C$ for 14 days, while another aliquot of pollen was stored at room temperature (RT), which

Table 5.2: Comparison of T_{on} and N_m values per gram residue after freeze-drying of BPWW measured with TINA and VODCA. Bold values represent $N_m(T_{on})$.

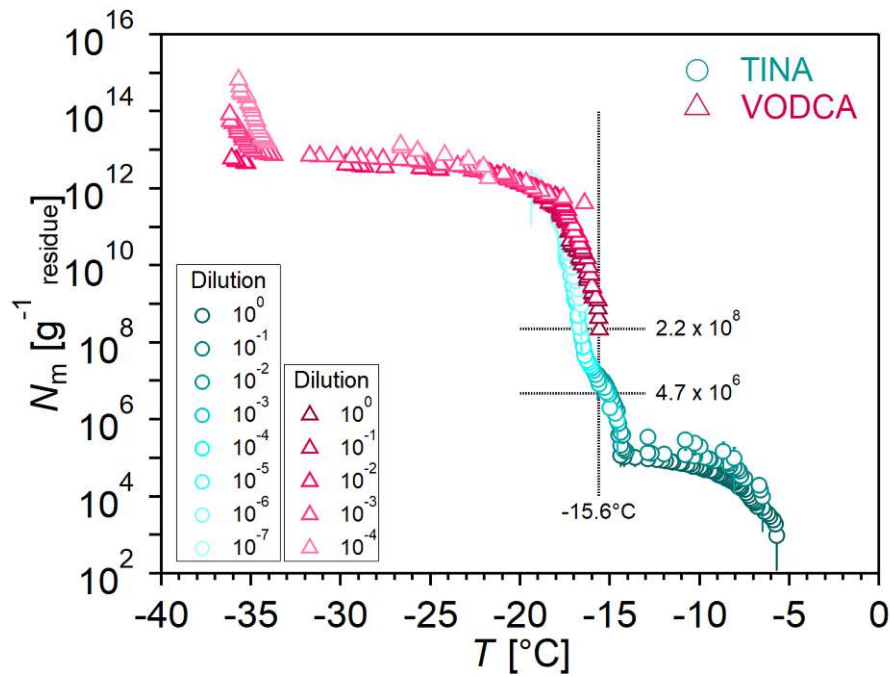| Temperature	N_m TINA	N_m VODCA
[°C]	$N_m(T)$ [g^{-1}]	$N_m(T)$ [g^{-1}]
$-5.7\,°\mathrm{C}$	$\mathbf{9.8 \times 10^2}$	-
$-15.6\,°\mathrm{C}$	4.7×10^6	$\mathbf{2.2 \times 10^8}$
$-19.4\,°\mathrm{C}$	1.6×10^{12}	1.1×10^{12}

Figure 5.4: Cumulative number of IN $N_m(T)$ per gram residue after freeze-drying in BPWW measured with TINA and VODCA. Turquoise circles show the TINA data, while pink triangles show the VODCA data.

is the usual storage method. Pollen A and B were tested. After 14 days BPWW from each aliquot was prepared according to section 4.1.2 and the INA was tested with TINA.

Figure 5.5 shows the freezing curves of the different samples. All samples froze heterogeneously since all droplets froze at a temperature of above $-15\,°\text{C}$. The UHQ water froze at about $-18\,°\text{C}$. The water background is higher than usual for the TINA setup, which in this case does not pose a problem since all analyzed samples froze at an even higher temperature. About $20\,\%$ of droplets froze above $-14\,°\text{C}$ with a small slope in the freezing curve starting between T_{on} of $-6.0\,°\text{C}$ to $-7.2\,°\text{C}$. After $-14\,°\text{C}$ all other droplets froze before reaching $-15\,°\text{C}$.

All samples show very similar freezing behaviour. Therefore, this experiment gives evidence that there is no influence of the storage condition on the freezing behaviour.
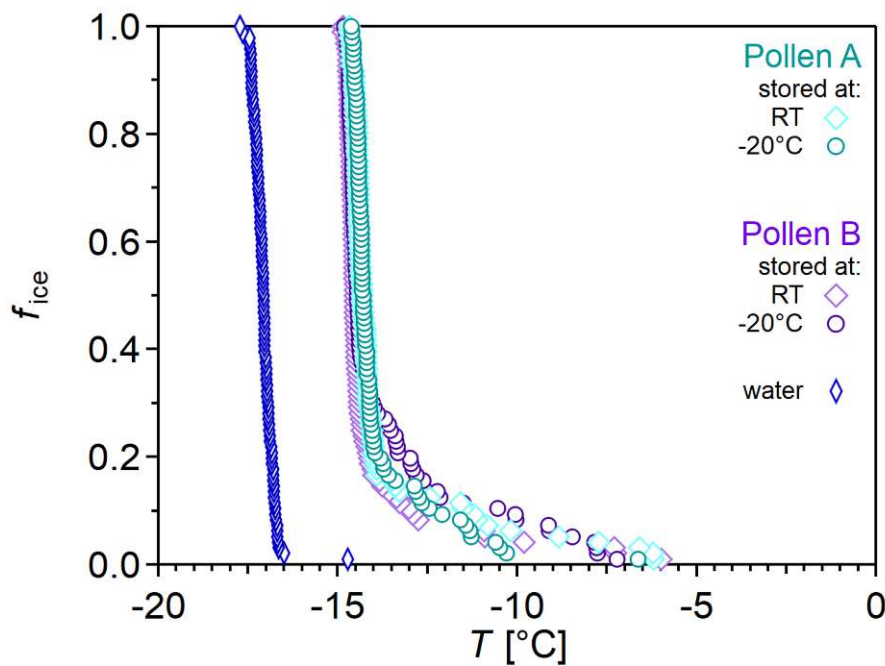

Figure 5.5: Freezing curves of BPWW prepared from pollen stored at two different temperatures measured with TINA. Two pollen aliquots - pollen A and B - were stored at room temperature (RT) and two at $-20\,°\text{C}$ to investigate a possible influence of the storage conditions on the freezing behaviour. In addition, water was measured as a reference.

5.2.4 Influence of ruptured pollen on the freezing behaviour

Many fresh birch pollen in the atmosphere rupture due to contact with water or high humidity, thereby releasing, amongst others, cytoplasmic material and SPPs [47].

Commercially bought pollen stored for a longer time or dried pollen often do not show this behaviour. To simulate pollen rupture and the release of cytoplasmic material, three pollen aliquots (from pollen A) were milled using a swing mill, twice dry and once wet (for details see section 4.2.1). From the milled pollen, BPWW was prepared (milled-BPWW) and the INA was measured with TINA.
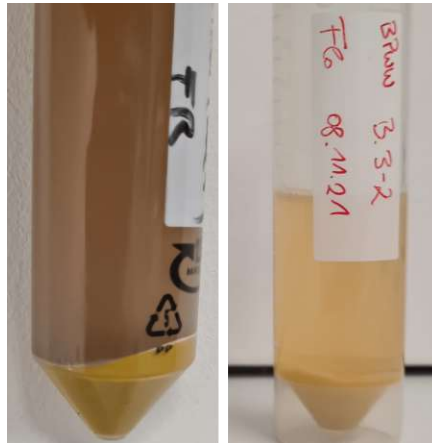
Figure 5.6: Comparison of milled (left) and regular (right) birch pollen suspended in water.

Figure 5.6 shows a comparison of regular and milled pollen suspended in water. The suspension with the milled pollen (left) is brown and much darker compared to the regular pollen suspension which is bright yellow. Figure 5.7 shows the freezing behaviour of the milled-BPWW compared to regular BPWW and water background. All samples froze heterogeneously and show similar freezing curves, with T_{on} at $-6.1\,°C$ to $-6.7\,°C$ and completely freezing before $-15\,°C$.

Besides the difference in suspension color, no significant difference in freezing behaviour can be recognized.

5.2.5 Summary and technical discussion

The measurement of BPWW using the TINA setup reveals three different T_{on} at $-18\,°C$, $-15\,°C$ and $-6\,°C$. While the freezing onset temperature at $-15\,°C$ has been previously reported by Pummer *et al.* [32] and Augustin *et al.* [45], the two freezing temperatures at $-15\,°C$ and $-18\,°C$ are also in accordance with O'Sullivan *et al.* [44] and Dreischmeier *et al.* [46]. In the supplement of Dreischmeier *et al.* [46] similar activity was reported, which however was interpreted in her PhD thesis Dreischmeier [108] as activity from the pollen grain rather than INMs. It is here the first time that the high T_{on} up to $-6\,°C$ is attributed to INMs.

INA above $-15\,°C$ as result of contamination?

Unfiltered BPWW was tested for microorganism contamination, since some microorganisms are known as effective ice nuclei, e.g. bacteria like *P. syringae* active at $-1\,°C$ [39], or fungi like *M. alpina* active at $-6\,°C$ [33] and *Fusarium spp.* active between $-1\,°C$ and $-6\,°C$ [40]. Even though contamination was found which showed INA, T_{on} was at $-15\,°C$ and $-20\,°C$ and not nearly as high as $-6\,°C$. The found microorganisms were observed using a microscope and found to be $2\,\mu m$ to $5\,\mu m$ in size. Therefore, the $0.2\,\mu m$ filter step in the standard BPWW preparation procedure, was filtering the microorganisms off regardless, since most of the known bacterial IN are membrane-bound proteins e.g. *P. syringae*. However, very few bacteria are known to secrete INMs like *Lysinibacillus parviboronicapiens* [109], but this is a quite uncommon characteristic.
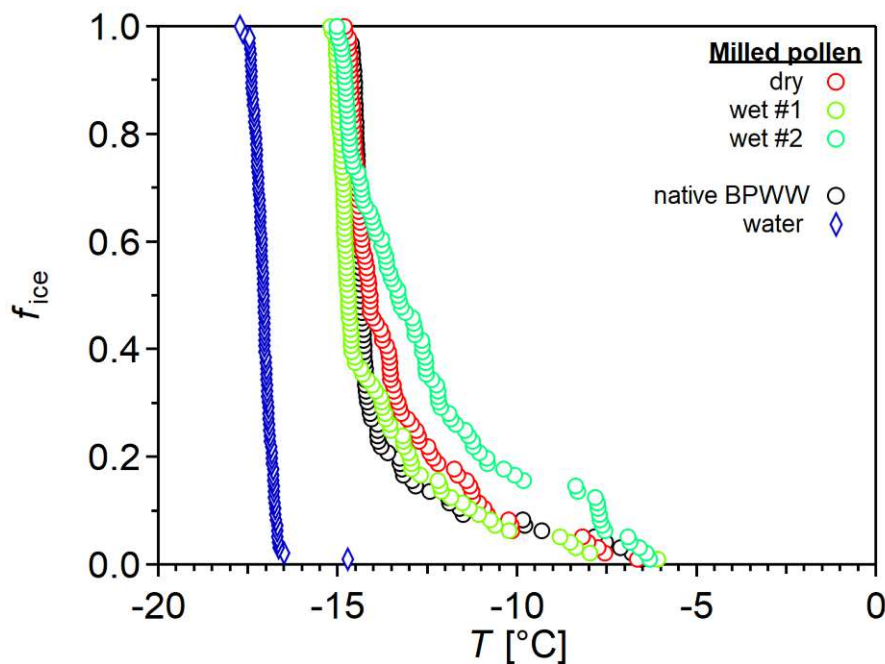
Figure 5.7: Freezing curves of BPWW prepared from regular and milled pollen to investigate a possible influence of the pollen rupture on the freezing behaviour. Two pollen aliquots were milled wet and one was milled wet. In addition water was measured as a reference.

In general, when working with biological samples the number of influencing factors is too high that not all can be tested for. For example the cultivation of microorganisms is always a selective process and not all microorganisms can be cultivated using conventional methods. Hence, there is a slight possibility that the cultivation did not include microorganisms producing the INMs active at $-6\,°C$ or the cultivation conditions did not induce the INM production within the organism, since cultivation conditions can strongly influence the metabolism of a microorganism and induce or repress the expression of certain metabolites. Overall it is rather unlikely that the INA up to $-6\,°C$ is caused by microorganisms.

Influence of measurement setup on INA results

The second verification experiment was the comparison of results of two different ice nucleation assays, namely TINA and VODCA (section 5.2.2). As mentioned in section 4.3.1, VODCA and TINA are complementary since they both have their unique advantages over the other, section 3.1 gives an overview of different assays and their characteristics. The same samples were measured with both setups, but they provide quite different results (see figure 5.4). The VODCA setup shows what was previously reported and recognized in contrast to the newly found activity at $-6\,°C$ using TINA. This may be due to the different sample droplet volumes. While TINA uses $3\,\mu L$ droplets, VODCA uses pL-sized droplets (see section 4.3.1). Since both measure a similar number of droplets in a single run, this leaves a factor of 10^6 difference in observed volume. This factor is found again when comparing the beginning of the N_m spectrum between VODCA, which starts at about $2.2 \times 10^8\,g^{-1}$, and TINA, which

starts at about $9.7 \times 10^2\,\mathrm{g}^{-1}$. This enormous difference in the observed volume can be simplified by the fact that in order to observe a reasonable amount of activity at $-6\,°\mathrm{C}$ with a VODCA-like setup would require the measurement of 1 million droplets, since in this case the probability to find this type of INM is highly unlikely in such small volumes and increases with increasing droplet volume. A single freezing event at this temperature in a single measurement is easily regarded as measurement artifact and therefore most likely not reported. This argument is even more convincing with respect to the evaluation of VODCA-like setups (picoliter-sized droplets), which is often still done manually, therefore the evaluation of 1 million droplets is unrealistic, if not for the proof of this exact problem. In summary the two measurement setups do not contradict each other but should be considered as complementary, which will be discussed in chapter 6.

Influence of storage conditions and pollen rupture

In addition to these experiments, the influence of storage conditions (section 5.2.3) and of pollen rupture (section 5.2.4) on the freezing behaviour was also tested. Both storage conditions resulted in similar freezing behaviour (figure 5.5), and also the freezing behavior of BPWW prepared from milled pollen and the whole pollen grain did not differ (figure 5.6). In both experiments only f_{ice} of the native samples was measured, for a deeper investigation and better understanding of the influence, dilutions could have been measured, as it brings quantitative information when calculating N_m. The main goal of these experiments was to see the influence of the freezing behaviour above $-15\,°\mathrm{C}$, which was achieved since all samples froze partly at $-15\,°\mathrm{C}$, where the second T_{on} is. If a sample completely freezes at $-6\,°\mathrm{C}$, it does not contain information about the amount of INMs at and below this temperature, because this is basically a signal overflow, which cannot be quantified unless the sample is diluted. This also means that there is no information about the influence of these two factors on the concentration of the INMs at $-15\,°\mathrm{C}$ and $-18\,°\mathrm{C}$, because a dilution series would be needed to get this observation. In summary, we can conclude that storage conditions and pollen rupture do not influence the freezing behaviour above $-15\,°\mathrm{C}$, and therefore, do not bring any additional arguments or conclusions to the origin of this activity.

Final remarks regarding the origin of the INA at $-6\,°\mathrm{C}$

Considering all experiments, the activity up to $-6\,°\mathrm{C}$ with high probability can be attributed to the birch pollen INMs rather than to any microorganism or experimental effects. Nevertheless, a small uncertainty remains, which can be reduced by a comprehensive study of birch pollen (*B. pendula*) of various origins, growing regions, and conditions with multiple measurement setups. Beyond that, there is the possibility of microorganisms as part of the microbiome of each tree, responsible for the ice nucleation activity above $-15\,°\mathrm{C}$. Finally, there will be uncertainty about the origin of the INMs active at $-6\,°\mathrm{C}$ (but also at lower temperatures) from *B. pendula* until the chemical composition and structure of the INMs are finally elucidated.

5.3 Freeze-thaw cycles

In a simple experiment the behavior of the INMs in multiple measurements, right after another was tested. Therefore, a dilution series of regular BPWW was measured using TINA. Right after reaching the lowest temperature of $-35\,°C$, where all droplets froze. After all droplets melted again a new measurement run was started. This freeze-thaw cycle was repeated 14-times.
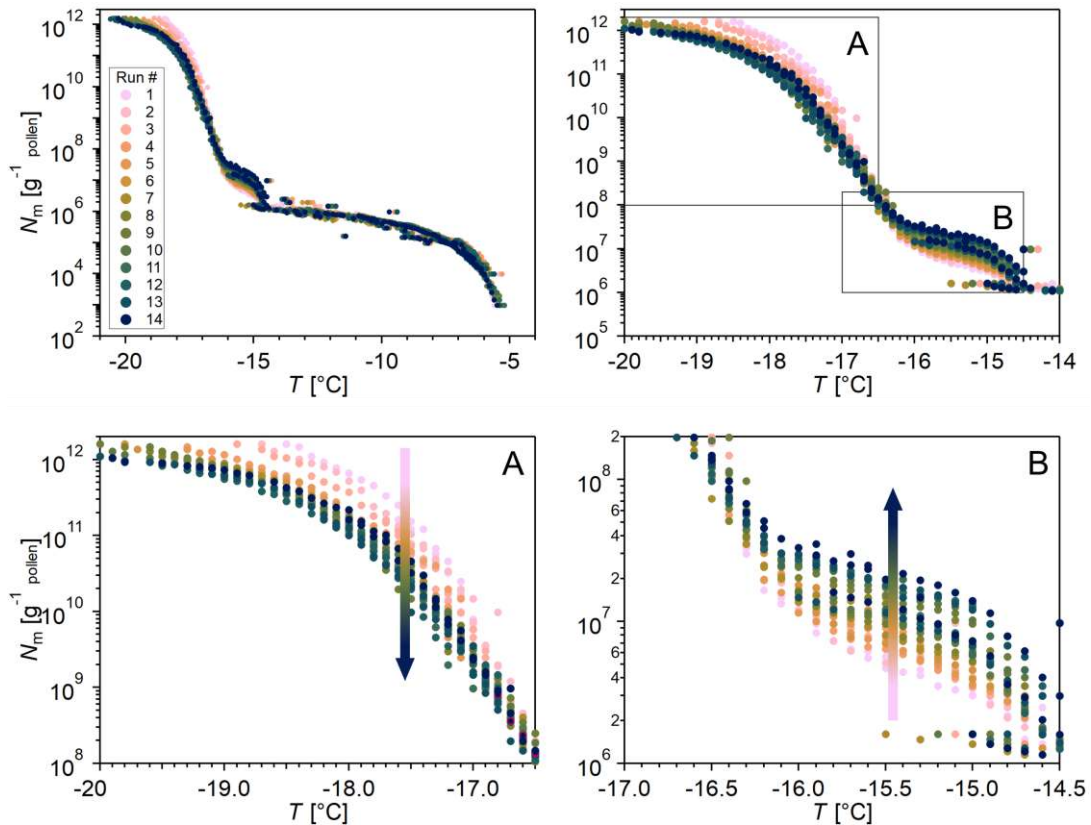

Figure 5.8: Series of the cumulative number of INMs ($N_m(T)$) of BPWW after 14 freeze-thaw-cycles (Run #), each freezing cycle was measured with TINA. Top left: N_m curves of all 14 measurements. Top right: Zoomed-in version of the left plot, with further zoomed-in regions A and B marked by boxes, which are depicted below. (A) shows the low temperature region, where a decrease in concentration with each run can be observed. (B) shows the high temperature region which shows the opposite trend of (A).

Figure 5.8 shows N_m curves per gram pollen of all 14 measurements. All measurements show consistent freezing behavior, with only minor variances. An interesting trend occurs between $-15\,°C$ and $-18\,°C$, which is zoomed in at the upper right graph. While the INMs at $-15\,°C$ seem to increase with each cycle, the INMs at $-18\,°C$ decrease. The bottom two graphs are zoomed into both of these regions as marked by boxes in the upper right graph. The clear trend of decreasing INM concentration between $-17\,°C$ to $-19\,°C$ with each cycle can be seen in box A, marked by the arrow. In the temperature region of $-14.5\,°C$ to $-16.5\,°C$ the concentration increases. Both concentrations change by about a factor of 10.

5.3.1 Summary and technical discussion

The freeze-thaw cycles show the consistency of the ice nucleation measurements throughout 14 measurements, only minor deviations occur. The trend of increasing INA at $-15\,°C$ while decreasing activity at $-18\,°C$ was unexpected and interestingly, the factors of increase and decrease are both about 10. This trend will be discussed in chapter 6.

5.4 Size analysis

5.4.1 Filtration series

The sizes of INMs from birch have been reported to be $>100\,kDa$ [32, 46, 59, 108]. To narrow down the size range the BPWW was filtered using five different MWCO (molecular weight cut off) filters with cut-off sizes of 10, 30, 50, 100 and $300\,kDa$ and the INA of the filtrates was measured, which includes molecules of the cut-off size and smaller. Pollen B were used to prepare the BPWW for this experiment.

Figure 5.9 shows the fraction of frozen droplets f_{ice} of the five cut-off filtrates and reference measurements of native BPWW (black circles) and a water blank (blue diamonds) measured with TINA (left) and VODCA (right). The TINA measurements show active IN down to sizes $<10\,kDa$. In contrast, the VODCA measurements show INA to sizes $<50\,kDa$. The INA within the $<50\,kDa$ fraction is quite low and only $13\,\%$ of droplets froze heterogeneously. The $<300\,kDa$ and $<100\,kDa$ fractions measured with TINA have an onset temperature T_{on} of $-14.5\,°C$, while the VODCA measurements show an onset temperature of $-16.5\,°C$. The fractions $<30\,kDa$ and $<10\,kDa$ show an T_{on} at $-17\,°C$ and below when measured with TINA. An overview of T_{on} is given in table 5.3. In general, the activity decreases with decreasing filter pore size. The blank measurement from TINA (UHQ water, not filtered but handled the same way as the samples) shows slight impurities and about $10\,\%$ of droplets froze before $-20\,°C$, which is the usual start of the homogeneous freezing temperature in the setup. The native sample here only shows small INA up to $-5.4\,°C$, indicating that this is a sample with less of the INMs active at high temperatures. This native sample was prepared for this experiment, and shows that the activity at $-6\,°C$ can vary from each batch of BPWW.

Table 5.3: Freezing onset temperatures T_{on} and T_{50} values of all cut-off size-fractions measured with TINA and VODCA. A grey value indicates homogeneous freezing.

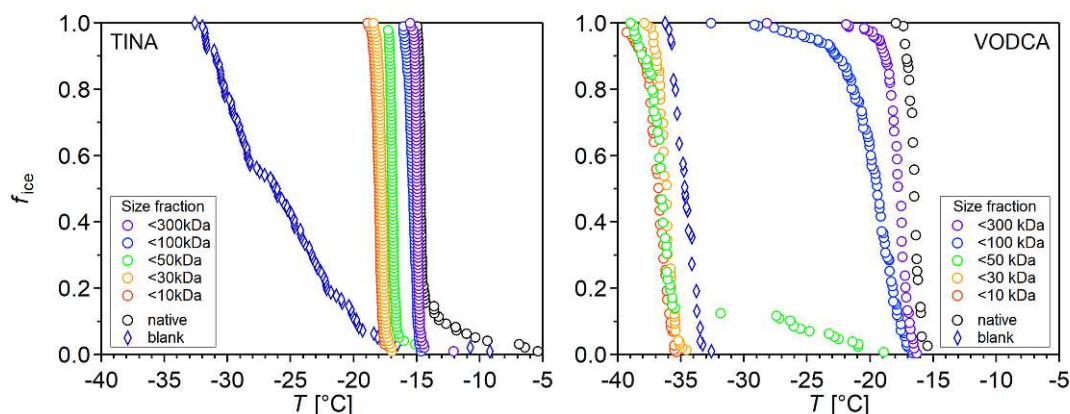| Size fraction	T_{on} [°C]		T_{50} [°C]	
[kDa]	TINA	VODCA	TINA	VODCA
native	-5.4	-15.4	-14.7	-16.5
< 300	-12.1	-15.4	-15.0	-16.5
< 100	-14.7	-15.7	-15.3	-17.1
< 50	-15.1	-18.9	-16.9	-36.6
< 30	-17.0	-34.6	-17.8	-36.1
< 10	-17.2	-35.4	-18.0	-36.8

Figure 5.9: Freezing experiments with different size fractions of the BPWW. Filtrates of 10, 30, 50, 100 and 300 kDa MWCO filtrations shown in red, orange, green, blue, and purple respectively. Pure water was used as a blank sample (blue diamonds) and native BPWW (black circles). Measured with TINA (left) and VODCA (right). It is assumed that molecules bigger than the filter size remain in the filter leaving the filtrate with molecules smaller than the filter size.

Size exclusion chromatography

Size exclusion chromatography (SEC) was performed with all size fractions i.e., all cut-off filtrates and all cut-off supernatants. The pure samples were injected into an HPLC with an SEC column (for details see section 4.3.2) and absorbance was measured at 220 nm. The injection volume was 10 µL. A native (i.e., unfiltered sample) was measured for comparison. The absorbance was not normalized.

In figure 5.10 the chromatograms of all filtrates and supernatants are depicted. The cut-off from all filters is at about 10 min, before all filtrates and after all supernatants show a decreased signal (compared to the native sample). Further distinction between the filter sizes is not possible. In general, all signals match with the native sample (supernatants before and filtrates after 10 min), therefore there is no contamination or loss of analyte. A correlation between the signals and INA is not possible.

Gel electrophoresis - SDS page

Figure 5.11 shows an image of the separation. The native sample has the highest intensity. The 300 kDa and 100 kDa show almost no difference in signals, the <10 kDa fraction does not show any bands, because the gel was not suitable for this size fraction. In general, with a smaller filter size, the high mass bands are lost. The upper of the two intense bands at 15 kDa is the pollen allergen Bet v 1 (at about 17 kDa) and the intense band at 25 kDa is Bet v 8 (27 kDa) [110]. The intense smeared band at 250 kDa occurs in all size fractions. The size is much larger than most filter sizes, but due to SDS and BME the proteins do not stay in their original shape and a direct correlation between filter size and SDS bands is not necessarily feasible.
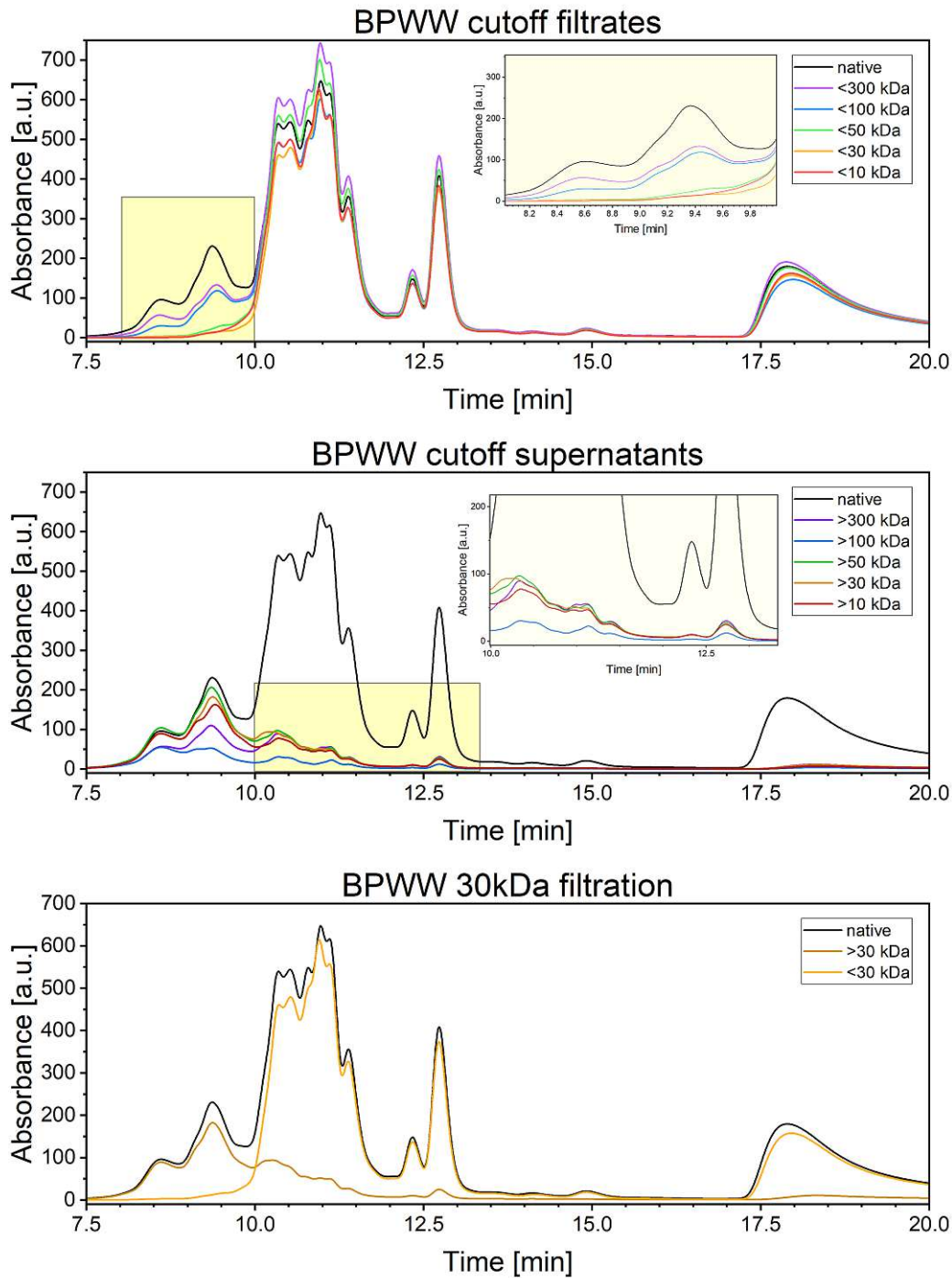
Figure 5.10: SEC chromatograms of all cut-off (10, 30, 50, 100 and 300 kDa) filtrates and supernatants and native BPWW (black). The cut-off can be seen at about 10 minutes, before the filtrates and after the supernatants show smaller signals than the native sample. The bottom chromatogram shows a direct comparison of the 30 kDa cut-off filtrate and supernatant.
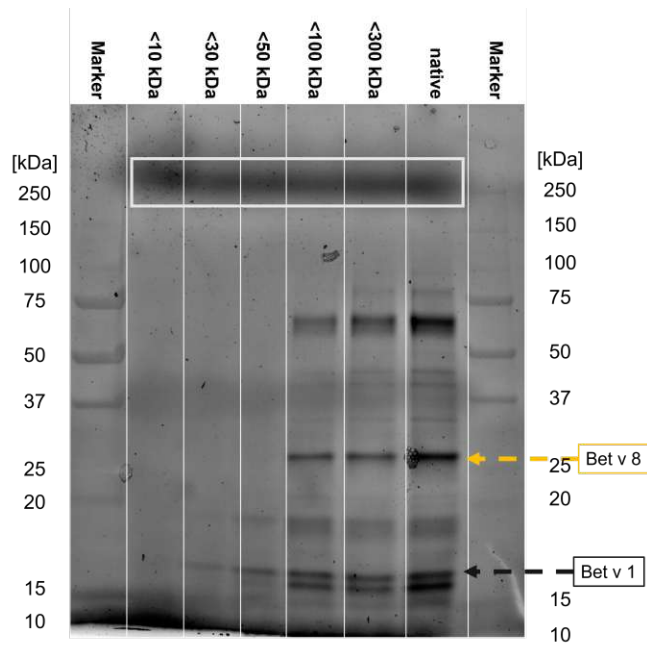
Figure 5.11: SDS page of BPWW filtrations. The outer lanes are markers with known molecular weights, which are given next to the lanes. An intense broad band is marked in light grey at about 250 kDa. The two birch pollen allergens Bet v 8 and Bet v 1 are marked with orange and black arrows.
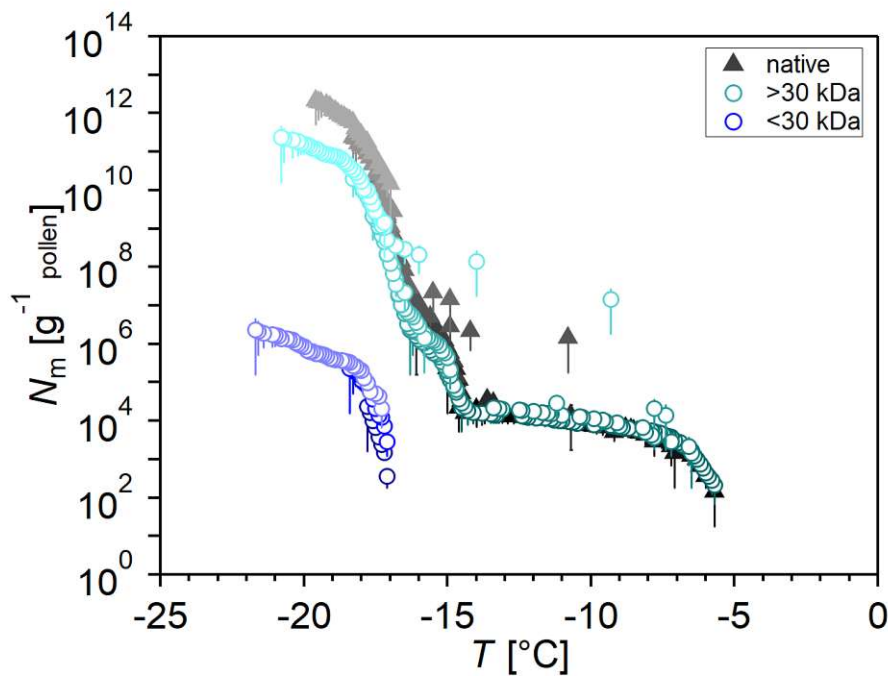

Figure 5.12: Cumulative number of IN (N_m) per gram pollen of BPWW compared to the filtrate and supernatant of the 30 kDa filtration measured with TINA. Native BPWW (black), 30 kDa filtration supernatant (turquoise) and filtrate (blue). The color gradient indicates 10-fold dilution steps, the lighter, the higher diluted the sample.

5.4.2 Single 30 kDa filtration

From a different batch of BPWW, another 30 kDa filtration was performed and from the supernatant and the filtrate, the dilutions were measured to perform quantitative comparison. For this experiment, pollen B were used to prepare the BPWW.

Figure 5.12 depicts N_m per gram pollen of the native sample, and the 30 kDa filtration supernatant and filtrate. The sample shows high concentrations of INMs starting at about $-5\,°C$. The supernatant concentration is almost identical to the native sample, except it has higher concentrations at the INMs at $-18\,°C$. The filtrate shows only activity at $-17\,°C$ and below and in much lower concentrations.

5.4.3 Summary and technical discussion

MWCO filtrations

Literature describes several cut-off filtration experiments performed with BPWW, all reporting the size of INMs to be $>100\,$kDa [32, 46, 59], since their 100 kDa filtrates did not show any INA. This type of experiment can be quite useful, because it can be used to purify the sample by a simple filtration.

INM purification was the initial goal of this experiment, but surprisingly the cut-off filtration experiments reveal INA even $<10\,$kDa (TINA results). The VODCA results show a different picture, they show that the INMs are $>30\,$kDa, as there was INA in the $<50\,$kDa filtrate. Hence, the TINA and VODCA results contradict each other. In addition, both results contradict the previously reported size of $>100\,$kDa [32, 46, 59, 108].

The single 30 kDa filtration, which was only measured with TINA, shows that the concentration of the INMs is greatly reduced in a single filtration step. The INA above $-17\,°C$ is completely lost and the activity between $-17\,°C$ to $-21\,°C$ is reduced by about a factor of 10^6. The lost activity could mean that INMs active above $-17\,°C$ are bigger than 30 kDa or more likely that the whole curve is shifted downwards through a dilution effect of the filtration and cut off at an INM concentration of about $1 \times 10^2\,g^{-1}$. At this point it has to be noted that the native sample from this experiment is different from the other filtrations, as is easily visible by the much higher INA above $-15\,°C$, therefore this filtration should not be directly compared to the other filtrations. However, the two experiments both show, that after a 30 kDa filtration freezing starts at about T_{on} $-17\,°C$ when measured with TINA.

Another notable trend is the decreasing T_{on} with decreasing filter size, especially in the TINA filtration series measurement. This could mean the three T_{on} found in section 5.2, correspond to three different INMs of different sizes. But, it could also fit to the theory of a downwards shift of the curve due to concentration, assuming the smaller the filter size, the higher the dilution effect.

In summary, the TINA results (INMs $<10\,$kDa) contradict the VODCA results (INMs $>30\,$kDa) and both contradict previous literature (INMs $>100\,$kDa). In addition, the TINA results show a decrease of T_{on} with decreasing filter size. There are multiple possible explanations for these contradictions, which will be discussed in the next chapter.

However, an important technical note is that MWCO filters do not strictly work at the certain mass (as the name suggests) but have an uncertainty of about 10 % to 20 % (according to the manufacturer), depending on e.g. shape of the macromolecule.

Therefore, the small activity in the 50 kDa filtrate measured with VODCA (13 % froze heterogeneously) could be due to the filter uncertainty. Further experiments focusing on the measurement of dilution series of all filtrates and in addition a sequential filtration, leaving only size fractions (e.g. between 30 kDa and 50 kDa), could improve our understanding of the INMs and the correlation of T_{on} and INM size.

Size exclusion chromatography and SDS page

SEC did not bring any conclusions, as the separation efficiency was not high enough to differentiate the filtrates or supernatants.

The results from the SDS page to some extent show that the filtrations worked since the bands of the larger proteins are removed in each fraction. The filter cutoff can not directly be correlated to the SDS page marker ladder since for SDS page the proteins are denatured, whereas the intact proteins which are filtered have varying shapes. Interestingly, a single band (at 250 kDa) is visible in all size fractions, and could therefore be the INM, since all fractions are ice nucleation active. However, we would then expect at least different concentrations respectively intensities in the picture. A direct correlation between this band and the INA is not possible. This band is quite unusual, since it did not keep in its lane, which could be a hint that this compound is more complex than a simple protein. However, it is more likely that the smeared band at 250 kDa is an artifact due to overloading or incomplete reaction with SDS and BME.

In summary, SEC and SDS page did not bring major conclusions. Native page could be more useful, since there proteins are not denatured and could afterwards be tested for INA. Also SEC is not necessarily the wrong method for this specific task, but would need much optimization to be utilized, but if done correctly can be used to purify INMs.

5.5 IAP and analytics

5.5.1 Ice affinity purification

BPWW is a complex sample containing many different components, which makes the analysis, component and structure elucidation of INMs a complicated task. IAP is a simple method to purify and concentrate ice affine molecules like INMs or AFPs. Different types of IAP methods exist, for this study a method developed by Ralph Schwidetzky was used [91]. The detailed procedure is given in 4.2.3. 1 h of IAP resulted in an ice plate of 426.97 g. The ice fraction was freeze-dried and filled up to a concentration of 7.21 mg$_{residue}$/g$_{water}$ which was also done for regular BPWW (for details see table 5.4).

Table 5.4: Preparation of before and after IAP samples.

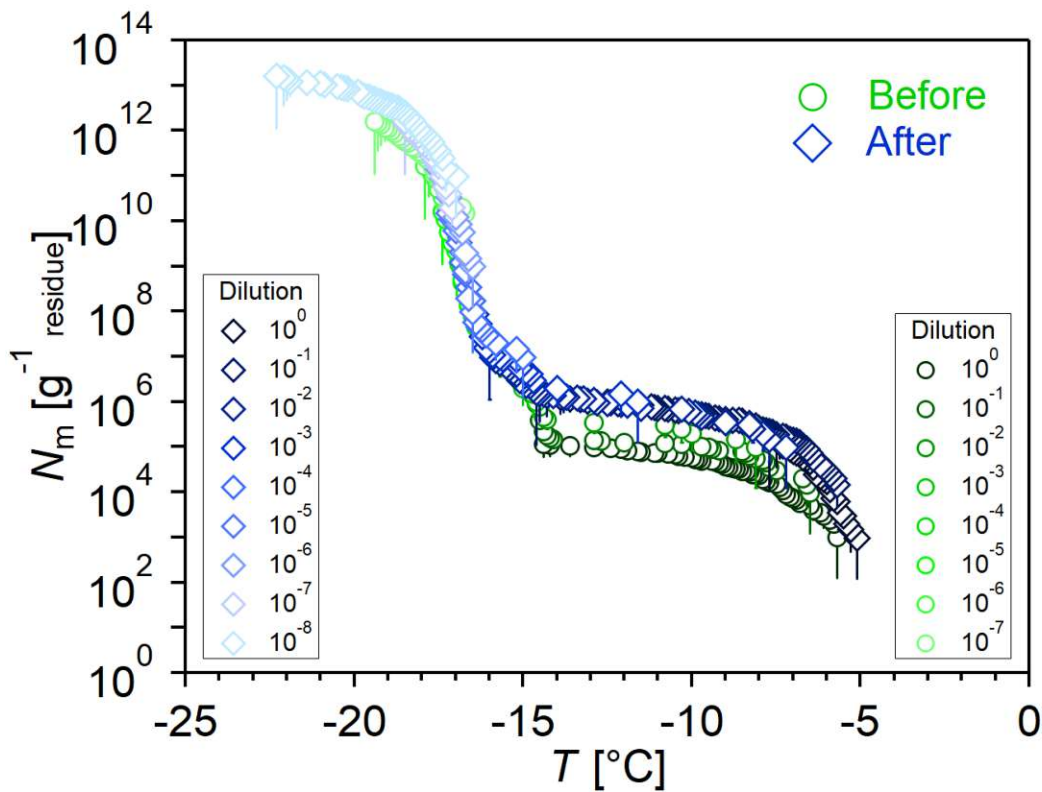| Sample	m_{BPWW}	$m_{residue}$	m_{water}	c_{sample}
	[g]	[g]	[g]	[mg$_{residue}$/g$_{water}$]
BPWW (Before IAP)	10.56	0.21	29.24	7.20
Ice fraction (After IAP)	426.97	0.30	41.57	7.21

Figure 5.13: Cumulative number of IN (N_m) of BPWW before and after ice affinity purification (IAP) measured with TINA. This graph shows the increase of INM concentration achieved through IAP.

Figure 5.13 shows the N_m curves of BPWW before (green) and after (blue) IAP per gram residue after freeze-drying. The samples have almost identical T_{on} at $-5.7\,°C$ before and $-5.1\,°C$ after IAP. After IAP shows higher concentrations, INMs active above $-15\,°C$ were especially concentrated, as the curve is shifted by a factor of about 10. At and below $-15\,°C$ the curves are almost identical, but a small shift of N_m can be seen at $-15\,°C$ and at $-19.5\,°C$.

These samples (before and after IAP) were then analyzed with different analytical methods and compared to find differences, which could lead to the understanding of INMs from birch pollen. The main goal was to find out the chemical nature of the INMs, if they are proteins, polysaccharides, or even something else.

5.5.2 Circular dichroism spectroscopy

Circular dichroism (CD) spectroscopy was measured of both samples. The measurements were carried out with a JASCO 1500 circular dichroism spectrometer, for procedure details see section 4.3.8. The samples were diluted about 1:5 (1 part sample to 5 parts overall) to obtain an optimal signal. The signals were background corrected and smoothed using the Savitzky-Golay algorithm.

Figure 5.14 shows the CD spectra of all samples. The spectra before and after IAP are quite similar with a maximum ellipticity at 190 nm followed by a decrease reaching a minimum at 210 nm. Thereafter the signal increases again rather slow until
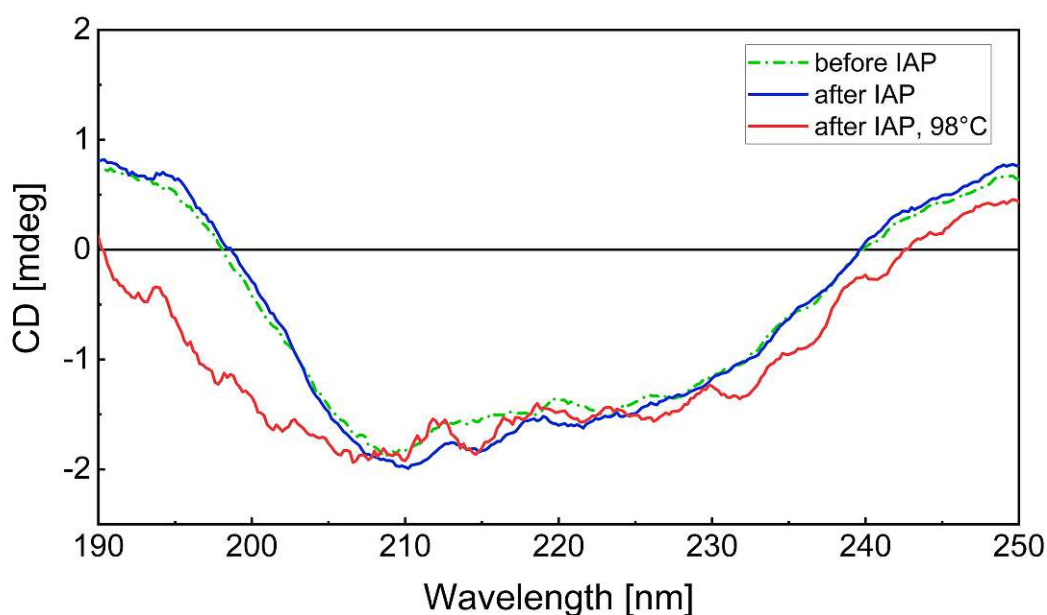
Figure 5.14: CD spectrum in mdeg (millidegree) against the wavelength nm before (green) and after (blue) IAP and after IAP heat treated for 1 h at 98 °C(red).

230 nm, where it increases faster until it reaches almost the maximum at 250 nm again. In the range of 210 nm to 225 nm the samples diverge, but only to a small extent. The spectrum changes after heat treatment at 98 °C for 1 h in the range of 190 nm to 210 nm, suggesting a small irreversible change of the proteins within the sample.

The sepctra are unusual and its deconvolution using the structural database does not allow a clear distinction into the common secondary protein structures of α-helix, β-turn, β-strand, or random coil. Compared to Greenfield [111] the signals could be a mixture of α-helix and anti-parallel β-sheets. Although these spectra are of highly purified proteins, whereas the BPWW samples still contain a complex mix of chemical components.

5.5.3   Bradford assay

A Bradford assay was conducted to compare the protein content before and after IAP. A calibration with seven standards was prepared with six measurements of each sample.

Figure 5.15 shows on the left the resulting calibration and the linear regression used to calculate the protein content in the samples. On the right is a box plot of the calculated protein content from the samples, which assumes a normal distribution. The protein content before IAP is $(17.4 \pm 4.4)\,\mu g_{protein}/mg_{residue}$ and after is $(20.1 \pm 2.0)\,\mu g_{protein}/mg_{residue}$. The given uncertainty is the standard deviation of 6 measurements, where each one of the 6 values is the average of a triplicate measurement. A t-test at 95 % confidence showed that there is no significant difference between the mean protein concentrations, assuming a normal distribution of the measurement values.

A protein content of $20\,\mu g_{protein}/mg_{residue}$ further means only 2 % by weight of the soluble molecules of BPWW are proteins.
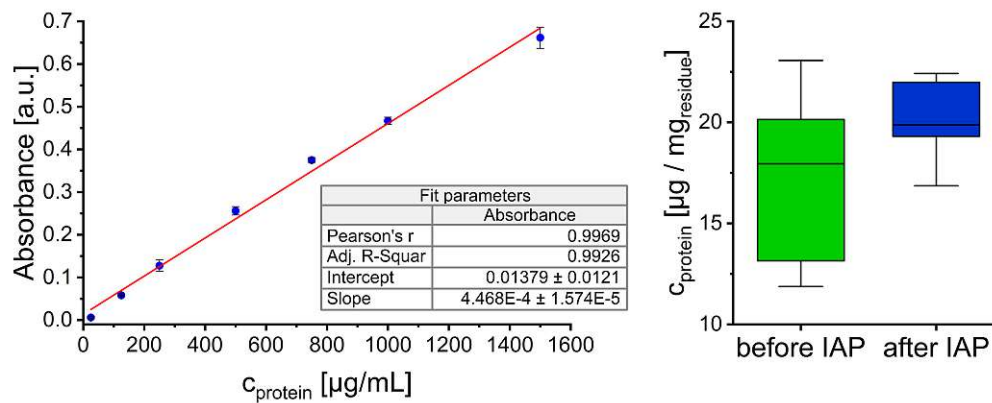
Figure 5.15: Protein content before and after IAP, measured using a Bradford assay. Left: Calibration using seven standards and a linear regression. The given uncertainties is the standard deviation of two measurements. Right: Box plot of a sixfold measurement of the sample in $\mu g_{protein}/mg_{residue}$ for BPWW before and after IAP, the whiskers show the whole range, while the box marks the first and third quartile and the line in the middle marks the median.

5.5.4 Gel electrophoresis

Two different SDS page gels were used to separate the proteins before and after IAP. A 10 % Mini-PROTEAN ©gel from BIORAD and a self cast 15 % gel were used. Both gels were stained using coomassie-blue. The detailed procedure is given in section 4.3.3. The 10 % gel was operated at a constant voltage of 150 V for 55 min. The 15 % gel was operated at a constant power of 20 mA for 120 min.

Figure 5.16 shows both gels. The 10 % gel (left) gives a better separation of the larger proteins, where no difference between the samples is visible. The band just below 75 kDa is more prominent after IAP, at closer look this is due to an error while staining and the band is visible before IAP as well. The 15 % gel (right) gives a better separation for the smaller proteins. There is only a small difference in the two bands between the 15 kDa to 20 kDa, where after IAP the upper band is more prominent but the lower band is more faint. The upper of the two bands is most likely the allergen Bet v 1, as mentioned in section 5.4.1. Interestingly in this gel the prominent smeared band at the top of the gel, as seen in the cut-off fractions gel (section 5.4.1), is not visible in either fraction.

In summary, the differences between the samples is rather minor.

5.5.5 Size exclusion chromatography

SEC was performed according to the procedure in section 4.3.2. The injection volume was 15 µL and the absorbance was measured at 220 nm.

Both samples show almost identical signals in the chromatogram (figure 5.17). There is a slight difference in intensities between 10.5 min to 11.5 min and at 12.5 min. The chromatogram is similar to the ones of the native sample in section 5.4.1. Hence, SEC does not allow to pinpoint a specific change in concentration of INMs or a significant purification effect through IAP.
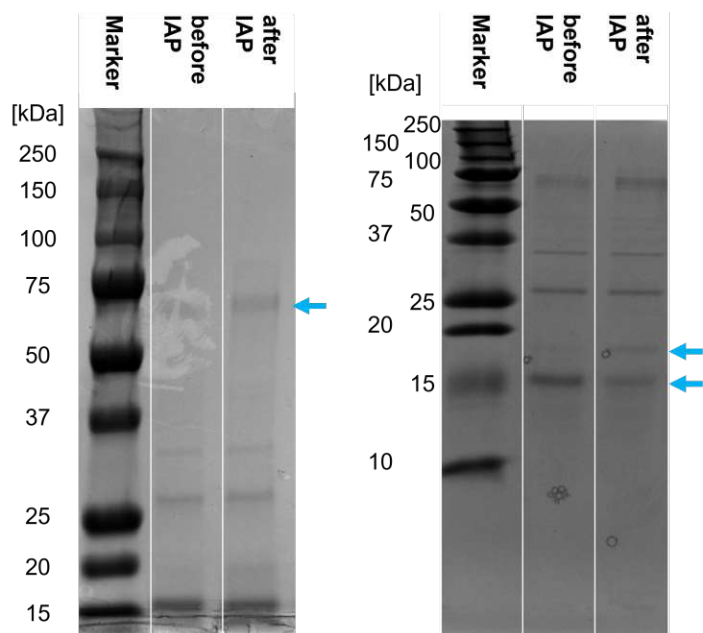
Figure 5.16: SDS page of BPWW before and after IAP. Left: 10 % Mini-PROTEAN ©gel from BIORAD. Right Self cast 15 % gel. Left lanes on both gels are markers. The bands that differ the most between the two samples are marked with a blue arrow.
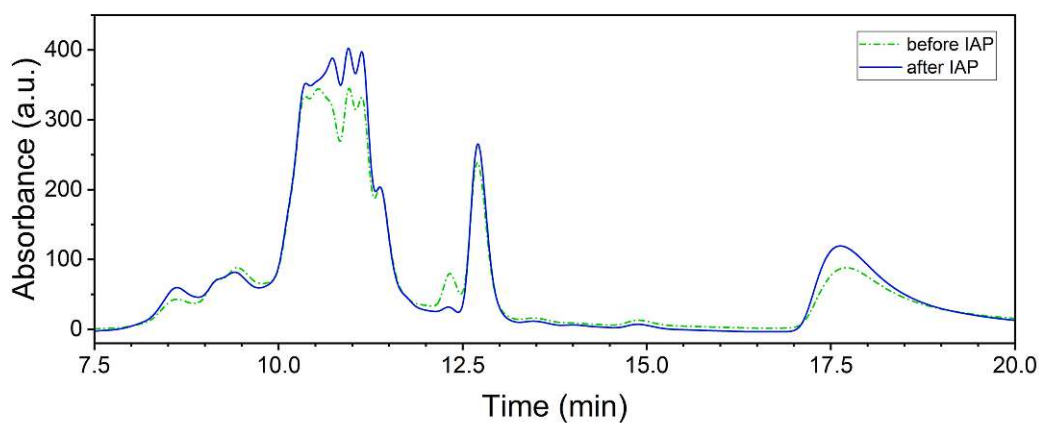

Figure 5.17: SEC chromatogram of BPWW before (green) and after (blue) IAP. Absorbance was measured at 220 nm.
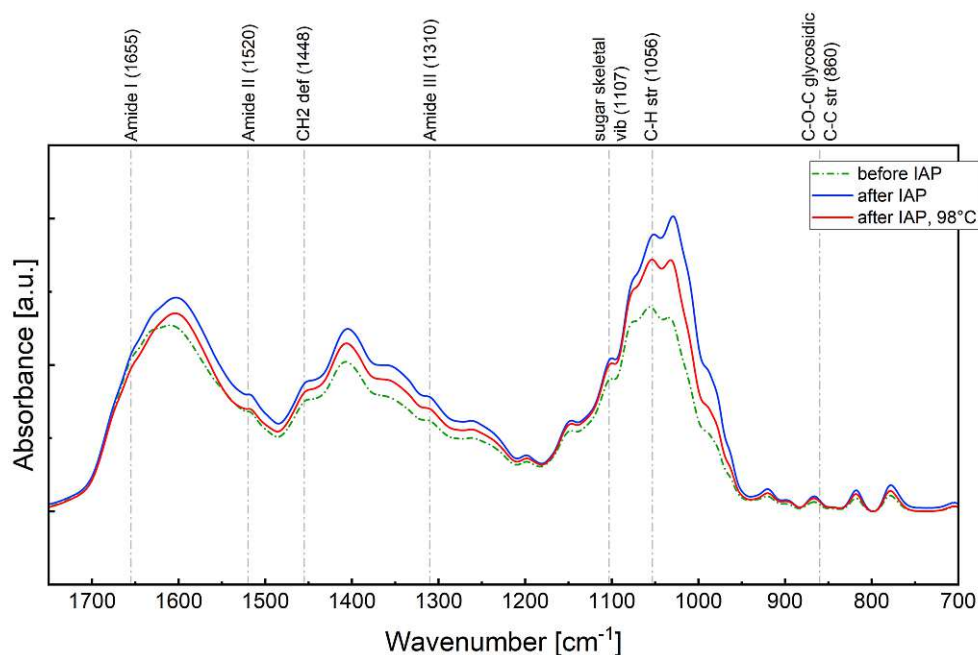
5.5.6 Infrared spectroscopy

Figure 5.18: Infrared spectrum of BPWW before (green) and after (blue) IAP, and after IAP heat treated at 98 °C for 1 h (red). The figure only depicts part of the whole spectrum, interpretation is done for the whole spectrum. The amide I (1655 cm^{-1}), II (1520 cm^{-1}), and III (1310 cm^{-1}) bands are marked.

Figure 5.18 shows IR spectra of the before and after IAP samples, the signals are normalized. Table 5.5 assigns the vibrations to the spectral bands. Socrates & Socrates [95] and Pummer *et al.* [112] was mostly used for the band assignment.

The spectra are almost identical except for a small overall shift of a few wavenumbers. The most prominent bands are not shown in the spectrum which are the O-H stretching and the C-H streching vibration. They are not shown because the first band is likely due to remaining water, and the second band is unsurprising for organic material. One of the most prominent bands shown in the spectrum is the H-O-H bending vibration at about 1600 cm^{-1}, which can also be attributed to water.

Bands hinting at polysaccharides (or sugars) are the C-O stretching vibration between 1200 cm^{-1} to 1030 cm^{-1}, the weak C-H stretching vibrations at 930 cm^{-1} to 760 cm^{-1} and the sugar skeletal vibration at 1107 cm^{-1}. Further bands are at 2900 cm^{-1} and 1460 cm^{-1} to 1200 cm^{-1}, these bands are various C-H vibrations found in many organic molecules and specific assignments in complex samples, as BPWW, is challenging. Same can be said about the O-H vibrations at 1460 cm^{-1} to 1200 cm^{-1} and 1080 cm^{-1} to 1030 cm^{-1}.

The spectrum shows the protein specific amide I, II, and III bands at 1655 cm^{-1}, 1520 cm^{-1}, and 1030 cm^{-1} respectively. The amide I band can be seen as shoulder at the water bending vibration around 1600 cm^{-1}. Another amide specific bands are bands between 900 cm^{-1} to 800 cm^{-1} corresponding to C-N-C vibrations. Although, in this spectrum below 900 cm^{-1} the C-N-C and C-H bands are weak.

Table 5.5: IR signals with according vibrations and (possible) assignment. The spectrum in figure 5.18 does not show the whole spectrum because it is zoomed in to the most important region.

Wavenumber [cm^{-1}]	Vibration	Assignment
$3700 - 2800$	O-H stretching	water, OH
$3000 - 2850$	C-H stretching	-
1655	Amide I	protein
1600	H-O-H bending	water
1520	Amide II	protein
$1460 - 1200$	C-H and O-H deformation	-
1448	CH2 deformation	-
1310	Amide III	protein
$1200 - 1030$	C-O stretching	(poly-)saccharide
1107	sugar skeletal vibration	polysaccharide
$1080 - 1030$	O-H deformation	water, OH
1056	C-H stretching	-
$930 - 760$	C-H deformation	polysaccharide
$900 - 800$	C-N-C stretching	Amides (proteins)
860	C-O-C glycosidic, C-C stretch	(polysaccharides)

5.5.7 Fluorescence spectroscopy

FEEM were also measured for both samples. Therefore the samples were measured pure and 1:1000 (part sample to parts overall) diluted with UHQ water. FEEM are gathered by measuring the emission intensity, of a sample at a certain excitation wavelength, for a number of different excitation wavelengths resulting in a 3D plot.

Figure 5.19 shows FEEM before (left) and after (right) IAP both undiluted (top) and 1:100 diluted (bottom). The FEEM of the undiluted samples are similar. Surprisingly, the diluted samples show completely different signals before and after IAP and even towards the undiluted samples. The difference to the diluted samples can be explained due to the inner filter effect of quercetin-3-O-sophoroside (Q3OS), as shown by Seifried *et al.* [113], which is the main UV/VIS absorbing component in birch pollen and therefore responsible for the yellow color. The much higher intensity before IAP can thereby also be explained, but the difference between the two diluted samples remains.

The emission at 300 nm to 400 nm at an excitation of 250 nm to 300 nm can be attributed to autofluorescnece of proteins. All natural proteins contain phenylalanine (Phe), tryptophan (Trp), and tyrosine (Tyr). Their excitable π-electrons allow for fluorescence when excited with 280 nm and emitting with a Stokes shift of about 50 nm at 330 nm [114]. This signal coincides with the FEEM reported by Burkart *et al.* [47], who assign these signals to the INMs of birch pollen. The amino acid fluorescence is about one order of magnitude smaller after IAP compared to before IAP, for both the diluted and undiluted sample. The diagonal signals seen in in the diluted samples are the scattering signals of water.
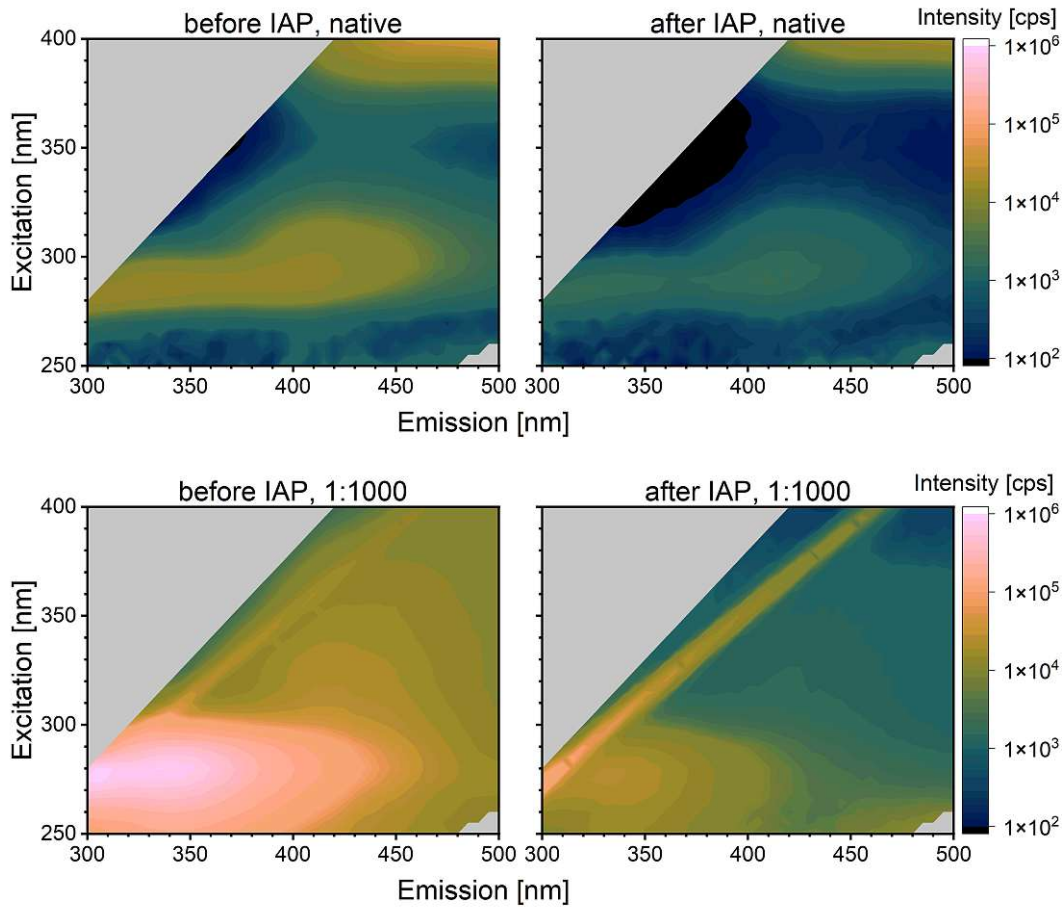
Figure 5.19: Fluorescence excitation-emission maps of BPWW before (left) and after (right) IAP, undiluted (top) and 1:1000 diluted (bottom). The color scale on the left shows the emission intensities, the color scale is logarithmic. The dilutions are depicted to avoid quenching of amino acids fluorescence (Ex: 275 nm, Em: 300 nm to 400 nm) as described by Seifried *et al.* [113], which can be observed here: only in the lower left graph (before IAP, diluted) this signal can be seen, especially in the undiluted graphs this signal is quenched and therefore about 2 to 3 orders of magnitude smaller.

5.5.8 Summary and technical discussion

Ice affinity purification - IAP

The use of IAP to purify and concentrate INMs from BPWW was successful, especially for the INMs above $-15\,°C$, where an increase of a factor of 10 was achieved. Since, both samples had the same concentration, we can deduce that the sample was also purified. Interestingly, the concentration of INMs below $-15\,°C$ did not increase as much. By absolute numbers these INMs could have increased by a similar amount, since the scale is logarithmic.

Generally, for a single IAP run, the result is quite promising. In most reports, IAP is done repeatedly for several runs, where the purified ice-fraction is then thawed and a subsequent run is done [71, 87–90]. Multiple IAP runs for BPWW could be very beneficial, due to the high complexity of the sample. Until now, most IAP studies were done on simpler samples, and even there the additional runs provide great improvements. The only limitation to multiple runs is the sample amount, but this does not pose a huge problem because large batches of BPWW can be prepared, since pollen are available for purchase in sufficient amounts. Although the BPWW preparation method has to be adapted since BPWW is mostly prepared in small volumes and the $0.2\,µm$ clog up after only a few milliliters.

Circular dichroism (CD) spectroscopy

The CD measurements showed protein-like signals, suggesting proteins to be in the sample before and after IAP. A difference between the samples cannot be seen, but this was not expected, since the protein contents are similar and sample dilution was adapted for ideal signals. The signal changed after heat treatment, most likely due to denaturation of proteins, but any further interpretation is challenging.

CD spectroscopy can be used to find secondary structures. For this purpose, highly purified protein samples are measured, hence for BPWW containing many different proteins (as seen in SDS page) the analysis of secondary structures is challenging. Further, only $2\,\%$ by weight of the soluble molecules are proteins, since large parts of the other components are unknown a possible influence of other molecules on the signal cannot be excluded.

Bradford assay

The protein content of BPWW before and after IAP was measured using a Bradford assay and showed no significant difference (t-test with a confidence level of $95\,\%$) between the mean values of six sample measurements each. Therefore, INA does not correlate with the protein content.

On a side note, a BCA assay was also performed, but due to interference caused by carbohydrates the assay did not deliver any reasonable results. A profound comparison of protein quantification methods of complex samples like aqueous birch pollen extracts (similar to BPWW) is given in Reinmuth-Selzle *et al.* [104]. They attested that most commonly used protein quantification methods can be suitable for these kinds of samples. But glycosylation of proteins can be problematic for BCA and Bradford assays. In contrast to this work, they were able to produce reliable results using a

BCA assay, since they removed substances $<3\,\mathrm{kDa}$ and thus eliminating many small sugars, which are known to interfere in BCA assays.

Gel electrophoresis - SDS page

The combination of two different gels allowed a good separation of all bands. Still, no significant difference before and after IAP was found. Since the protein content and the bands are almost unchanged, this suggests that most proteins remained in the ice fraction during IAP. Interestingly, the smeared band from the gel in section 5.4 is missing. A clear reason for this could not be identified. The only difference in handling was the freeze-drying of the IAP samples, whereas the cut-off filtered samples were not.

Size exclusion chromatography - SEC

SEC did only show minor difference after IAP, which are hard to interpret on their own. It was also not able to separate all analytes, which is not surprising given the high number of components. Repeated IAP cycles, as described before, could lead to a better purification and then SEC might be able to give hints to what changes, as a pre-step to a preparative SEC where the fractions are collected and tested for INA.

Infrared spectroscopy

Protein and polysaccharide signals can be seen in both IR spectra. A difference in the samples was not visible, except for a loss of intensity between $1000\,\mathrm{cm}^{-1}$ to $1100\,\mathrm{cm}^{-1}$. The heat treated sample did not show a difference to the regular sample. Even the protein signals (amide bands) did not change, which is not quite surprising, since denaturation caused by heat only changes protein folding by breaking hydrogen bonds. Thus, chemical bonds, mostly responsible for IR bands. However, a small shift in wavenumbers could be expected, since the hydrogen bonds can influence the bond strength. Actually, Montemurro *et al.* [115] were able to quantify bovine milk proteins purely off of IR data from the milk without sample pretreatment, based on the interplay of the amide I and II band using statistical models. While at first glance the situation seems comparable, milk proteins are well studied compared to proteins from pollen.

In summary, the IR spectra show protein and polysaccharide signals. Before and after IAP samples differed mostly in intensities especially between $1000\,\mathrm{cm}^{-1}$ to $1100\,\mathrm{cm}^{-1}$, which are likely rather unspecific C-H stretching vibration. Generally, the interpretation of an IR spectrum of a complex sample is always tricky, due to the threat of over-interpretation of simple signals such as the C-H vibrations, which can be found in many organic molecules.

Fluorescence spectroscopy

The FEEM revealed a difference in the samples after dilution. The dilution minimized the inner filter effect as described by Seifried *et al.* [113]. In figure 5.19 a difference before and after IAP was observed. The autofluorescence signal of amino acids (Ex: 275 nm, Em: 300 nm to 400 nm) is about one order of magnitude smaller after IAP, for both the diluted and the undiluted samples. However, the Bradford assay results (see figure 5.15) suggests the overall protein content did not change significantly after

IAP. This suggests IAP brings a net loss of aromatic amino acids (phenylalanine, tryptophan, and tyrosine) which are responsible for these signals.

Burkart *et al.* [47] assign this signal to INMs and hence INA which contradicts the results depicted in figure 5.19.

5.6   Heat treatments

The last chapter (chapter 5.5) showed that within BPWW protein signals can indeed be found, although a direct correlation of INMs to protein signals was not evident. Pummer *et al.* [32] speculated, that INMs from birch pollen are polysaccharides, but later reports concluded proteins might be involved in the INA of birch pollen [47]. While polysaccharides are heat stable molecules, proteins can be denatured by heat, by breaking hydrogen bonds and unfolding a protein and e.g. thereby losing its enzymatic activity. From this simple principle, the idea of heat treatment of BPWW arose. Therefore, BPWW after IAP was heated to 40 °C, 78 °C and 98 °C in closed Eppendorf tubes for 1 hour and INA was tested before and after. Further, particle sizes in solution using dynamic light scattering (DLS) and circular dichroism (CD) spectroscopy was measured to investigate the effect on these signals.

5.6.1   Effect of heat on INA

Figure 5.20 shows the $N_m(T)$ curve per gram residue after freeze-drying as function of T of BPWW after IAP, and four samples heated to 40 °C, 78 °C and 98 °C for 1 h and to 98 °C for 24 h. The overall concentration decreases with increasing heat and duration. After 40 °C for 1 hour, INA above -15 °C remains but is decreased by about a factor of 10, while INA below -15 °C remains unchanged. After 1 h at 78 °C, INA above -15 °C is completely lost. Only at 98 °C the INA below -15 °C decreases by a factor of about 100 at -18 °C. This activity additionally decreases by a factor 100 after 24 h at 98 °C. In general, a trend of decreasing INA with increasing heat and duration was observed.

5.6.2   Dynamic light scattering

Figure 5.21 shows the hydrodynamic radius R_h of the heat-treated samples (except the 24 h at 98 °C), the error is estimated at 10 % of the value. R_h before IAP is about 980 nm, almost double the 550 nm after IAP. The heat-treated samples show a decrease in particle size with increasing incubation temparture, similar to the INA. R_h decreases from 550 nm after IAP, to 500 nm after 1 h at 40 °C, to 350 nm after 1 h at 78 °C, and to 260 nm after 1 h at 98 °C. All R_h values are bigger than the 0.2 μm (200 nm) filter used during the BPWW preparation. This can be explained by the hydration shell, which is included in R_h.

5.6.3   Summary and technical discussion

Generally, INA decreased when exposed to heat. The activity decreased with increasing temperature and duration of heat exposure. At first glance, the INMs active above -15 °C are less heat stable than the INMs below -15 °C. However, since the INMs active at higher temperatures occur in much lower numbers. The effect is more
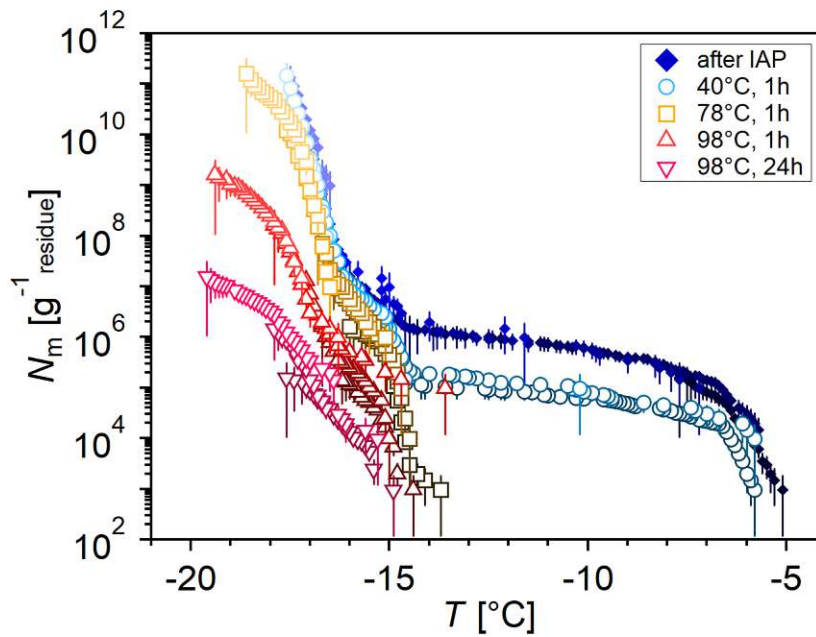
Figure 5.20: Cumulative number of INMs ($N_m(T)$) per gram residue after freeze-drying in heat treated BPWW measured with TINA. The error was calculated using the Gaussian error propagation. BPWW after IAP was once heated to 40 °C, 78 °C and 98 °C for 1 h (light blue circles, yellow squares, red upward triangles) and to 98 °C for 24 h (pink downward triangles). INA was measured using TINA. Native BPWW after IAP (solid dark blue diamonds, from figure 5.13) are also plotted for reference.
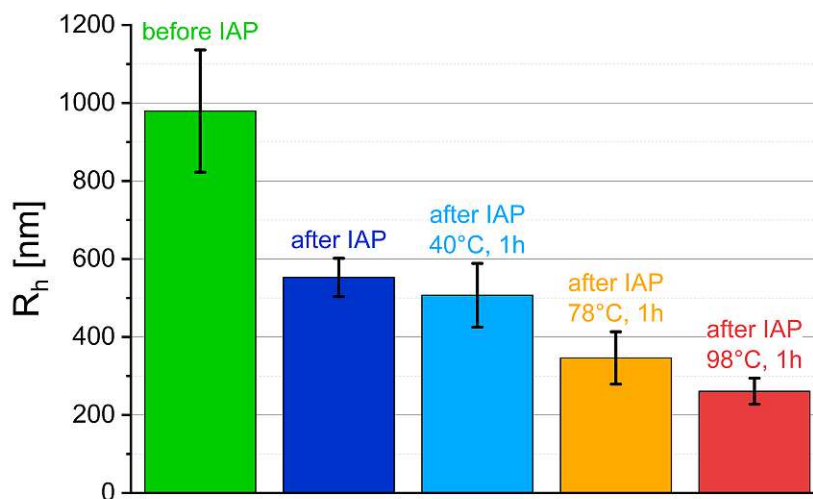

Figure 5.21: Hydrodynamic radius R_h of particles in solution of BPWW before and after IAP and heat treated samples.

prominent as they fall below the detection limit, while the INMs below $-15\,°\text{C}$ are just slightly shifted downwards. Similarly, the longer duration of the heat treatment, the more INMs are deactivated (or destroyed) since the sample treated at $98\,°\text{C}$ for $24\,\text{h}$ shows a significant decrease in INM concentration overall.

The DLS measurements showed a correlation of decreasing particle size (derived from the measured R_h value) with decreasing INA. However, the DLS measurements only show the biggest particles within the sample, which do not have to be the INMs.

Chapter 6

In depth discussion of INMs

The discussion is separated into three main parts. First, Tables 6.1 and 6.2 summarize all experiments, showing the main conclusions and technical limitations. The second part is section 6.1 and will mainly discuss the two tables, put the main findings into perspective, and finally, result in a new hypothesis for birch INMs. The third part is section 6.2, which will discuss the influence of droplet size when measuring INA.

6.1 New insights to birch INMs

6.1.1 At what temperature are birch INMs active?

TINA measurements of BPWW (see section 5.2) showed three steps with T_{on} of BPWW at $-6\,°C$, $-15\,°C$ and $-18\,°C$ respectively. Previously only two steps with T_{on} at $-15\,°C$ and $-18\,°C$ have been reported for BPWW [44, 46]. Although the activity at $-6\,°C$ was not recognized before, Dreischmeier *et al.* [46] depicted a similar activity at a temperature of up to $-6\,°C$. Surprisingly in her Ph.D. thesis Dreischmeier [108] attributed this activity to the pollen grain rather than the INMs.

The presented results clearly show that the pollen grains can not be responsible for this remarkably high T_{on}, as the $0.2\,\mu m$ filtration in the BPWW preparation procedure removes all pollen grains. The filters used have pore sizes of $0.2\,\mu m$, and birch pollen has sizes of around $20\,\mu m$. Even small fragments and SPPs (with sizes of $0.25\,\mu m$ to $4.5\,\mu m$) are filtered off as shown by Pummer *et al.* [32].

Interestingly, the INA up to $-6\,°C$ varied between different batches of BPWW. A possible explanation is contamination of pollen since the INA varied, and microorganisms are usually linked to activity at these high temperatures ($-10\,°C$ and above), e.g. bacteria like *P. syringae* or fungi like *Fusarium spp*. We even found microorganisms on some pollen batches, which is unsurprising as tree pollen is a biological sample collected from living trees in farms or forests, which are non-sterile environments per se. The microorganisms are likely bacteria due to their small size of $2\,\mu m$ to $5\,\mu m$. Cultivation under various conditions showed that they indeed show INA, but only at and below $-15\,°C$. Since most known bacterial IN are membrane-bound proteins (e.g. *P. syringae*), the $0.2\,\mu m$ filtration removes the bacteria and thus the INMs. The variation in INA at up to $-6\,°C$ is likely due to the biological nature of the sample. Unlike most commercial chemicals, biological samples can vary and are not always the same.

Table 6.1: Overview of results (1)

Experiment	Main conclusion	Technical limitation
Section 5.1: Background measurements of INA setups (page 43)		
TINA	Homogeneous nucleation starts at $-21\,°C$	no measurements below $-21\,°C$ possible
VODCA	Homogeneous nucleation starts at $-32\,°C$	no measurements below $-32\,°C$ possible
Section 5.2: Ice nucleation activity of birch pollen (page 44)		
TINA	T_{on} at $-6\,°C$, $-15\,°C$ and $-17\,°C$	Variation between BPWW batches
Microorganisms	Contamination found, active $<-15\,°C$	Cultivation is a selective process
Storage & rupture	No influence	-
INA setup	Different results	See section 6.2
Section 5.3: Freeze-thaw cycles (page 52)		
Freeze-thaw cycles	High reproducibility, Simultaneous N_m decrease at $-18\,°C$ with increase at $-15\,°C$	-
Section 5.4: Size analysis (page 53)		
MWCO filtrations	TINA: INMs $<10\,$kDa, T_{on} decreases with decreasing size; VODCA: INMs $>30\,$kDa	Filter uncertainty $10\,\%$ to $20\,\%$; Filtration likely causes dilution effect
Single 30kDa filtration	N_m concentration decreases by 10^6	-
SEC	-	Would need optimization
SDS Page	MWCO distinguishable	Gel likely overloaded

Table 6.2: Overview of results (2)

Experiment	Main conclusion	Technical limitation
Section 5.5: IAP and analytics (page 58)		
IAP	N_m above $-15\,°C$ increased by factor 10	Multiple IAP cycles might improve result
CD spectroscopy	Protein-like signals	No further interpretation because other components might interfere with signal
Bradford assay	No significant change in total protein content before and after IAP	Possible interference from small sugars
SDS Page	Minor difference before and after IAP	-
SEC	Minor signal differences before and after IAP	would need optimizing
IR spectroscopy	Protein and polysaccharide signals	-
Fluorescence spectr.	After IAP less intensity in autofluorescenct amino acid region	-
Section 5.6: Heat treatments (page 68)		
TINA	INA decreases with time and temperature of heat treatment; INA $>-15\,°C$ affected by $40\,°C$, lost at $78\,°C$; INA $<-15\,°C$ more stable but also affected	-
DLS	R_h decreases with increasing temperature of heat treatment	Only shows biggest particles, which are not necessarily INMs

73

Still, a slight uncertainty remains because a few bacteria that secrete INMs have been found, like *Lysinibacillus parviboronicapiens* [109]. In addition, cultivating microorganisms is always a selective process. Hence, even the most thorough testing would not lead to complete certainty. We can even question whether it is necessary to determine if the INA stems from pollen or microorganisms. Assuming these INMs are from microorganisms growing on pollen and the whole tree as part of the tree's microbiome and the microbiome being similar for the whole species, the origin is less critical when these INMs enter the atmosphere and nucleate ice, influencing weather and climate.

In additional experiments, we found that the storage conditions and pollen rupture did not influence the INA. Interestingly, the results varied when using different INA measurement setups. However, after various experiments, we hypothesize that TINA and VODCA do not contradict each other but are complementary. Therefore we have to refer to section 6.2, which discusses the influence of droplet size on INA measurements.

Finally, we conclude that all three T_{on} ($-6\,°C$, $-15\,°C$ and $-18\,°C$) originate from INMs from the pollen. The biological nature of the sample likely causes the varying concentration between $-6\,°C$ to $-15\,°C$. Still, minor uncertainties remain regarding the microorganism contamination, which is unlikely to be dissolved.

6.1.2 What size are birch INMs?

BPWW was filtered with five different MWCO filters (10, 30, 50, 100 and 300 kDa), and the INA of the filtrates was measured using TINA and VODCA. These simple filtrations are an easy way to gather information about the size of the INMs. Previous studies reported INMs from birch pollen to be >100 kDa [32, 46]. In contrast, our results showed INMs are <10 kDa according to TINA or >30 kDa according to VODCA. For the VODCA measurements, we must add that the activity in the 50 kDa filtrate was low and, the filter uncertainty is about 10 % to 20 %. Therefore the INMs could also be >50 kDa. Nonetheless, the TINA results, the VODCA results, and the literature values all contradict each other.

The TINA results further show decreasing T_{on} with decreasing filter size, which could mean larger INMs are active at higher temperatures. Since INMs at lower temperatures occur in higher numbers (up to 10^6 more), filtration could be seen as a dilution.. The measured dilution series of the single 30 kDa filtration shows that the activity between $-6\,°C$ to $-15\,°C$ is lost, which could mean INMs >30 kDa are the ones active in this range. The graph also shows that the concentration of INMs active between $-15\,°C$ to $-21\,°C$ is reduced by a factor of 10^6. Assuming the filtration is a simple dilution, then the graph will shift to lower concentrations, as we observe. The limit of detection will cut off the graph at a particular concentration, which will then define T_{on}. This effect can explain the TINA results, assuming the smaller filters cause higher dilutions since more INMs remain in the filter. The dilution, or downward shifted graph, explains the decreasing T_{on} with decreasing filter size and the decreasing concentration between $-15\,°C$ to $-21\,°C$.

However, filtration as a simple dilution effect still needs to explain the contradiction of the TINA and VODCA results and why both contradict previous studies. Section 6.2 will discuss the influence of droplet volume on INA measurements. In short, the smaller the droplet volume in the INA assay, the lower the sensitivity. This effect explains that the less sensitive VODCA setup (pL droplets) does not measure INA in

the small filtrates, unlike the TINA setup (µL droplets). Furthermore, past INA and MWCO filtration studies used pL INA assays [32, 46]. These studies still contradict the VODCA results. However, they mostly use sequential filtrations, so the filtrate of the largest filter is filtered again using the next smaller filter. Hence, the dilution is higher with each filtration step, unlike the single filtrations from this work.

The SEC and the SDS Page measurements did not bring any additional information, except that the filtrates show different bands and, differentiation of filtrates is possible, at least with SDS Page.

To summarize, the INMs are <10 kDa, and the filtration liekly causes a dilution effect. We suggest that the combination of high dilution effects and low sensitivity INA assays leads to the INMs appearing much bigger than they actually are, as reported in previous studies [32, 46, 59].

6.1.3 What are birch INMs from a chemical perspective?

The main goal of this thesis is to gather more information or even elucidate the chemical nature of birch INMs. This knowledge will allow us to track birch INMs in the atmosphere and reveal their influence on weather and climate.

Some studies suggest birch INMs are polysaccharides [32, 46, 59]. The main arguments for polysaccharides are high temperature stability up to 187 °C and various chemical and enzymatic experiments [32, 46, 59]. Raman and IR spectra support arguments suggesting polysaccharides. In contrast, other studies suggest proteins to be at least involved [47, 73, 74]. For example, Burkart *et al.* [47] argue for proteinaceous involvement, supported by fluorescence measurements and a decrease in INA after chemical treatment aimed at denaturing proteins. Burkart *et al.* [47] also suggest glycoproteins, which explain polysaccharide and proteinaceous signals. However, there is no final conclusion yet.

Firstly we focused on purifying the INMs using IAP. After IAP, INA increased, and hence INMs were purified. Especially the INA between -6 °C to -15 °C was increased by a factor of 10. The purified "after IAP" sample was then analyzed and compared to the "before IAP" at the same concentration to get more insights to understand the chemistry of birch INMs.

As measured in previous studies, IR spectra showed protein and polysaccharides signals. Before and after IAP only showed minor deviations, not allowing further interpretation of the chemical nature of INMs. Also, SEC showed minor changes, but no further interpretations were possible. SDS Page shows that proteins of varying sizes are indeed in the sample, but also, in this case, the deviations were too minor for further interpretation. Interestingly, fluorescence spectroscopy showed that after IAP, the signal of autofluorescent amino acids (Phe, Trp, Tyr) decreased by a factor of 10. However, the Bradford assay shows no significant change in protein content. In combination, the results suggest a net loss of Phe, Trp, and Tyr, which means that the purified ice affine proteins have fewer aromatic acids. CD spectroscopy clearly shows protein-like signals. However, we cannot rule out other substances interfering with the signals.

In literature, many INM studies involve heat treatments to distinguish biological from inorganic IN since biomolecules are generally less heat stable. Polysaccharides, although large biomolecules, are usually heat stable, while proteins denature and lose their activity. Therefore we tested the influence of heat on our sample. Interestingly,

the INA at high temperatures ($-6\,°\mathrm{C}$ to $-15\,°\mathrm{C}$) was strongly affected by heat. The INA between $-6\,°\mathrm{C}$ to $-15\,°\mathrm{C}$ decreased after $1\,\mathrm{h}$ at $40\,°\mathrm{C}$ and lost after $1\,\mathrm{h}$ at $78\,°\mathrm{C}$. The INA at lower temperatures was more heat stable but not unaffected, as it strongly decreased after heat treatment at $98\,°\mathrm{C}$. The heat treatments show that birch INMs are affected by relatively low heat ($<100\,°\mathrm{C}$), suggesting proteins are involved. Furthermore, IR and CD spectra of a heat-treated sample ($1\,\mathrm{h}$ at $98\,°\mathrm{C}$) were measured. While the IR shows almost no difference, the CD spectra show that the signal is strongly affected in the first region ($190\,\mathrm{nm}$ to $210\,\mathrm{nm}$).

In summary, proteins and polysaccharides were found even in a purified sample. The heat treatments strongly suggest the INMs to be proteinaceous or proteins to be at least involved in the INA of birch pollen. However, a definitive answer is impossible since no experiment showed a clear correlation to INA. In future experiments, additional IAP cycles would be beneficial to purify the sample even more. Also, mass spectroscopy could finally offer the last missing piece of this puzzle.

6.1.4 Agglomerate hypothesis

From each set of experiments, we made separate conclusions. This section will combine all three conclusions and produce a new hypothesis for INMs from birch pollen. To recap, these three main conclusions were explained in the last three sections:

- We found three distinct steps with T_{on} at $-6\,°\mathrm{C}$, $-15\,°\mathrm{C}$ and $-18\,°\mathrm{C}$ in INA measurements from BPWW. Although some uncertainties remain, we conclude INMs from birch pollen cause all three T_{on}.

- We suggest the INMs are $<10\,\mathrm{kDa}$ and hence much smaller than the previously reported $>100\,\mathrm{kDa}$[32, 46, 59]. We explain that filtration likely causes a dilution effect and how the combination of high dilutions and low sensitivity INA assays leads to the INMs appearing much bigger than they are.

- Regarding the chemical composition of INMs, we found proteins and polysaccharide signals. The heat treatments strongly suggest that the INMs are proteinaceous or that proteins are at least involved in the INA of birch pollen. Also, complex glycoproteins such as INMs are possible.

From all these arguments we suggest INMs from birch pollen are large agglomerates built up from smaller subunits. The small units can act as IN at relatively low temperatures of about $-18\,°\mathrm{C}$. If the subunits agglomerate to larger structures, they become more effective at nucleating ice, pushing T_{on} to temperatures up to $-6\,°\mathrm{C}$. High concentrations can induce agglomeration of the subunits. The larger the agglomerates, the higher the T_{on}, whereas medium-sized agglomerates are most common and have T_{on} at $-15\,°\mathrm{C}$, and massive aggregates are very rare and show INA up to $-6\,°\mathrm{C}$.

The agglomerate hypothesis can explain the three different T_{on} and the significant concentration differences between them, which are multiple orders of magnitude. This concentration difference has a massive impact on the results of the INA measurements (see section 6.2).

Hence, the observed MWCO filtration results, suggest the filtrations cause a massive dilution effects, as shown in the single 30 kDa filtration. Many small subunits pass the filter, but not all, resulting in a dilution. Afterward, the subunits can agglomerate again and show INA. Interestingly, it could also explain the observation of the freeze-thaw cycle experiment.

The hypothesis explains the concentration decrease at $-18\,°C$ and increase at $-15\,°C$ observed during the multiple freeze-thaw cycles if we suppose repeated freezing induces agglomeration of the smaller INMs (active at $-15\,°C$) to form larger agglomerates that are active at $-15\,°C$. However, the INMs active at $-6\,°C$ are unaffected, possibly because this agglomeration requires specific conditions, which can explain why they only occur in such low numbers compared to the other INMs. Furthermore, we hypothesize that freeze drying could induce agglomeration since the residual molecules come close when removing the solvent. Proteins have large hydration shells in water, making it even harder for the subunits to agglomerate. The large hydration shells are likely what we see in our DLS measurements since particles with radii of 0.5 µm (figure 5.21 after IAP) would not pass through the 0.2 µm filter used in the BPWW preparation procedure.

The agglomerates have a relatively weak affinity, allowing gentle heat to break them apart. The results from DLS support this if the large agglomerates dissolve by heat, decreasing the INA. Moreover, if some proteinaceous subunits act as glue, and we denature them, the INA is lost, which explains our heat treatment results. However, we are unsure if all subunits are the same or if some could be polysaccharides or glycoproteins.

Further experiments will have to test the agglomeration hypothesis. This could involve multiple IAP cycles to purify the INMs even more. An experiment to test agglomeration could be to increase the concentration of the sample, e.g. by removing the solvent and testing INA afterward. Thorough analytics (e.g. mass spectrometry, IR, fluorescence) of a highly purified sample will also resolve the chemical structures of the subunits.

6.2 The influence of droplet size on ice nucleation measurements

The two different results of INA activity of BPWW measured with the two setups (shown in figure 5.4) are likely due to the difference in the analyzed sample volumes and hence sensitivity. This section discusses the limitations and advantages of both setup types. It explains the hypothesis that they are complementary and, when used together, can yield a complete picture of the INA of a particular sample.

Higher droplet volumes, as used in TINA, inevitably lead to a higher volume of the analyzed sample and, therefore, higher chances of finding IN. Thus the detection of rare IN is possible (as from BPWW at $-6\,°C$). This increase in sensitivity, however, leads to a higher background due to the volume dependency of T_{hom} 1.2.1. It has an immediate effect when comparing the freezing temperature of pure water: $T_{water}(\text{TINA})$ is about $-20\,°C$ to $-25\,°C$ and $T_{water}(\text{VODCA})$ is about $-32\,°C$ to $-35\,°C$. Hence, VODCA (and other pL assays) allows the observation of INA to about $10\,°C$ lower than TINA (and other microliter assays). Figure 6.1 on the bottom shows the increased background compared to VODCA on the right.

The upper graph of figure 6.1 shows that, according to the hypothesis, the smaller droplet volumes lead to decreased sensitivity and, therefore, a blind spot for rare IN. Measuring the same sample with both setups leads to a complete picture of the INA of a sample (see figure 5.4). A remedy for this problem could be a setup using extremely high numbers of picoliter droplets, e.g. one million droplets per sample following the argument from above, where the factor between microliter and picoliter is 10^6. In order to be practical, such a setup would need automated picoliter droplet generation and detection. Such IN-assays exist but are mostly used to study homogeneous ice nucleation [116, 117]. The setup of Stan *et al.* [116] at the time had the fastest acquisition time, with 75 measurements per second (1 measurement equals one droplet), but still would need about 4 hours of pure measurement time to measure one million droplets of a single sample.

Generally, investigating a sample with different measurement setups seems beneficial as each setup has its advantages. One factor yet to be discussed is the difference in the droplet surrounding. In VODCA (and most pL assays), sample droplets are emulsified in a solvent, while in TINA, the droplets are in a cavity. The droplet shape and its interface could further influence the freezing behavior. In VODCA, a paraffin oil surrounds the droplets, which is highly apolar. Hence, apolar substances could accumulate at the interface or even diffuse into the oil. If the INMs are apolar and diffuse into the apolar matrix, the INM concentration reduces. With TINA, the chance of substances diffusing into the PCR plate is extremely low. Still, the material could influence the arrangement of molecules, e.g. an accumulation of the apolar substances on the apolar plastic surface of the PCR tray.

In summary, many parameters still need to be taken into account when it comes to the study of heterogeneous ice nucleation and the setups used for these studies. However, we are confident that combining two INA assays, one with pL and one with μL droplets, yields a more complete picture of IN in any sample.

For our results this means, since the large, highly effective agglomerates only occur in small numbers, less sensitive INA assays do not detect them. Previous studies [32, 44–46] used similar assays and therefore did not detect this activity. Dreischmeier [108] detected activity up to $-6\,°\mathrm{C}$ but attributed this activity to the pollen grain.
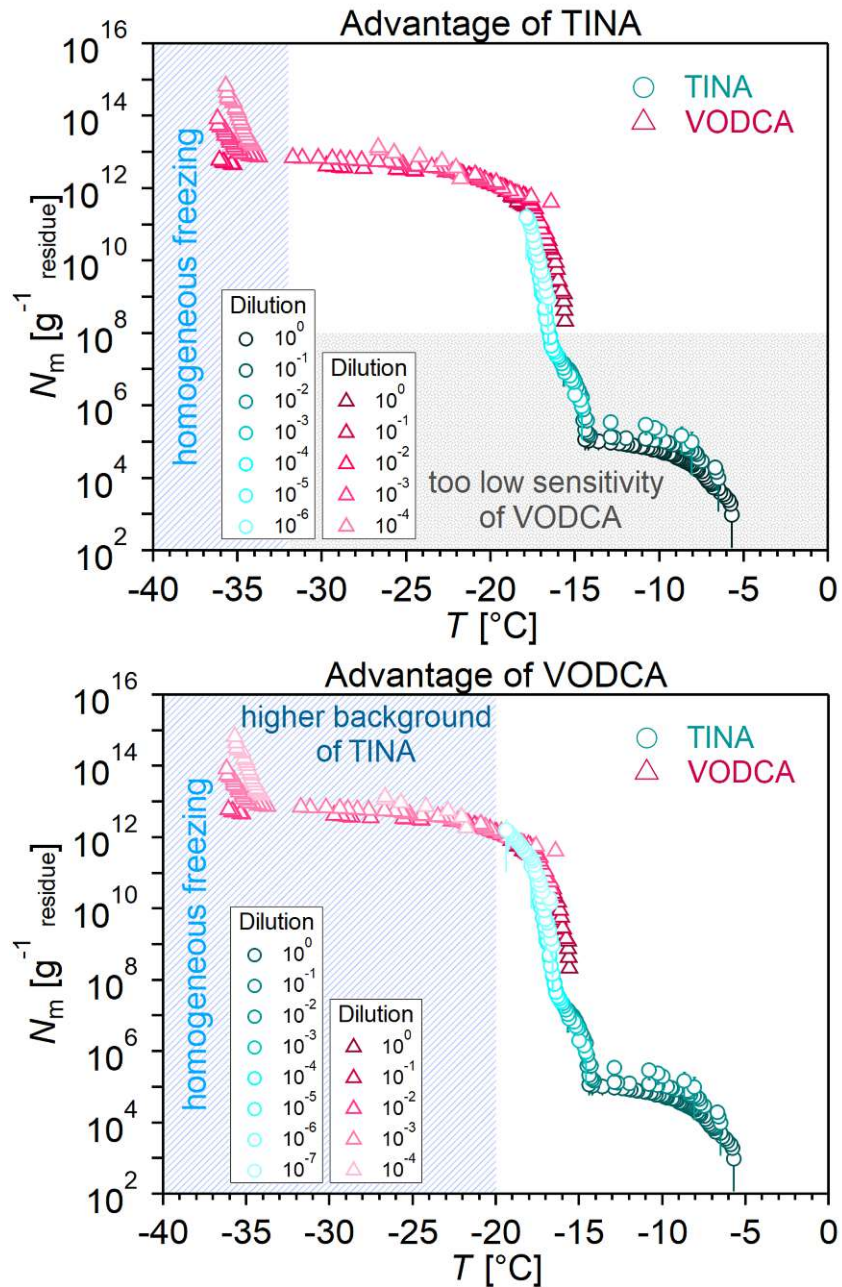
Figure 6.1: A comparison of the advantages of the TINA and VODCA setups. On the top, the advantage of TINA is shown: the higher sensitivity, due to a higher droplet volume. On the bottom, the advantage of VODCA is shown: lower background due to the smaller droplets.

Chapter 7

Conclusion

In times of climate change, understanding our climate is more critical than ever. Therefore, we must understand the influencing factors, such as biological ice nucleation. Moreover, this will help to build more accurate models, which is vital for future predictions and will help to understand what measures can be taken to preserve a habitable climate on our planet.

With this purpose, we try to understand INMs from the pollen of the species *Betula pendula*. The INMs from birch pollen were, among other pollen, the ones with the highest INA. Huge birch forests all over the globe could serve as a potential INM source and thereby significantly influence cloud glaciation and, thus, climate. This work combines various ice nucleation and analytical measurements, all representing different pieces of the same puzzle, which on their own only yield small information but, in sum, allow significant conclusions.

INA of birch INMs at temperatures up to -6°C

Ice nucleation measurements of BPWW with the TINA setup revealed INA at three different temperatures: $-6\,°C$, $-15\,°C$ and $-18\,°C$. While the latter two temperatures have been previously reported [44, 46], the INA activity at $-6\,°C$ is novel. After various experiments, we conclude that this activity stems from the pollen. However, we can not exclude all possible interferences. Throughout all measurements done for this work, the activity at $-6\,°C$ varied more than at the other freezing temperatures, probably due to the relatively lower concentration. For this reason, previous studies did not recognize this activity or attribute it to the pollen grain [32, 46]. However, this region is observable due to increased sensitivity from VODCA to TINA.

The sensitivity issue is discussed in section 6.2 and visualized in figure 5.4. The proposed hypothesis could require reevaluating INA studies of many pollen and other substances.

The size of birch INMs can be below $10\,\mathrm{kDa}$

We found INA after we filtered the INMs from BPWW through a $10\,\mathrm{kDa}$ MWCO filter. Thus, birch INMs are much smaller than the previously reported $>100\,\mathrm{kDa}$ [32, 46]. T_{on} of the fraction $<10\,\mathrm{kDa}$ was about $-18\,°C$. The $<100\,\mathrm{kDa}$ fraction had a T_{on} of $-15\,°C$. Thus, birch INMs probably have a bigger size range (of at least a factor of 10) than the previously reported $>100\,\mathrm{kDa}$ [32, 46]. Interestingly, we found a decrease

in T_{on} with decreasing size, which could be a dilution effect, as the INMs active at lower temperatures occur in much higher numbers.

Additionally, we found a decreasing INM concentration after heat treatment with increasing temperatures. In combination with the DLS measurements, we saw a decreasing size of particles in the solution. This suggests smaller INMs show lower T_{on}, assuming the DLS measurements show the INM sizes rather than any other large particles or molecules present in the sample.
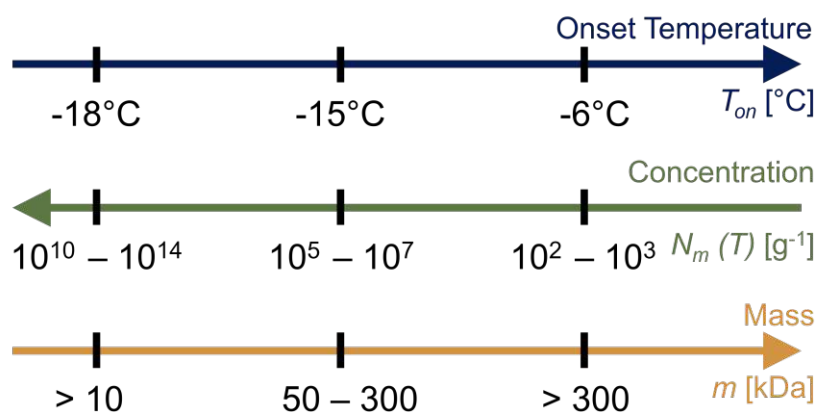
Figure 7.1: Illustration of the results: First arrow shows the three reported T_{on} (blue); Second arrow shows the concentration (N_m) range of INMs g^{-1} pollen (green), each corresponding to the three temperatures shown directly above; The third arrow shows the mass of the INMs active the the corresponding temperature (marked at first arrow) according to the MWCO filtrations (yellow). The arrows point to increasing numbers (temperature, concentration, mass).

IAP successfully increased INM concentration

We were able to concentrate the INMs active above $-15\,°\mathrm{C}$ by a factor of 10 after a single cycle of IAP. We did not directly quantify the purification of the INMs but indirectly assume it through the increasing INM concentration.

Are birch INMs proteins or polysaccharides?

Polysaccharides were long thought to be the INM from birch pollen [32, 44, 46], but some studies suggest proteins [47, 73, 119] as INMs similar to many bacterial INMs such as *inaZ* from *P. syringae* [31].

We observed protein signals with various analytical methods - fluorescence, IR, and CD spectroscopy. IR spectroscopy, in addition, also showed polysaccharide signals. It is clear that in BPWW, we can find polysaccharides and proteins. We could not observe a direct correlation between the protein or polysaccharide signals and INA with these methods. However, we measured the protein content before and after IAP and did not observe a significant change. Thus, although proteins are in the BPWW, their concentration did not increase with the increasing INA after IAP. At the same time, heat treatments of $1\,\mathrm{h}$ up to $98\,°\mathrm{C}$ significantly decrease INA. Since polysaccharides are usually quite heat-stable, this would suggest proteins as INMs.
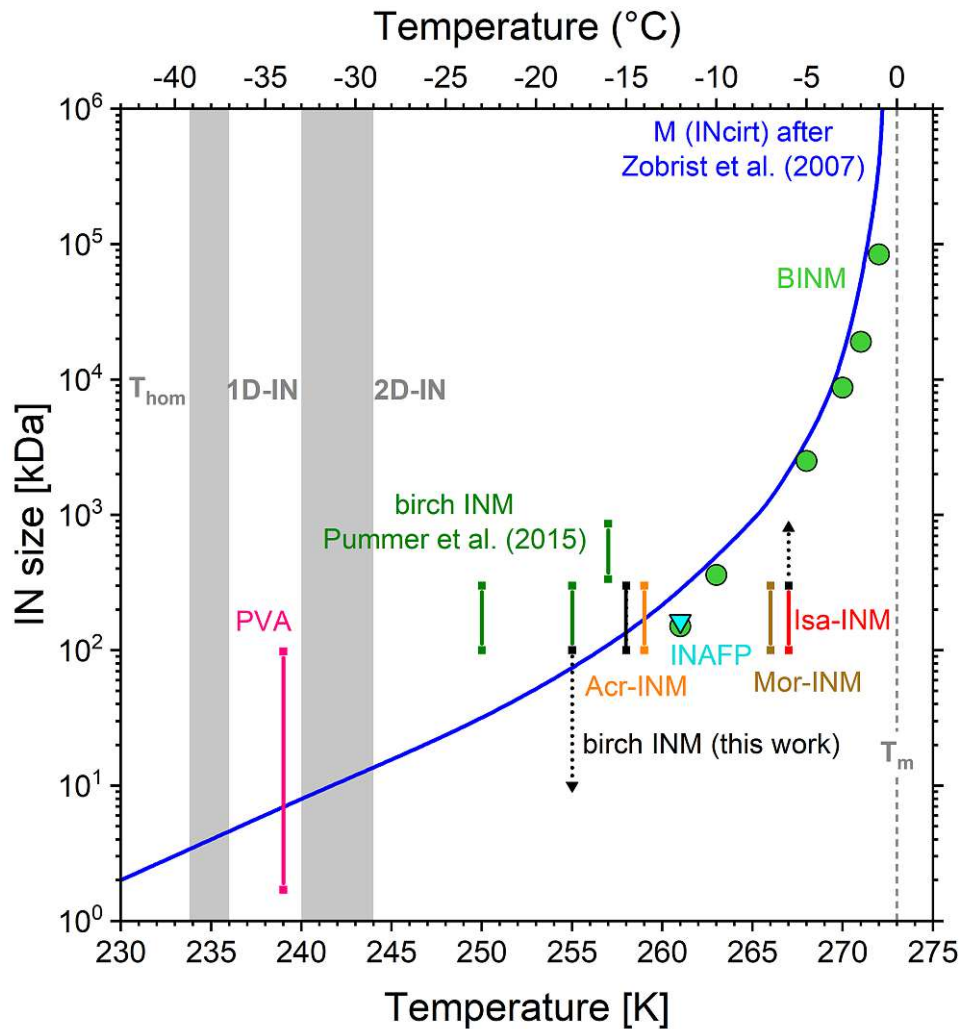
Figure 7.2: The dependence of the freezing temperature on size for different types of IN, adapted from figure 4 of Pummer *et al.* [59]. The blue curve is the calculated critical ice cluster size derived from classical nucleation theory [118]. The results from this thesis are added into the graph (in black) and show that the newly found sizes for birch INMs, fit better to the blue curve, than the previous reported results [59]. The dotted lines and arrows mark the possible size range of the domains, since only the cutoff size of the filter is known (square). The graph further shows the region where it is assumed that domains of 1-D and 2-D templates act as IN. The grey areas mark the transition regions between the domains. The acronyms Acr, Isa, and Mor stand for *Acremonium implicatum*, *Isaria farinosa*, *Mortierella alpina*.

Agglomerate hypothesis

Combining all results, we suggest INMs from birch pollen are large agglomerates built up from small subunits. The small units can act as IN at relatively low temperatures of about $-18\,°\text{C}$. If the subunits agglomerate to larger structures, they become more effective at nucleating ice, pushing T_{on} to temperatures up to $-6\,°\text{C}$. High concentrations can induce agglomeration of the subunits. The larger the agglomerates, the higher the T_{on}. We hypothesize that the agglomerates have a relatively weak affinity, allowing gentle heat to break them apart, which leads to reduced INA. Moreover, if some proteinaceous subunits act as glue, and we denature them, then INA is lost due to hindered re-agglomeration. However, we have yet to determine if all subunits are the same or if some could be polysaccharides or glycoproteins.

Final remarks and outlook

In this work, we found that although we know a bit about INMs from birch pollen, there are still many unknowns. Past studies might have overlooked some essential aspects, such as a T_{on} of up to $-6\,°\text{C}$. Also, the size range is different than previously reported. These two aspects are most likely due to the measurement setups used. Showing the wide variety of freezing setups is problematic since two setups can see two completely different pictures. As we have done here, a combination of setups seems beneficial if not necessary.

Furthermore, although we took significant steps forward by postulating our agglomerate hypothesis, we did not identify the INMs from birch pollen. Future studies can use advanced mass spectrometry and proteomics after multiple IAP steps, which could offer the final piece of information missing in the complex puzzle of birch INMs.

Once we understand birch INMs, it will likely be easier to identify INMs from other trees and plants. Additionally, we can work towards understanding ice nucleation mechanisms from these INMs and other biological items. Further, using the INM as a marker in specialized measurement setups will help understand cloud glaciation's impact. A pretty exciting approach could be measuring vertical protein and polysaccharide concentration profiles with drone-based setups, as shown by Bieber *et al.* [17]. This information will allow the calculation of a biological IN flux, which modelers can use to improve understanding of birch's local and global impact or, more generally, tree INMs.

References

1. Crutzen, P. J. in *Earth System Science in the Anthropocene* 13–18 (Springer-Verlag, Berlin/Heidelberg, 2006).

2. IPCC. *Global Warming of 1.5°C: IPCC Special Report on impacts of global warming of 1.5°C above pre-industrial levels in context of strengthening response to climate change, sustainable development, and efforts to eradicate poverty* 1st ed. (Cambridge University Press, 2022).

3. IPCC. *Impacts, Adaptation and Vulnerability. Contribution of Working Group II to the Sixth Assessment Report of the Intergovernmental Panel on Climate Change* 1st ed. (Cambridge University Press, 2022).

4. IPCC. *Summary for Policymakers. In: Climate Change 2021: The Physical Science Basis. Contribution of Working Group I to the Sixth Assessment Report of the Intergovernmental Panel on Climate Change* 3-32 (Cambridge University Press, Cambridge, UK and NY,USA, 2021).

5. Barry, R. G. & Hall-McKim, E. A. *Essentials of the Earth's Climate System* (Cambridge University Press, 2014).

6. Barry, R. G. & Hall-McKim, E. A. *Essentials of the Earth's climate system* 259 pp. (Cambridge University Press, Cambridge ; New York, 2014).

7. Barry, R. G. & Chorley, R. J. *Atmosphere, weather and climate: Eighth edition* Publication Title: Atmosphere, Weather and Climate: Eighth Edition (2003).

8. Wallace, J. M. & Hobbs, P. V. in *Atmospheric Science (Second Edition)* 1–23 (Academic Press, San Diego, 2006).

9. Lamb, D. & Verlinde, J. *Physics and chemistry of clouds* 584 pp. (Cambridge University Press, Cambridge ; New York, 2011).

10. Lohmann, U., Lüönd, F. & Mahrt, F. *An introduction to clouds: From the microscale to climate* Publication Title: An Introduction to Clouds: From the Microscale to Climate (2016).

11. Ickes, L., Welti, A., Hoose, C. & Lohmann, U. Classical nucleation theory of homogeneous freezing of water: thermodynamic and kinetic parameters. *Physical Chemistry Chemical Physics* **17.** Publisher: The Royal Society of Chemistry, 5514–5537 (2015).

12. Volmer, M. & Weber, A. Keimbildung in übersättigten Gebilden. *Zeitschrift für Physikalische Chemie* **119U,** 277–301 (1926).

13. Turnbull, D. & Fisher, J. C. Rate of Nucleation in Condensed Systems. *The Journal of Chemical Physics* **17,** 71–73 (1949).

References

14. Murray, B. J., O'sullivan, D., Atkinson, J. D. & Webb, M. E. Ice nucleation by particles immersed in supercooled cloud droplets. *Chemical Society Reviews* **41** (2012).

15. Pruppacher, H. R. & Klett, J. D. in *Microphysics of Clouds and Precipitation* 9–55 (Springer Netherlands, Dordrecht, 1978).

16. Balibar, S. & Caupin, F. Nucleation of crystals from their liquid phase. *Comptes Rendus Physique* **7,** 988–999 (2006).

17. Bieber, P., Seifried, T. M., Burkart, J., Gratzl, J., Kasper-Giebl, A., Schmale, D. G. & Grothe, H. A Drone-Based Bioaerosol Sampling System to Monitor Ice Nucleation Particles in the Lower Atmosphere. *Remote Sensing* **12** (2020).

18. Wang, P. K. *Physics and Dynamics of Clouds and Precipitation* (2013).

19. Durant, A. J. Evaporation freezing by contact nucleation inside-out. *Geophysical Research Letters* **32,** L20814 (2005).

20. Kanji, Z. A., Ladino, L. A., Wex, H., Boose, Y., Burkert-Kohn, M., Cziczo, D. J. & Krämer, M. Overview of Ice Nucleating Particles. *Meteorological Monographs* **58,** 1.1–1.33 (2017).

21. Niedermeier, D., Shaw, R. A., Hartmann, S., Wex, H., Clauss, T., Voigtländer, J. & Stratmann, F. Heterogeneous ice nucleation: Exploring the transition from stochastic to singular freezing behavior. *Atmospheric Chemistry and Physics* **11** (2011).

22. Vali, G. Quantitative Evaluation of Experimental Results an the Heterogeneous Freezing Nucleation of Supercooled Liquids. *Journal of the Atmospheric Sciences* **28** (1971).

23. Pruppacher, H. R. & Klett, J. D. *Microphysics of clouds and precipitation* 2nd rev. and enl. ed. *Atmospheric and oceanographic sciences library* **v. 18.** 954 pp. (Kluwer Academic Publishers, Dordrecht ; Boston, 1997).

24. DeMott, P. J., Prenni, A. J., Liu, X., Kreidenweis, S. M., Petters, M. D., Twohy, C. H., Richardson, M. S., Eidhammer, T. & Rogers, D. C. Predicting global atmospheric ice nuclei distributions and their impacts on climate. *Proceedings of the National Academy of Sciences* **107,** 11217–11222 (2010).

25. Niedermeier, D., Augustin-Bauditz, S., Hartmann, S., Wex, H., Ignatius, K. & Stratmann, F. Can we define an asymptotic value for the ice active surface site density for heterogeneous ice nucleation? *Journal of Geophysical Research: Atmospheres* **120,** 5036–5046 (2015).

26. Mertes, S., Verheggen, B., Walter, S., Connolly, P., Ebert, M., Schneider, J., Bower, K. N., Cozic, J., Weinbruch, S., Baltensperger, U. & Weingartner, E. Counterflow Virtual Impactor Based Collection of Small Ice Particles in Mixed-Phase Clouds for the Physico-Chemical Characterization of Tropospheric Ice Nuclei: Sampler Description and First Case Study. *Aerosol Science and Technology* **41,** 848–864 (2007).

27. Kanji, Z. A., Florea, O. & Abbatt, J. P. D. Ice formation via deposition nucleation on mineral dust and organics: dependence of onset relative humidity on total particulate surface area. *Environmental Research Letters* **3,** 025004 (2008).

28. Vonnegut, B. The Nucleation of Ice Formation by Silver Iodide. *Journal of Applied Physics* **18,** 593–595 (1947).

29. Häusler, T., Witek, L., Felgitsch, L., Hitzenberger, R. & Grothe, H. Freezing on a Chip-A new approach to determine heterogeneous ice nucleation of micrometer-sized water droplets. *Atmosphere* **9** (2018).

30. Niehaus, J. & Cantrell, W. Contact Freezing of Water by Salts. *The Journal of Physical Chemistry Letters* **6,** 3490–3495 (2015).

31. Green, R. L. & Warren, G. J. Physical and functional repetition in a bacterial ice nucleation gene. *Nature* **317,** 645–648 (1985).

32. Pummer, B. G., Bauer, H., Bernardi, J., Bleicher, S. & Grothe, H. Suspendable macromolecules are responsible for ice nucleation activity of birch and conifer pollen. *Atmospheric Chemistry and Physics* **12** (2012).

33. Fröhlich-Nowoisky, J., Hill, T. C., Pummer, B. G., Yordanova, P., Franc, G. D. & Pöschl, U. Ice nucleation activity in the widespread soil fungus Mortierella alpina. *Biogeosciences* **12** (2015).

34. Lohmann, U. & Feichter, J. Global indirect aerosol effects: a review. *Atmospheric Chemistry and Physics* **5,** 715–737 (2005).

35. Matus, A. V. & L'Ecuyer, T. S. The role of cloud phase in Earth's radiation budget. *Journal of Geophysical Research: Atmospheres* **122,** 2559–2578 (2017).

36. Lau, K. M. & Wu, H. T. Warm rain processes over tropical oceans and climate implications. *Geophysical Research Letters* **30** (2003).

37. Hoose, C. & Möhler, O. Heterogeneous ice nucleation on atmospheric aerosols: a review of results from laboratory experiments. *Atmospheric Chemistry and Physics* **12,** 9817–9854 (2012).

38. Morris, C. E., Georgakopoulos, D. G. & Sands, D. C. Ice nucleation active bacteria and their potential role in precipitation. *Journal de Physique IV (Proceedings)* **121,** 87–103 (2004).

39. Maki, L. R., Galyan, E. L., Chang-Chien, M. M. & Caldwell, D. R. Ice nucleation induced by pseudomonas syringae. *Applied microbiology* **28** (1974).

40. Pouleur, S., Richard, C., Martin, J. & Antoun, H. Ice nucleation activity in Fusarium acuminatum and Fusarium avenaceum. *Applied and Environmental Microbiology* **58** (1992).

41. Diehl, K., Matthias-Maser, S., Jaenicke, R. & Mitra, S. K. The ice nucleating ability of pollen: Part II. Laboratory studies in immersion and contact freezing modes. *Atmospheric Research* **61** (2002).

42. Diehl, K., Quick, C., Matthias-Maser, S., Mitra, S. K. & Jaenicke, R. The ice nucleating ability of pollen Part I: Laboratory studies in deposition and condensation freezing modes. *Atmospheric Research* **58** (2001).

43. Pummer, B. G. *Ice nucleation activity of pollen and fungal spores* PhD thesis (Technische Universität Wien, Vienna, 2013).

44. O'Sullivan, D., Murray, B. J., Ross, J. F., Whale, T. F., Price, H. C., Atkinson, J. D., Umo, N. S. & Webb, M. E. The relevance of nanoscale biological fragments for ice nucleation in clouds. *Scientific Reports* **5** (2015).

45. Augustin, S., Wex, H., Niedermeier, D., Pummer, B., Grothe, H., Hartmann, S., Tomsche, L., Clauss, T., Voigtländer, J., Ignatius, K. & Stratmann, F. Immersion freezing of birch pollen washing water. *Atmospheric Chemistry and Physics* **13** (2013).

46. Dreischmeier, K., Budke, C., Wiehemeier, L., Kottke, T. & Koop, T. Boreal pollen contain ice-nucleating as well as ice-binding 'antifreeze' polysaccharides. *Scientific Reports* **7.** Number: 1 Publisher: Nature Publishing Group, 41890 (2017).

47. Burkart, J., Gratzl, J., Seifried, T. M., Bieber, P. & Grothe, H. Isolation of subpollen particles (SPPs) of birch: SPPs are potential carriers of ice nucleating macromolecules. *Biogeosciences* **18** (2021).

48. Taylor, P. E., Flagan, R. C., Miguel, A. G., Valenta, R. & Glovsky, M. M. Birch pollen rupture and the release of aerosols of respirable allergens. *Clinical <html_ent glyph="@amp;" ascii="&"/> Experimental Allergy* **34,** 1591–1596 (2004).

49. Bacsi, A., Choudhury, B., Dharajiya, N., Sur, S. & Boldogh, I. Subpollen particles: Carriers of allergenic proteins and oxidases. *Journal of Allergy and Clinical Immunology* **118,** 844–850 (2006).

50. Grote, M., Valenta, R. & Reichelt, R. Abortive pollen germination: A mechanism of allergen release in birch, alder, and hazel revealed by immunogold electron microscopy. *Journal of Allergy and Clinical Immunology* **111,** 1017–1023 (2003).

51. Wozniak, M. C., Solmon, F. & Steiner, A. L. Pollen Rupture and Its Impact on Precipitation in Clean Continental Conditions. *Geophysical Research Letters* **45,** 7156–7164 (2018).

52. Steiner, A. L., Brooks, S. D., Deng, C., Thornton, D. C. O., Pendleton, M. W. & Bryant, V. Pollen as atmospheric cloud condensation nuclei. *Geophysical Research Letters* **42,** 3596–3602 (2015).

53. Mikhailov, E. F., Ivanova, O. A., Nebosko, E. Y., Vlasenko, S. S. & Ryshkevich, T. I. Subpollen Particles as Atmospheric Cloud Condensation Nuclei. *Izvestiya, Atmospheric and Oceanic Physics* **55,** 357–364 (2019).

54. D'Amato, G., Liccardi, G. & Frenguelli, G. Thunderstorm-asthma and pollen allergy. *Allergy* **62,** 11–16 (2007).

55. Suphioglu, C., Singh, M., Taylor, P., Knox, R., Bellomo, R., Holmes, P. & Puy, R. Mechanism of grass-pollen-induced asthma. *The Lancet* **339,** 569–572 (1992).

56. Felgitsch, L., Baloh, P., Burkart, J., Mayr, M., Momken, M. E., Seifried, T. M., Winkler, P., Schmale, D. G. & Grothe, H. Birch leaves and branches as a source of ice-nucleating macromolecules. *Atmospheric Chemistry and Physics* **18** (2018).

57. Seifried, T. M., Bieber, P., Felgitsch, L., Vlasich, J., Reyzek, F., Schmale, D. G. & Grothe, H. Surfaces of silver birch (Betula pendula) are sources of biological ice nuclei: In vivo and in situ investigations. *Biogeosciences* **17** (2020).

58. Seifried, T. M., Reyzek, F., Bieber, P. & Grothe, H. Scots Pines (Pinus sylvestris) as Sources of Biological Ice-Nucleating Macromolecules (INMs). *Atmosphere* **14,** 266 (2023).

59. Pummer, B. G., Budke, C., Augustin-Bauditz, S., Niedermeier, D., Felgitsch, L., Kampf, C. J., Huber, R. G., Liedl, K. R., Loerting, T., Moschen, T., Schauperl, M., Tollinger, M., Morris, C. E., Wex, H., Grothe, H., Pöschl, U., Koop, T. & Fröhlich-Nowoisky, J. Ice nucleation by water-soluble macromolecules. *Atmospheric Chemistry and Physics* **15** (2015).

60. Gute, E., David, R. O., Kanji, Z. A. & Abbatt, J. P. Ice Nucleation Ability of Tree Pollen Altered by Atmospheric Processing. *ACS Earth and Space Chemistry* **4** (2020).

61. Seifried, T. M., Bieber, P., Kunert, A. T., Schmale, D. G., Whitmore, K., Fröhlich-Nowoisky, J. & Grothe, H. Ice Nucleation Activity of Alpine Bioaerosol Emitted in Vicinity of a Birch Forest. *Atmosphere* **12,** 779 (2021).

62. Hoose, C., Kristjánsson, J. E. & Burrows, S. M. How important is biological ice nucleation in clouds on a global scale? *Environmental Research Letters* **5,** 024009 (2010).

63. O'Connor, D. J., Healy, D. A., Hellebust, S., Buters, J. T. M. & Sodeau, J. R. Using the WIBS-4 (Waveband Integrated Bioaerosol Sensor) Technique for the On-Line Detection of Pollen Grains. *Aerosol Science and Technology* **48,** 341–349 (2014).

64. Oteros, J., Pusch, G., Weichenmeier, I., Heimann, U., Möller, R., Röseler, S., Traidl-Hoffmann, C., Schmidt-Weber, C. & Buters, J. T. Automatic and Online Pollen Monitoring. *International Archives of Allergy and Immunology* **167,** 158–166 (2015).

65. Tummon, F., Adamov, S., Clot, B., Crouzy, B., Gysel-Beer, M., Kawashima, S., Lieberherr, G., Manzano, J., Markey, E., Moallemi, A. & O'Connor, D. A first evaluation of multiple automatic pollen monitors run in parallel. *Aerobiologia* (2021).

66. Huang, S., Hu, W., Chen, J., Wu, Z., Zhang, D. & Fu, P. Overview of biological ice nucleating particles in the atmosphere. *Environment International* **146,** 106197 (2021).

67. Abe, K., Watabe, S., Emori, Y., Watanabe, M. & Arai, S. An ice nucleation active gene of *Erwinia ananas*: Sequence similarity to those of *Pseudomonas* species and regions required for ice nucleation activity. *FEBS Letters* **258,** 297–300 (1989).

68. Hill, T. C. J., Moffett, B. F., DeMott, P. J., Georgakopoulos, D. G., Stump, W. L. & Franc, G. D. Measurement of Ice Nucleation-Active Bacteria on Plants and in Precipitation by Quantitative PCR. *Applied and Environmental Microbiology* **80,** 1256–1267 (2014).

69. Orser, C., Staskawicz, B. J., Panopoulos, N. J., Dahlbeck, D. & Lindow, S. E. Cloning and expression of bacterial ice nucleation genes in Escherichia coli. *Journal of Bacteriology* **164,** 359–366 (1985).

70. Pandey, R., Usui, K., Livingstone, R. A., Fischer, S. A., Pfaendtner, J., Backus, E. H. G., Nagata, Y., Fröhlich-Nowoisky, J., Schmüser, L., Mauri, S., Scheel, J. F., Knopf, D. A., Pöschl, U., Bonn, M. & Weidner, T. Ice-nucleating bacteria control the order and dynamics of interfacial water. *Science Advances* **2,** e1501630 (2016).

71. Lukas, M., Schwidetzky, R., Kunert, A. T., Backus, E. H., Pöschl, U., Fröhlich-Nowoisky, J., Bonn, M. & Meister, K. Interfacial Water Ordering Is Insufficient to Explain Ice-Nucleating Protein Activity. *Journal of Physical Chemistry Letters* **12** (2021).

72. Kunert, A. T., Pöhlker, M. L., Tang, K., Krevert, C. S., Wieder, C., Speth, K. R., Hanson, L. E., Morris, C. E., Schmale III, D. G., Pöschl, U. & Fröhlich-Nowoisky, J. Macromolecular fungal ice nuclei in <i>Fusarium</i>: effects of physical and chemical processing. *Biogeosciences* **16,** 4647–4659 (2019).

73. Tong, H. J., Ouyang, B., Nikolovski, N., Lienhard, D. M., Pope, F. D. & Kalberer, M. A new electrodynamic balance (EDB) design for low-temperature studies: Application to immersion freezing of pollen extract bioaerosols. *Atmospheric Measurement Techniques* **8** (2015).

74. Felgitsch, L., Bichler, M., Burkart, J., Fiala, B., Häusler, T., Hitzenberger, R. & Grothe, H. Heterogeneous Freezing of Liquid Suspensions Including Juices and Extracts from Berries and Leaves from Perennial Plants. *Atmosphere* **10,** 37 (2019).

75. Christner, B. C. Bioprospecting for microbial products that affect ice crystal formation and growth. *Applied Microbiology and Biotechnology* **85,** 481–489 (2010).

76. Watabe, S., Abe, K., Hirata, A., Emori, Y., Watanabe, M. & Arai, S. Large-scale Production and Purification of an *Erwinia ananas* Ice Nucleation Protein and Evaluation of Its Ice Nucleation Activity. *Bioscience, Biotechnology, and Biochemistry* **57,** 603–606 (1993).

77. Davies, P. L. Ice-binding proteins: a remarkable diversity of structures for stopping and starting ice growth. *Trends in Biochemical Sciences* **39,** 548–555 (2014).

78. Schnell, R. C. & Vali, G. Biogenic Ice Nuclei: Part I. Terrestrial and Marine Sources. *Journal of the Atmospheric Sciences* **33.** Publisher: American Meteorological Society Section: Journal of the Atmospheric Sciences, 1554–1564 (1976).

79. Knopf, D. A., Alpert, P. A., Zipori, A., Reicher, N. & Rudich, Y. Stochastic nucleation processes and substrate abundance explain time-dependent freezing in supercooled droplets. *npj Climate and Atmospheric Science* **3** (2020).

80. Diehl, K., Debertshäuser, M., Eppers, O., Schmithüsen, H., Mitra, S. K. & Borrmann, S. Particle surface area dependence of mineral dust in immersion freezing mode: Investigations with freely suspended drops in an acoustic levitator and a vertical wind tunnel. *Atmospheric Chemistry and Physics* **14** (2014).

81. Rogers, D. C. Development of a continuous flow thermal gradient diffusion chamber for ice nucleation studies. *Atmospheric Research* **22** (1988).

82. Kunert, A. T., Lamneck, M., Helleis, F., Pöschl, U., Pöhlker, M. L. & Fröhlich-Nowoisky, J. Twin-plate Ice Nucleation Assay (TINA) with infrared detection for high-Throughput droplet freezing experiments with biological ice nuclei in laboratory and field samples. *Atmospheric Measurement Techniques* **11** (2018).

83. Miller, A. J., Brennan, K. P., Mignani, C., Wieder, J., David, R. O. & Borduas-Dedekind, N. Development of the drop Freezing Ice Nuclei Counter (FINC), intercomparison of droplet freezing techniques, and use of soluble lignin as an atmospheric ice nucleation standard. *Atmospheric Measurement Techniques* **14** (2021).

84. Raymond, J. A. & Fritsen, C. H. Semipurification and Ice Recrystallization Inhibition Activity of Ice-Active Substances Associated with Antarctic Photosynthetic Organisms. *Cryobiology* **43,** 63–70 (2001).

85. Sharma, B., Sahoo, D. & Deswal, R. Single-step purification and characterization of antifreeze proteins from leaf and berry of a freeze-tolerant shrub seabuckthorn (Hippophae rhamnoides). *Journal of Separation Science* **41.** Publisher: John Wiley & Sons, Ltd, 3938–3945 (2018).

86. Nguyen, C. T., Yuan, M., Yu, J. S., Ye, T., Cao, H. & Xu, F. Isolation of ice structuring collagen peptide by ice affinity adsorption, its ice-binding mechanism and breadmaking performance in frozen dough. *Journal of Food Biochemistry* **42.** Publisher: John Wiley & Sons, Ltd, e12506 (2018).

87. Adar, C., Sirotinskaya, V., Bar Dolev, M., Friehmann, T. & Braslavsky, I. Falling water ice affinity purification of ice-binding proteins. *Scientific Reports* **8,** 11046 (2018).

88. Marshall, C. J., Basu, K. & Davies, P. L. Ice-shell purification of ice-binding proteins. *Cryobiology* **72** (2016).

89. Tomalty, H. E., Graham, L. A., Eves, R., Gruneberg, A. K. & Davies, P. L. Laboratory-scale isolation of insect antifreeze protein for cryobiology. *Biomolecules* **9** (2019).

90. Kuiper, M. J., Lankin, C., Gauthier, S. Y., Walker, V. K. & Davies, P. L. Purification of antifreeze proteins by adsorption to ice. *Biochemical and Biophysical Research Communications* **300,** 645–648 (2003).

91. Schwidetzky, R. *To freeze or not to freeze : Investigating ice-binding proteins and the role in biological ice nucleation* PhD thesis (Johannes Gutenberg University, Mainz, 2022).

92. Demtröder, W. *Molecular Physics: Theoretical Principles and Experimental Methods* 1st ed. (Wiley, 2005).

93. Hertel, I. V. & Schulz, C.-P. *Atome, Moleküle und optische Physik 2* (Springer Berlin Heidelberg, Berlin, Heidelberg, 2010).

94. Hollas, J. M. *Modern spectroscopy* 4th ed. 452 pp. (J. Wiley, Chichester ; Hoboken, NJ, 2004).

95. Socrates, G. & Socrates, G. *Infrared and Raman characteristic group frequencies: tables and charts* 3rd ed. 347 pp. (Wiley, Chichester ; New York, 2001).

96. *Bioanalytik* (eds Kurreck, J., Engels, J. W. & Lottspeich, F.) 4. Auflage (Springer Spektrum, Berlin [Heidelberg], 2022). 1183 pp.

97. *Bioanalytics: analytical methods and concepts in biochemistry and molecular biology* (eds Lottspeich, F. & Engels, J. W.) (Wiley-VCH, Weinheim, 2018). 1110 pp.

98. *Analytical applications of circular dichroism* (eds Purdie, N. & Brittain, H. G.) *Techniques and instrumentation in analytical chemistry* **v. 14** (Elsevier, Amsterdam ; New York, 1994). 348 pp.

99. Lakowicz, J. R. *Principles of fluorescence spectroscopy* 3rd ed. 954 pp. (Springer, New York, 2006).

100. Makowski, L., Berkowitz, S. A. & Houde, D. J. in *Biophysical Characterization of Proteins in Developing Biopharmaceuticals* 171–209 (Elsevier, 2015).

101. Sakho, E. H. M., Allahyari, E., Oluwafemi, O. S., Thomas, S. & Kalarikkal, N. in *Thermal and Rheological Measurement Techniques for Nanomaterials Characterization* 37–49 (Elsevier, 2017).

102. Liu, F., Lakey, P. S. J., Berkemeier, T., Tong, H., Kunert, A. T., Meusel, H., Cheng, Y., Su, H., Fröhlich-Nowoisky, J., Lai, S., Weller, M. G., Shiraiwa, M., Pöschl, U. & Kampf, C. J. Atmospheric protein chemistry influenced by anthropogenic air pollutants: nitration and oligomerization upon exposure to ozone and nitrogen dioxide. *Faraday Discussions* **200,** 413–427 (2017).

103. Ziegler, K., Kunert, A. T., Reinmuth-Selzle, K., Leifke, A. L., Widera, D., Weller, M. G., Schuppan, D., Fröhlich-Nowoisky, J., Lucas, K. & Pöschl, U. Chemical modification of pro-inflammatory proteins by peroxynitrite increases activation of TLR4 and NF-ϰB: Implications for the health effects of air pollution and oxidative stress. *Redox Biology* **37,** 101581 (2020).

104. Reinmuth-Selzle, K., Tchipilov, T., Backes, A. T., Tscheuschner, G., Tang, K., Ziegler, K., Lucas, K., Pöschl, U., Fröhlich-Nowoisky, J. & Weller, M. G. Determination of the protein content of complex samples by aromatic amino acid analysis, liquid chromatography-UV absorbance, and colorimetry. *Analytical and Bioanalytical Chemistry* **414,** 4457–4470 (2022).

105. Schwidetzky, R., Lukas, M., YazdanYar, A., Kunert, A. T., Pöschl, U., Domke, K. F., Fröhlich-Nowoisky, J., Bonn, M., Koop, T., Nagata, Y. & Meister, K. Specific Ion–Protein Interactions Influence Bacterial Ice Nucleation. *Chemistry - A European Journal* **27** (2021).

106. Schwidetzky, R., Kunert, A. T., Bonn, M., Pöschl, U., Ramløv, H., DeVries, A. L., Fröhlich-Nowoisky, J. & Meister, K. Inhibition of Bacterial Ice Nucleators Is Not an Intrinsic Property of Antifreeze Proteins. *The Journal of Physical Chemistry B* **124,** 4889–4895 (2020).

107. Schwidetzky, R., Sun, Y., Fröhlich-Nowoisky, J., Kunert, A. T., Bonn, M. & Meister, K. Ice Nucleation Activity of Perfluorinated Organic Acids. *Journal of Physical Chemistry Letters* **12** (2021).

108. Dreischmeier, K. *Heterogene Eisnukleations- und Antigefriereigenschaften von Biomolekülen* PhD thesis (Universität Bielefeld, 2019).

109. Failor, K. C., Schmale, D. G., Vinatzer, B. A. & Monteil, C. L. Ice nucleation active bacteria in precipitation are genetically diverse and nucleate ice by employing different mechanisms. *The ISME Journal* **11,** 2740–2753 (2017).

110. Ziemianin, M., Waga, J., Czarnobilska, E. & Myszkowska, D. Changes in qualitative and quantitative traits of birch (Betula pendula) pollen allergenic proteins in relation to the pollution contamination. *Environmental Science and Pollution Research* **28,** 39952–39965 (2021).

111. Greenfield, N. J. Using circular dichroism spectra to estimate protein secondary structure. *Nature Protocols* **1** (2007).

112. Pummer, B. G., Bauer, H., Bernardi, J., Chazallon, B., Facq, S., Lendl, B., Whitmore, K. & Grothe, H. Chemistry and morphology of dried-up pollen suspension residues: Chemistry and morphology of pollen suspension residues. *Journal of Raman Spectroscopy* **44,** 1654–1658 (2013).

113. Seifried, T. M., Bieber, P., Weiss, V. U., Pittenauer, E., Allmaier, G., Marchetti-Deschmann, M. & Grothe, H. Fluorescence signal of proteins in birch pollen distorted within its native matrix: Identification of the fluorescence suppressor quercetin-3-O-sophoroside. *Analytical and Bioanalytical Chemistry* (2022).

114. Pöhlker, C., Huffman, J. A. & Pöschl, U. Autofluorescence of atmospheric bioaerosols - fluorescent biomolecules and potential interferences. *Atmospheric Measurement Techniques* **5,** 37–71 (2012).

115. Montemurro, M., Schwaighofer, A., Schmidt, A., Culzoni, M. J., Mayer, H. K. & Lendl, B. High-throughput quantitation of bovine milk proteins and discrimination of commercial milk types by external cavity-quantum cascade laser spectroscopy and chemometrics. *The Analyst* **144,** 5571–5579 (2019).

116. Stan, C. A., Schneider, G. F., Shevkoplyas, S. S., Hashimoto, M., Ibanescu, M., Wiley, B. J. & Whitesides, G. M. A microfluidic apparatus for the study of ice nucleation in supercooled water drops. *Lab on a Chip* **9.** Publisher: The Royal Society of Chemistry, 2293–2305 (2009).

117. Edd, J. F., Humphry, K. J., Irimia, D., Weitz, D. A. & Toner, M. Nucleation and solidification in static arrays of monodisperse drops. *Lab on a Chip* **9.** Publisher: The Royal Society of Chemistry, 1859–1865 (2009).

118. Zobrist, B., Koop, T., Luo, B. P., Marcolli, C. & Peter, T. Heterogeneous Ice Nucleation Rate Coefficient of Water Droplets Coated by a Nonadecanol Monolayer. *The Journal of Physical Chemistry C* **111,** 2149–2155 (2007).

119. Felgitsch, L. *Ice nucleation activity of boreal plants with focus on birch trees* PhD thesis (Wien, 2019).

List of Abbreviations

AFP	Antifreeze proteins
BME	ß-Mercaptoethanol
BPWW	Birch pollen washing water
CCN	Cloud condensation nuclei
CD	Circular dichroism
DFA	Droplet freezing assay
DLS	Dynamic light scattering
EEM	Excitation emission map
EM	Electromagnetic
FTIR	Fourier-transform-infrared (spectroscopy)
HPLC	High performance liquid chromatography
HS	Hydrosat©
IAP	Ice affinity purification
IBM	Ice binding molecule
ICP	Inductively coupled plasma
IN	Ice nuclei
INA	Ice nucleation activity
INM	Ice nucleating macromolecule
IR	Infrared
IRE	Internal reflection element
MCT	Mercury cadmium telluride
MS	Mass spectrometry
MWCO	Molecular weight cut-off
Phe	Phenylalanine
PCR	Polymerase chain reaction
PES	Polyethersulfone
RT	Room temperature
SDS	Sodium dodecyl sulfate
TINA	Twin-plate ice-nucleation assay
Trp	Tryptophane
Tyr	Tyrosine
VODCA	Vienna optical droplet analyzer

List of Symbols

a	total number of evaluated droplets.
c	speed of light
d	dilution factor
E	energy
f_{ice}	fraction of frozen droplets
h	Planck's constant
m	mass
N_m	cumulative number of IN
s	freezing events within a temperature bin
T	Temperature
T_{on}	freezing onset temperature
V	volume
V_{drop}	average droplet volume
V_{wash}	volume of the initial suspension
λ	wavelength
ν	frequency

List of Figures

List of Tables